ISTANBUL TECHNICAL UNIVERSITY ★ GRADUATE SCHOOL OF SCIENCE ENGINEERING AND TECHNOLOGY

**MANUFACTURE AND TESTING
OF A COMPOSITE DRIVESHAFT
FOR AUTOMOTIVE APPLICATIONS**

M.Sc. THESIS

Samet TATAROĞLU

Department of Aeronautical and Astronautical Engineering

Aeronautical and Astronautical Engineering Programme

DECEMBER 2015

ISTANBUL TECHNICAL UNIVERSITY ★ GRADUATE SCHOOL OF SCIENCE ENGINEERING AND TECHNOLOGY

**MANUFACTURE AND TESTING
OF A COMPOSITE DRIVESHAFT
FOR AUTOMOTIVE APPLICATIONS**

M.Sc. THESIS

**Samet TATAROĞLU
(511111167)**

Department of Aeronautical and Astronautical Engineering

Aeronautical and Astronautical Engineering Programme

Thesis Advisor: Prof. Dr. Halit S. TÜRKMEN

DECEMBER 2015

İSTANBUL TEKNİK ÜNİVERSİTESİ ★ FEN BİLİMLERİ ENSTİTÜSÜ

**KOMPOZİT MALZEMELİ BİR ŞAFTIN
OTOMOTİV UYGULAMALARI İÇİN
ÜRETİMİ VE TESTİ**

YÜKSEK LİSANS TEZİ

**Samet TATAROĞLU
(511111167)**

Uçak ve Uzay Mühendisliği Anabilim Dalı

Uçak ve Uzay Mühendisliği Programı

Tez Danışmanı: Prof. Dr. Halit S. TÜRKMEN

ARALIK 2015

Samet TATAROĞLU, a **M.Sc.** student of ITU **Graduate School of Science Engineering and Technology** student ID 511111167, successfully defended the **thesis** entitled "**MANUFACTURING AND TESTING OF A COMPOSITE DRIVESHAFT FOR AUTOMOTIVE APPLICATIONS**", which he prepared after fulfilling the requirements specified in the associated legislations, before the jury whose signatures are below.

Thesis Advisor: **Prof. Dr. Halit S. TÜRKMEN**   ....
Istanbul Technical University

Jury Members: **Prof. Dr. Vedat Z. DOĞAN**   ....
Istanbul Technical University

                                       Assoc. Prof. Dr. Zafer KAZANCI   ....
Turkish Air Force Academy

Date of Submission: 27 November 2015
Date of Defence: **25 December 2015**

To my family

and

My other-half,

FOREWORD

First and foremost, I would like to thank my family for all the care and endless support they provided to me. They are the ones made me who I am today…

I would like to specially thank my advisor, Prof. Dr. Halit S. TÜRKMEN, for all the advices and counsel he provided me during the course of this study. Without his guidance this study would not be possible. I am also grateful for the opportunity of working with Prof. Dr. Vedat Z. DOĞAN and Prof. Dr. Zahit MECİTOĞLU, for all their technical assistance during the course of our project.

I would like to thank research assistants Erdem AKAY and Sedat SÜSLER for their valuable assistance during laboratory work. Laboratory technician Müslüm ÇAKIR has proved himself to be an invaluable workmate, I would also like to thank him for all his hard work and endeavor.

A. Aykut ŞEN and Sibel KAYA of Ford Otosan has been supportive of our work, whenever and wherever needed. I am grateful to be able to work with professionals like them.

Emrah ÖLMEZBAŞ of MAKSAV Inc. has provided us every means that is available to him during the course of coupon manufacturing. Although we have not been able to achieve a desired outcome, I would like thank and wish him success in his business life.

All the employees of Adalar Makina has consecrated their endeavor for our study and shown a great hospitality during the time we spent in Polatlı, Ankara. I would like to kindly thank them all, especially my dear colleagues Ender BİDAV and Serkan ESKİCİOĞLU.

I would like to thank Mehmet İsmet BAYRAKLI of Çalışanlar Naval Works for his technical competence and professional ethics. I wish we could have been able to work together beforehand, rather than the final stages of our project.

Last but not least, I would like to thank my other-half for completing me…

December 2015   Samet TATAROĞLU
                                                                    (Engineer)

x

TABLE OF CONTENTS

ABBREVIATIONS

2-D : 2 Dimensional
3-D : 3 Dimensional
2WD : Two Wheel Drive
4WD : Four Wheel Drive
ACP : ANSYS Composite PrepPost
AISI : American Iron and Steel Institute
APDL : ANSYS Parametric Design Language
ASTM : American Society for Testing and Materials
AWD : All Wheel Drive
°C : Degree Celsius
CAD : Computer Aided Design
CFRP : Carbon Fiber Reinforced Plastic
CLT : Classical Laminate Theory
CMT : Cold Metal Transfer
CNC : Computer Numeric Control
CTE : Coefficient of Thermal Expansion
DPM : Degrees Per Minute
°F : Degree Fahrenheit
FEA : Finite Element Analysis
FWD : Front Wheel Drive
GPa : Gigapascal
GTO : Grand Turismo Omologato
h : Hour
Hz : Hertz
IMSA : International Motor Sports Association
ISO : International Standards Organization
ITU : Istanbul Technical University
kg : Kilogram
km : Kilometer
lbs. : Pound
m : Meter
min : Minute
mPa·s : Millipascal-second
mm : Millimeter
MPa : Megapascal
N : Newton
Nm : Newton-meter
NVH : Noise Vibration Harshness
Pa·s : Pascal-second
PMC : Polymer Matrix Composite
PTU : Power Transfer Unit
RPM : Revolutions Per Minute
RWD : Rear Wheel Drive
SAE : Society of Automotive Engineers
TIG : Titanium Inert Gas
UD : Unidirectional

LIST OF TABLES

LIST OF FIGURES

MANUFACTURE AND TESTING OF A COMPOSITE DRIVESHAFT FOR AUTOMOTIVE APPLICATIONS

SUMMARY

Automotive driveshafts are generally manufactured from steel or aluminum material and constructed in multiple pieces to avoid bending resonance. Composite materials have emerged as an alternative solution for torque tube material recently, enabling reduction to a single piece due to higher values of axial moduli.

In this thesis; design, manufacture and testing of a composite driveshaft is sought, which is to replace a 2-piece metallic driveshaft on a heavy weight commercial vehicle. Carbon/Epoxy composite torque tube of the driveshaft is to be produced by filament winding, regarding fundamentals of the method are also presented. Torque tube is modelled by utilizing Classical Laminate theory in analytical domain; numerical model was developed with finite element method. Material properties obtained from the literature is used for the initial evaluation of models.

Manufacturing of composite materials is a complex issue and material properties depend on many parameters. The properties of actual material may differ from catalogue values found in the literature. To address that issue, test plate production is carried out in accordance with ISO 1268. Specimens are cut from test plates and mechanical properties are determined by testing per regarding ASTM standards.

End connections constitute, perhaps the most interesting and challenging issue about producing a composite driveshaft. In this particular design, end connections, which are machined from blocks of C50 material, are planned to be co-cured with filament wound carbon/epoxy shaft tube. An adhesive layer of epoxy would develop between them and its strength is investigated in order to transmit the design torque safely. In order to ensure safer transmission, hexagonal shape for the joint is chosen to provide coupling between the shaft and joint. An appropriate amount of taper is given to provide a smooth inner bore and continuous layers.

Manufacturing setup consists of the mandrel body and end connections mounted on it. Masking tape is applied to cylindrical surfaces in order to preserve them and release agent is applied on all surfaces bar the connection geometry. Carbon fibers, which are impregnated with epoxy resin system, would be wound on this setup. After curing cycle, the mandrel would be removed thus leaving a composite cylinder adhered to the end connections, which is our composite driveshaft in either test rig or vehicle configuration. Some problems had been encountered on conic hexagonal connection geometry during trial windings so draping analyses of connection geometries were carried out. Conic hexagonal connection geometry has been replaced with a polygonal section.

Static and fatigue testing of the prototype shafts are planned. A torsion test rig is designed to be employed on the MTS322.21 universal testing system for transforming the axial force of the system into a torque loading by the utilization of a torque arm.

A prototype driveshaft has been manufactured but rig tests are yet to commence. 28 kilograms of weight saving is achieved which constitutes to 35% of the structure. Design requirements are fulfilled, except for the natural frequency which might be attributed to the lower moduli of the production material. Better planning of the filament winding process would yield a production material with better properties resulting in further weight savings and a higher natural frequency for a production shaft.

KOMPOZİT MALZEMELİ BİR ŞAFTIN OTOMOTİV UYGULAMALARI İÇİN ÜRETİMİ VE TESTİ

ÖZET

Kardan şaftı, arkadan itişli araçlarda torku şanzımandan arka aksa aktararak süspansiyonun bağıl hareketlerini kompanse eden sistemdir. Şaftın gövdesini meydana getiren tork tüpü, ağırlığı düşürmek ve eğilme/burulma rijitliği sağlamak açısından genellikle içi boş imal edilirken; tek, iki veya üç parçalı olabilir. Malzeme olarak çoğunlukla çelik veya alüminyum kullanılırken imalatta çeşitli kaynak teknikleri uygulanabilir. Kompozit malzemeler de tork tüpü için son dönemlerde yeni bir alternative olarak ortaya çıkmıştır.

Tork tüpü için kompozit malzeme kullanmanın en temel avantajı, eğilme rezonansı tarafından kısıtlanmakta olan şaft boyunun uzatılabilmesine imkan vermesidir. Kompozit bir tork tüpü, daha yüksek elastisite modülü sayesinde, şaft boyunun uzamasıyla iki parçalı yapının tek parçaya indirilebilmesini sağlar. Bu durumda aracın sürüş karakterinde iyileştirmeler sağlanmasının yanı sıra, daha yalın bir yapıyla üretim zamanının kısalması, envanter maliyetlerinin düşürülmesi ve bakım kolaylığı sağlanır. Maliyet açısından bakıldığında ise; kompozit bir şaftın üretimi metal muadiline göre daha karmaşık ve pahalı gibi gözükse de, bir kompozit şaft ömür devri içerisinde metal bir şafttan daha ucuza malolacak şekilde tasarlanıp üretilebilir.

Metalik malzemeler otomotiv uygulamaları için şaft tasarımında geleneksel bir seçim olmakla birlikte; ağırlık, yorulma dayanımı/ömrü ve kritik hız açısından teknolojik sınırlara ulaşmış durumdadır. Otomotiv şaftı tasarımlarını ileriye taşımak açısından çeşitli öneriler getirilmiş olsa da bunu şaft ağırlığını arttırmadan yapabilen bir çözüm henüz sunulamamıştır. Tork tüpü olarak elyaf takviyeli kompozit yapıların kullanılması performans limitlerinin ağırlık artışına sebep olmadan sağlanabilmesi potansiyelini taşımaktadır. Buradan hareketle tezin amacı; bir ağır ticari araç uygulamasında kullanılmak üzere, iki parçalı çelik bir şaftı değiştirecek tek parçalı kompozit bir şaftın tasarlanması, üretimi ve testidir.

Mevcut tez çalışması; T.C. Bilim, Sanayi ve Teknoloji Bakanlığı ile Ford Otosan'ın desteklemiş olduğu 0529.STZ.2013-2 kodlu SAN-TEZ projesinin ürünüdür.

Tasarım çalışmaları literatürden elde edilen malzeme verileriyle başlatılmış olup tork tüpü analitik olarak katman teorisi ve nümerik olarak da sonlu elemanlar analizi yoluyla modellenmiştir. Şaftın bir başlangıç modeli oluşturulmasının ardından, kupon üretimi ve testleri yoluyla üretim malzemesinin mekanik özellikleri belirlendikten sonra güncellenmiştir. Üretimi yapılan prototip şaftın burulma durumundaki statik ve yorulma mukavemetinin belirlenmesi amacıyla bir test düzeneği tasarlanmıştır. Şaftın dinamik karakteristikleri modal testler yoluyla belirlenecektir. Çalışmanın son adımı ise prototipi üretilip statik, yorulma ve modal davranışı düzenek üzerinde belirlenen şaftın araç üzerinde test edilmesi olacaktır.

Otomotiv uygulamalarında kullanılacak bir şaftın temel performans isterleri, kritik hız, burulma ve burkulma dayanımı ile yorulma ömrü olarak belirtilebilir. Metal bir şaftın tasarımında şaft kesidi, üzerine gelen belirli bir tasarım torku ile malzemenin izin verilebilir kesme gerilmesine göre kolayca belirlenebilir. Metal şaftlardan farklı olarak kompozit şaftlarda değiştirilebilecek parametre sayısı daha fazla olması sonucunda elastik sabitlerin düzenlenebilmesi yoluyla performans isterlerini karşılayabilen, birden çok daha fazla sayıda şaft seçeneğinin tasarımı mümkün olabilmektedir.

Temel tasarım hedefi; çalışma hızından daha yüksek bir kritik hız, azami torktan daha yüksek bir burkulma torku ve Tsai-Wu gibi bir hasar kriteri uygulandığında arzu edilen bir dayanım oranı sağlanırken ağırlığın minimumda tutulabilmesidir.

Statik tork iletimi, burkulma yük katsayısı ve doğal eğilme frekansı mevcut tasarımda göz önüne alınan temel tasarım kriterleridir. Şafttan belirli bir yorulma ömrü de istenmekte olup bunun belirlenmesi tamamen deneysel yollarla gerçekleştirilecektir. Tasarım kriterleri; 17000Nm değerindeki bir azami torkun iletimi, burkulma kararlılığı, 130Hz değerindeki doğal eğilme frekansı ve ±6800Nm değerindeki değişken torkta 300.000 çevrimlik yorulma ömrü olarak özetlenebilir.

Şaftın analitik modeli bir EXCEL dokümanı yardımıyla oluşturulmuştur. Katman teorisi ve Tsai-Wu hasar kriteri uygulanarak azami tork yüküne dayanım oranı bulunmuştur. Doğal eğilme frekansı ve kritik burkulma torku da çeşitli formüllerden yararlanılarak hesaplanmıştır.

Şaft, nümerik olarak, sonlu elemanlar analizi yöntemiyle modellenmiştir. ANSYS ACP ve Mechanical APDL ortamında iki farklı yapı oluşturulmuş olup eleman ağları aynı olmakla birlikte sınır koşullarında çeşitli farklılıklar mevcuttur. Şaft, bir ucundan sabiltlenmişken diğer ucunda tanımlanmış bir merkezi düğüm noktası yardımıyla tork yükü uygulanmıştır. Yapı, toplamda 1650 SHELL181 elemanıyla modellenmiştir.

Burkulma analizi, şaftın burkulma kararlılığını ortaya koymak üzere gerçekleştirilmiştir. Burkulma analizinde kullanılan model ve uygulanan sınır koşulları static analiz ile aynıdır.

Modal analiz ise şaftın doğal frekansları ve mod şekillerinin tespit edilerek eğilme frekansları ve modlarının belirlenmesi amacıyla gerçekleştirilmiştir. Şaft tamamen serbest durumdayken incelenmiş olup modal analiz sırasında herhangi bir sınır koşulu veya yük uygulanmasına gerek bulunmamaktadır.

İç çapı 120mm olan A modelleri ve 140mm olan B modelleri olmak üzere toplamda 10 farklı şaft modeli oluşturulup analitik ve nümerik modellerden elde edilen sonuçlar tasarım kriterleri ile karşılaştırılarak bir tablo halinde verilmiştir. Katman sayıları A1 ve B1 başlangıç modellerinden Tsai-Wu dayanım oranına göre itere edilmiş olup diğer tasarım kriterlerinin değerlerine göre de farklı katman dizilimleri oluşturulmuştur.

Kompozit malzemelerin üretimi, birçok değişkene bağlı karmaşık bir konu olup literatürden alınan malzeme verileri ile atölyede üretilen malzemenin özellikleri birbirinden büyük farklılıklar gösterebilmektedir. Bu durumun yarattığı belirsizliğin giderilebilmesi amacıyla ISO 1268 standardı referans alınarak test plakaları üretilmiş, bu test plakalarından kesilen numuneler de ilgili ASTM standartlarına göre testlere tabi tutularak üretim malzemesinin mekanik özellikleri belirlenmiştir.

Üretim malzemesinin mekanik özelliklerinin belirlenmesi amacıyla test plakasından numuneler kesilerek MTS322.21 üniversal test cihazı üzerinde kupon testleri gerçekleştirilmiştir. Çekme testi için ASTM D3039, basma testi için ASTM D6641 ve kesme testi için de ASTM D3518 standartları referans alınmıştır. Modül ve Poisson Oranı gibi verilerin elde edilebilmesi için numuneler üzerine gerinim ölçerler yerleştirilmiştir. Mekanik özellikleri belirlenen üretim malzemesinin yoğunluğu da ASTM D792 standardı referans alınarak belirlenmiştir.

Piyasadaki mevcut uygulamalar hakkında fikir vermesi amacıyla bazı örnek şaftlar temin edilmiş olup bunlardan alınan numunelere de yoğunluk testi uygulanmıştır. Örnek şaftlara yoğunluk testi uygulanmasının amacı, belirli bir elyaf ve matris yoğunluğu üzerinden elyaf hacim oranının tahmin edilebilmesidir.

Üretim malzemesinin mekanik özelliklerinin belirlenmesinden sonra analitik ve nümerik şaft modellerinin buna göre güncellenmesi gerekliliği doğmuştur. Analizlerin güncellenmesinden sonra 120mm iç çaplı A modellerinden performans isterlerinin

düşük değerleri nedeniyle vazgeçilmiştir. Bunu takiben 130mm iç çapa sahip C modeli şaftlar oluşturulmuş, katman sayısı ve dizilimi de performans isterlerine göre belirlenmiştir.

Kompozit bir şaft tasarımının teknik açıdan en ilginç kısımlarından birini de kompozit boru ile şaft mafsallarının bağlantısı oluşturmaktadır. Literatürde farklı ifadeler mevcut olmakla birlikte, bu çalışmada "uç bağlantısı" ifadesi kullanılacaktır. Kompozit şaft uygulamalarındaki uç bağlantıları yapıştırmalı ve sıkı geçmeli bağlantı olmak üzere iki temel gruba ayrılabilir.

GKN tarafından daha önce bu konu üzerinde çalışılmış olup çok düşük ağırlığa sahip bir kompozit şaft tasarımı ortaya konmuştur. Teufelberger GmbH şirketi de bu konu üzerinde T-IGEL adını verdiği ticari bir çözüm üretmiştir. Konu ile ilgili bir patent araştırması gerçekleştirilmiş olup, farklı tarihlere ait 111 adet patent derlenmiştir. Tedarik edilmiş olan örnek şaftların da uç bağlantıları tahribatlı muayene ile incelenerek mevcut diğer ticari uygulamalar hakkında bilgi edinilmiştir.

Uç bağlantı parçalarının, C50 yapı çeliği blok malzemeden talaşlı işlemle imal edilmesi ve kompozit sargı ile birlikte fırında kürtlenirken yapıştırılması planlanmıştır. Bu durumda uç parçası ile kompozit sargı arasında bir yapıştırıcı katmanı oluşacaktır ve bu katmanın istenen torku güvenli bir şekilde iletebilmesi için mukavemeti açısından kontrol edilmesi gerekmektedir. Yapıştırıcının kesme modülü, yapıştırıcı katman kalınlığı ve yapışma uzunluğu gibi parametrelerin değişimi ile yapıştırıcı içerisindeki kayma gerilmesi dağılımının farklı tasarımlar içerisinde nasıl değiştiği çeşitli eğriler yardımıyla incelenebilmektedir. Eğrilerdeki gerilmelerin tepe noktaları yapıştırıcının kesme mukavemeti ile karşılaştırılarak uç parçası ve kompozit boru arasındaki ayrılmanın nereden ve nasıl başlayabileceği değerlendirilebilir. Bu hesabın yapılmasının temel sebebi yapıştırıcının kesme mukavemeti sınırları içerisinde kalabilmesini sağlayacak, güvenli bir yapıştırma boyunun belirlenebilmesidir. Bunun yanında yapıştırma boyu, uç parça geometrisini de belirleyen önemli etkenlerden biridir. Şekil bağı yardımıyla tasarım torkunun daha güvenli bir şekilde iletimini sağlamak açısından uç parçalarının altıgen bir keside sahip olması düşünülmüştür. Bunun yanında kompozit boru ile uç parçasının iç çapının dirseksiz bir şekilde birleşebilmesi, yapışma alanının arttırılıp kesme gerilimi dağılımının iyileştirilebilmesi için parçaya bir miktar koniklik de verilmiştir. İletmek istediğimiz tork değerinin yüksekliğinden dolayı parçanın tüm ayrıntıları buna göre şekillendirilmiştir.

Üretilecek prototip şaftın düzenek ve araç üzerinde test edilecek iki farklı türevi olacaktır. Araç şaftında uç parçaları ile mafsallar bir yüzük yardımıyla kaynatılacak iken test şaftı üzerinde yuvalı ve flanşlı olmak üzere iki uçta da farklı birleştirme parçaları bulunacaktır. Bunlardan biri test düzeneği mili ile birlikte çalışabilmesi için yuvalı, diğeri de test düzeneği üzerindeki brakete bağlanabilmesi için flanşlı olacaktır. Uç bağlantı parçalarının tasarım ve imalatı süresince filaman sargı yöntemiyle imalata uygunluğunu sağlamak açısından prototip şaftları üretecek firma olan Adalar Makina'nın değerlendirmeleri ve onayı alınmıştır. Parçaların mukavemeti sonlu elemanlar analizi yoluyla kontrol edilmiş, uygun yerlerden sabitlenerek 35000Nm tasarım torku altıgen konik bağlantı geometrisi üzerinden uygulanmıştır. Sonlu elemanlar modelinin yakınsayabilmesi açısından eleman ağının oluşturulmasında iteratif seçenekler kullanılmıştır.

Sarım konfigürasyonu mandrel gövdesi ve üzerine geçirilmiş bağlantı parçalarından oluşmaktadır. Mandrel yüzeylerine maskeleme bandı uygulanarak koruma sağlanması amaçlanmıştır. Uç bağlantı parçaları hariç tüm yüzeylere kalıp ayırıcı uygulanmaktadır. Reçine emdirilmiş karbon elyaf, belirlenen katman sayısı ve dizilimi

dahilinde bu yapı üzerine sarılacak ve kürleme işlemi bittikten sonra mandrel flanşlı bağlantı parçası içerisinden çıkarılarak kompozit boru ve ona yapışmış uç bağlantı parçaları olarak test şaftı elde edilecektir.

Prototip şaft imalatından önce deneme sarımları gerçekleştirilmiş ve bu deneme sarımları süresince çeşitli sorunlarla karşılaşılmıştır. Mandrelin dairesel yüzeyleri üzerine oldukça düzenli sarımlar yapılabilirken uç parçalarının altıgen konik geometrisi üzerinde elyaf bandının istenen konumdan kaydığı ve dağıldığı gözlemlenmiştir. Geometrinin burada esas problemi teşkil ettiği anlaşılmış, problemli ve uygun geometriler serim(draping) analizi yoluyla incelenmiştir. Serim analizinde incelenen geometri dörtgen elemanlarla kaplanmakta ve bu elemanların çarpılmasına göre elyafın arzu edilen yönden ne kadar sapacağı kestirilebilmektedir. Başta altıgen konik geometri olmak üzere çeşitli ihtimaller değerlendirilmiştir. Kolaylık için sarım yüzeylerinin çeyreği modellenmiş ve şekil bağı sağlayabilirken elyaf sarımına müsait bir poligon uç bağlantı geometrisi geliştirilmiştir.

Üretilen prototip şaftın statik ve yorulma testleri de ayrıca planlanmıştır. İTÜ UUBF bünyesindeki Kompozit Yapı Laboratuvarı'nda mevcut MTS322.21 üniversal test cihazı üzerinde kullanılacak bir burulma test düzeneği tasarlanıp imal ettirilmiştir. MTS322.21 eksenel yönde ±100kN maksimum kuvvet sağlayabilen bir test cihazıdır ancak burulma testi için eksenel bir kuvvet tek başına yeterli değildir. Eksenel yükün tork yüküne dönüştürülebilmesi için bir kol tasarlanmış, cihaz ve masaları üzerinde uygun şekilde mafsallanmıştır. Test düzeneği parçaları ve montajı CATIA V5 ortamında tasarlanmış, deney torkuna dayanımı da ANSYS ortamında gerçekleştirilen sonlu elemanlar analizleriyle ortaya konmuştur.

Mevcut durumda prototip şaftın imalatı tamamlanmış olup MTS322.21 cihazı üzerinde devam etmekte olan testlerden dolayı montajı mümkün olmamış, prototip şaftın testlerine başlanamamıştır.

Sonuç olarak, 2 parçalı çelik malzemeli bir şaftı değiştirecek tek parçalı kompozit bir şaftın tasarımı ve prototip üretimi gerçekleştirilmiştir. Mevcut durumda yapının %35'ine denk gelen 28 kilogramlık bir ağırlık kazancı sağlanmıştır. Kritik hız dışındaki performans isterleri sağlanmış olup bu durumun sebebi de esas olarak üretim malzemesinin düşük modül değeridir. Kupon üretimi sırasında arzu edilen elyaf hacim oranı ve mekanik özelliklere sahip bir malzemenin elde edilememiş olduğunu da ayrıca eklemek gerekir. Filaman sargı üretim sürecinin daha iyi bir şekilde planlanması ve yönetimiyle daha iyi özelliklere sahip bir malzemenin üretilebilmesi mümkün olup, bu durumda hem daha fazla ağırlık kazancı sağlanabilir hem de kritik hızı daha yüksek olan bir şaft tasarımı ortaya konabilir.

1. INTRODUCTION

The basic function of a driveline system, various layouts are provided in Figure 1.1, is to transmit torque and rotation from the transmission to the wheel hubs. Driveshaft is the system which transmits torque from transmission to rear axle whilst compensating suspension movements on RWD vehicles. [1]
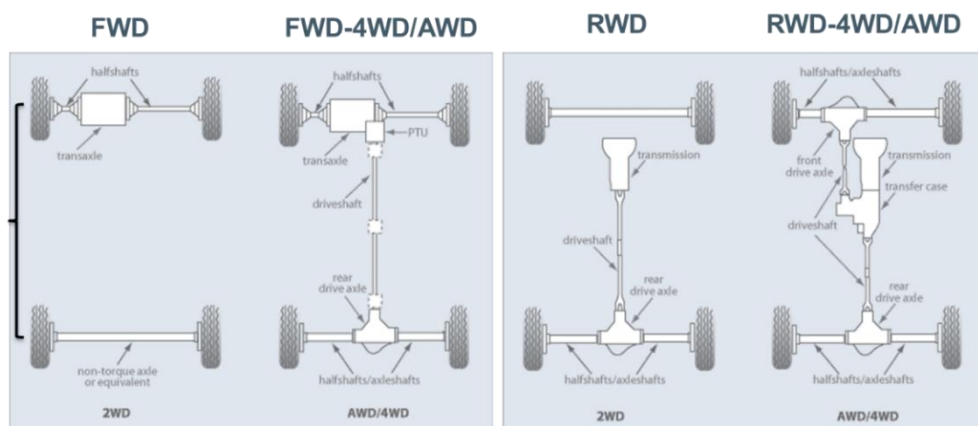
Figure 1.1: Driveline layouts [1].

Primary functions of a driveshaft might be listed as:

- Transmission of rotation/torque between major components
- Permission of axial/angular driveline movement [1]

A generic driveshaft assembly is illustrated in Figure 1.2.

Key

1) Bolts
2) Torque tube
3) Snap ring
4) Flange yoke
5) Universal joint
6) Snap ring
7) Slip yoke
8) Universal joint
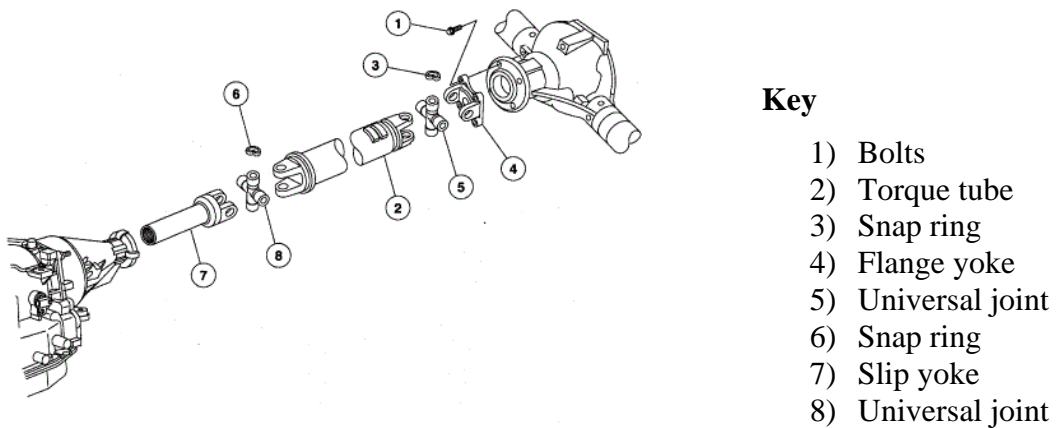
Figure 1.2: Driveshaft assembly (Url-1).

Driveshafts are usually hollow, to reduce weight, with a properly large diameter to provide strength and bending/torsion stiffness. They come in 1-piece, 2-piece, and 3-piece tubular versions, as can be seen in Figure 1.3. [1]

Figure 1.3: 1-piece, 2-piece and 3-piece driveshafts [1].

Steel shafts are generally of smaller diameter, ranging from 2.5 to 3.5". There are various wall thickness combinations with diameter. Production might be carried out either with friction or magnetic arc welding. Plasma/Cold Metal Transfer (CMT), laser or CO_2 welding options are also available.

40-50% lighter shafts might be produced with 1-piece aluminum tubing when compared with a 2-piece steel driveshaft. They can be constructed of multiple diameters ranging between 3.5-5.5". There are various wall thickness combinations with diameter. Swaging of aluminum tubes is also an option. Aluminum shaft assemblies might be produced by friction or Titanium inert gas (TIG) welding.

Composite/carbon fiber tubes are generally 40% lighter but 350% stiffer than aluminum counterparts. 1st bending mode frequency would be higher thus providing a bigger figure of maximum speed.

1-piece composite tubing may replace a 2-piece steel setup due to tailorability of the material. This provides some tunable noise, vibration and harshness (NVH) characteristics as well. End yokes are press fit into shaft tubing of composite materials. [1]

1.1 Purpose of Thesis

Metallic materials are the conventional choice for automotive drivelines; driveshafts of steel and aluminum materials are in service on millions of motor vehicles today. Eventually, they have reached the peak point of their performance, regarding weight limits, fatigue life/strength and critical speed. Various solutions for the elimination of these inherent limitations have been proposed; such as flywheels, harmonic dampers, multiple shafts with additional bearings and heavy rubber shock absorbers etc. These

proposals have shown limited success, always at the expense of increased weight, rotational inertia and resistance in drivelines. [2], [3]

The purpose of this thesis is the manufacturing and testing of a composite driveshaft to replace a conventional 2-piece steel driveshaft of a heavy weight commercial vehicle. The use of fiber reinforced plastics as tubing material has the potential of solving most of the current driveline problems without incorporating additional weight.

A good starting point is that there are no examples of composite driveshafts being utilized in any production vehicle of Turkish origin. In addition, no serial production heavy weight commercial vehicle has been noted to use composite driveshaft till this date either, most of the applications are for passenger cars. These are two primary motivations behind present study.

1.2 Literature Review

Composite materials have been in focus from a structural point of view recently; applications and correspondingly the literature of composite materials are growing for quite some time. Adoption of composite materials has been started by aerospace industries, however they are used much more widely in other industrial applications, such as sporting goods today, a fact which is obvious from Figure 1.4.
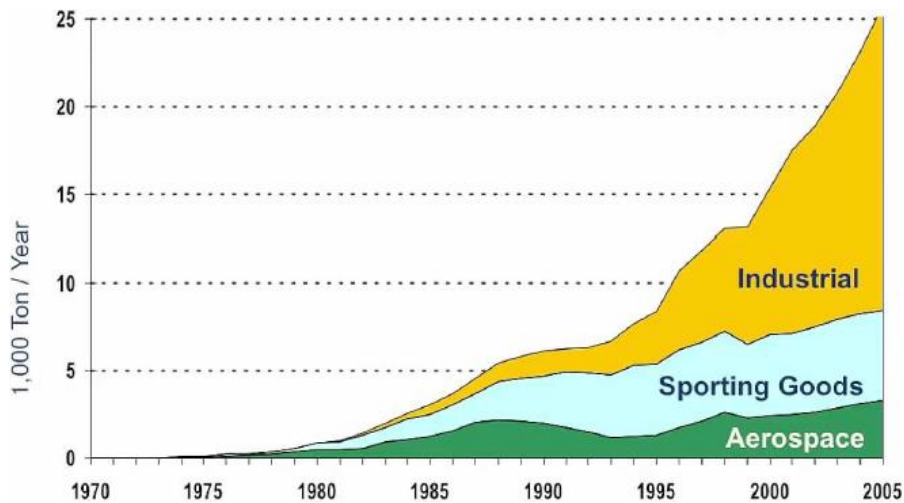
Figure 1.4: Composite production in different industries [4].

Composite market for automotive industry is around 30% of total production on a weight basis in 2005; as a comparison, same figure is a rough 10% for aerospace industry.

Current trend within the composites industry is the reduction of costs, by development of more automated methods for manufacturing integrated composite products of highly optimized design. Increasing demand of non-aerospace industries for composite materials are reinforcing these trends due to larger market volume and higher production rates. Meeting these very high production rates, especially for automotive industry, will be a significant challenge for the composite industry in the near future. Development of better analysis tools for the prediction of lifetime for composite structures and effective methods of recycling them after useful life are two issues gaining importance mainly due to increasing demand of non-aerospace industries. [5]

Basic advantage of replacing metals with composite materials for automotive driveshaft applications is that they render the increase of shaft length possible, which is otherwise constrained by bending resonance. Expression of critical speed is given in (1.1).

$$N_c = (C/L^2) \cdot (E/\rho \cdot I/A)^{0.5} \tag{1.1}$$

N_c is shaft critical speed, L is shaft length, I is tube second moment of area, A is cross sectional area of tube and C is a constant.

Space constraints limit the external diameter of a driveshaft, leaving the only way to increase critical speed increasing specific modulus which is defined by E/ρ. By using a fiber reinforced composite, it is possible to arrange the fiber orientations layer by layer so that bending modulus of the torque tube would be higher whilst specific gravity is lower. That situation leads to a favorable specific bending modulus and an enhanced critical speed, which can be observed in Figure 1.5. [6]
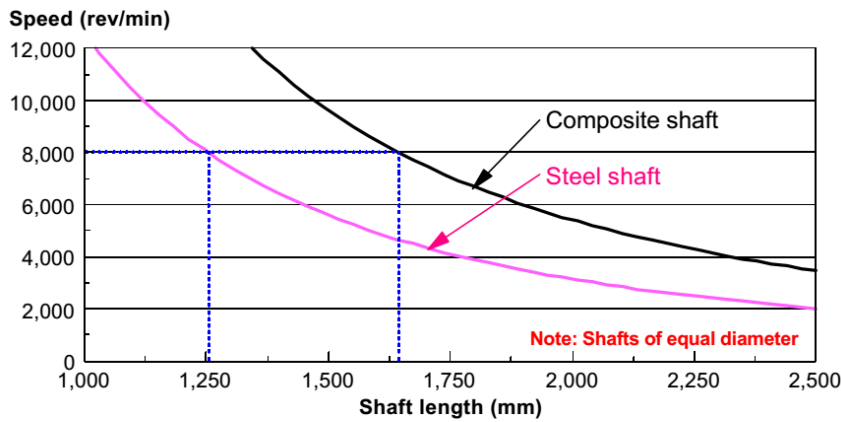
Figure 1.5: Critical speed-length curve for automotive driveshafts [6].

Not only bending but also torsional vibrations could pose serious problems for driveline systems. Mazziotti in 1960 [7] reviewed and analyzed torsional vibrations associated with drivelines. As his conclusion, amplification or decay of the vibrations being transmitted through a driveline is possible so that the driveline should be operated at no less than 1.5 times the (torsional) natural frequency of the system. In comparison, Rossoni [8] makes the general recommendation that critical speeds should be avoided by a 10% margin, regardless of the mode of the vibration.

In order to assist in a better design of truck drivelines, Spicer division of Dana published SAE paper #942322 [9] which describes a detailed torsional analysis of truck drivelines utilizing computer simulations. The paper approves Maziotti's findings and concludes that torsional vibrations cause comfort problems for occupants and result in component failures. Torsional vibrations also create additional dynamic loads on top of the mean static torque transmitted through the driveline which could easily cause catastrophic fatigue failures of dynamic components. In addition, they are responsible for wear problems at springs, splines, gear teeth, etc. eventually leading to the failure of these components. In addition, the paper presents a detailed list of references on the torsional vibrations and their effects on automotive drivelines.

Excessive rotating masses might cause power losses in a driveline; 17-22% of the power generated by the engine is lost to the rotating mass in a driveline according to Texas A&M University. [10] Reducing the amount of rotating mass would help to decrease these losses. Composite driveshafts are lighter in weight, requiring less energy to spin thus increasing the amount of the power transmitted to the wheels.

Nature of the composite materials, fibers oriented in a resinous binder, provides driveshafts a certain amount of tailorability to meet specific operational characteristics so that they can match requirements of various applications. As an example for that, carbon fiber driveshafts can be designed to be more flexible under torsional loading. [2] This increased amount of torsional flexibility might help to absorb impact loads resulting from torque spikes due to "clutch pop". According to some automotive manufacturers [11], that increased torsional flexibility of a driveshaft can effectively increase the fatigue life of all other driveline components connected to it.

Steel driveshafts longer than 1500mm are manufactured in two pieces to increase natural bending frequency, which is inversely proportional to the square of the length

and proportional to the square root of the specific modulus. Composite materials with higher values of specific moduli, e.g. in the case of carbon/epoxy exceeds four times that of aluminum, make it possible to replace 2-piece metallic driveshaft with a single piece composite driveshaft which provides a higher critical speed and ultimately maintains a higher margin of safety. [3]

Reduction of a 2-piece driveshaft into 1-piece results in significant reductions in weight and noise, vibration and harshness. Damping capability of composites could also absorb shock loads, reducing wear on dynamic components as well as increasing tire traction. [2] The use of a single torque tube would provide additional benefits such as reduced assembly time, inventory cost, ease of maintenance and part simplicity. [3] By that way a composite design of a driveshaft could help to simplify the design, engineering and production of a vehicle floor pan. [6] Van Laarhoven [12] notes additional benefits of a composite driveshaft as corrosion resistance and a near zero coefficient of thermal expansion, which provides the shaft assembly an ability to withstand greater degrees of misalignment than conventional 2-piece metallic driveshafts.

Polymer matrix composites, such as glass or carbon fibers in an epoxy matrix, provide better fatigue characteristics because the fibers act as a stop mechanism for the growth of micro cracks in resin structure. For that reason, composites are also less susceptible to the effects of stress concentrations which are created by notches and holes, than metals. [3], [13] Fatigue strength comparison of CFRP and 7075-T6 aluminum are provided in Figure 1.6 for tension and compression-tension cases.
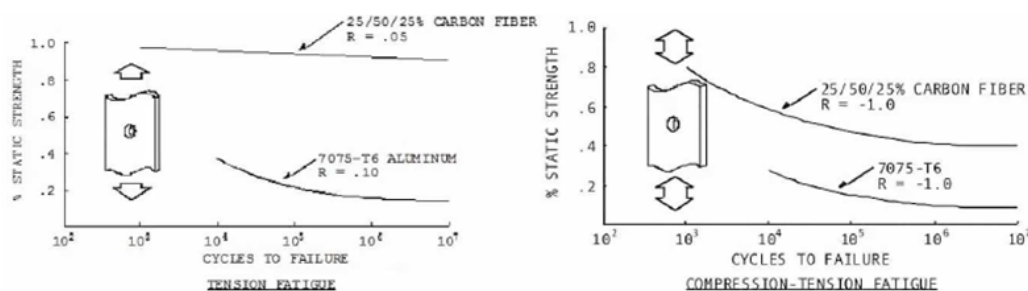
Figure 1.6: Fatigue characteristics of CFRP and 7075-T6 aluminum [4].

Besides providing a higher fatigue strength, polymer matrix composites also offer additional benefits such as vibration damping and an excellent corrosion resistance over metals, as mentioned before. For drivelines of extended length when a critical speed of 7500 RPM or above is required; steel, aluminum and even glass/epoxy would have severe design limitations due to a lack of axial moduli. Even when the cost is a

strong driver, hybrids of glass and carbon epoxy could be utilized to optimize the cost versus performance. Length versus critical speed curve of such hybrid driveshafts of carbon-glass/epoxy would lie between the curves representing carbon/epoxy and glass/epoxy materials, respectively. [14] Fourney and Poesch [15] concludes that vibrations in structures made from graphite composites are damped more rapidly than structures made from metals, evidently from their damping results. Mentioned damping characteristics would also differ between composite materials of various designs, depending on reinforcement type and orientation.

Vibrational strain and time graphics of a graphite composite and 1020 steel are provided in Figure 1.7, which clearly indicates superior vibrational damping characteristics of composites. Enhancement of fatigue life is also an established fact, resulting from the vibrational damping characteristics of composite materials. Due to the damping of vibrations, forces and amplitudes are not transmitted and the result is a definitely lower fatigue loading away from vibrational sources and connecting parts. In contrast to notch sensitivity or crack propagating/stress intensifying characteristics of metals, composite structures act as crack stoppers. In a composite structure, micro cracks in the resin can only propagate very short distances before running into round holes occupied by fibers, which are natural crack stoppers. [15]
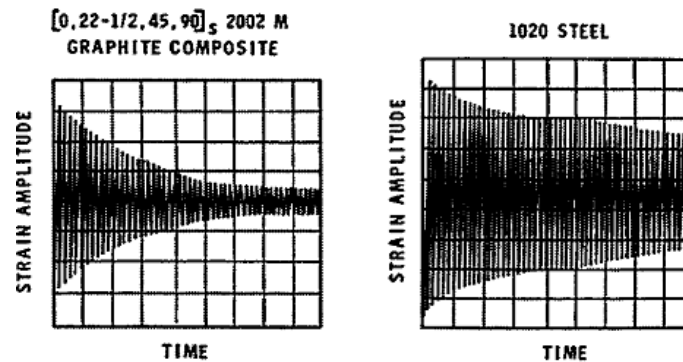
Figure 1.7: Vibration damping of PMCs [15].

Crash behavior is a principal design consideration for a driveshaft and an area which composite driveshafts could offer competitive opportunities. Conventional 2-piece metallic shafts can buckle at the center bearing in any direction depending on the joint position at impact, which is visualized in Figure 1.8; it is impossible to determine the axial force and energy absorbed by them in a frontal crash. [6]
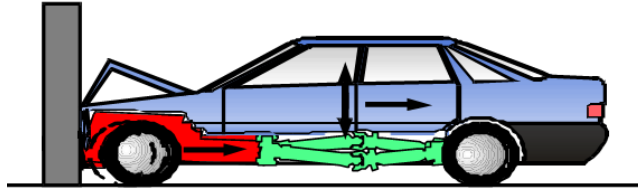
Figure 1.8: Frontal crash behavior of a conventional shaft [6].

Due to their fibrous nature embedded in a polymeric matrix, composites can absorb a fair amount of energy upon impact. Composite driveshafts would break apart rather than entering passenger compartment, catapulting vehicle or whipping a broken end through a tank or valuable cargo during an accident. [2] A failed steel driveshaft may project shrapnel in all directions; however, a composite torque tube would break into smaller fiber fragments, which is seen in Figure 1.9, that constitute it, upon failure. [11]

Figure 1.9: A failed composite driveshaft (Url-2).

A defined axial force-displacement behavior is the target for crash-optimization of a driveshaft, which would ultimately mean a controlled energy absorption characteristic.

Weight saving is a strong driver for any composite design case, which is also valid for composite driveshaft programs. Weight reduction, in particular, secures fuel consumption improvements in considerations for environmental protection. Cost competitiveness is a key issue for all cases regarding composites. Together with all their benefits regarding weight savings and reduction of emission during the operational phase of a vehicle; considering scraping, disposal has become a recent focus of attention regarding the widespread use of composites in automotive industry. [6]

Thermoplastics soften and might be reshaped upon heating, thus they could offer a considerably higher chances for recycling. In contrast, thermoset matrices would burn, yet maintain shape upon heating which limits the amount of options regarding disposal. [2]

High quality carbon or glass fibers might be recovered from scrap thermoset matrix composites by combustion in a fluidized bed. Oxidation of thermoset matrix helps liberating clean filaments of glass/carbon fibers which can then be collected and reused in other products and applications. [6] As a worst case option, a thermoset matrix composite can be burned and ground with the addition of some fuel such as powdered coal etc. which would produce heat that can be utilized in other processes. [2]

Regarding from a perspective of cost, manufacturing a composite driveshaft might be a little bit more complex than their metallic counterparts; however, total installed price of a composite driveshaft can be managed to cost lower than a conventional 2-piece metallic shaft.

As for investigating previous applications of composite driveshafts, a carbon fiber driveshaft helped Dan Gurney's All American Racers (Toyota Celica) win the IMSA GTO championship in 1987. The result was dead smooth driveshaft performance all the way to the engine's limit of 9,000RPM, instead of the metal shaft's limit of 8,000RPM, which contributed heavily to winning the 1987 GTO title. [2]

The Renault Espace Quadra, for which the driveline layout is illustrated in Figure 1.10, launched in 1988, was the pioneering application for composite driveshafts in production vehicles. The floor was in any case sensitive to noise and vibration inputs, which were improved by the absence of a driveshaft center support bearing. [6] The composite driveshaft system weighed 5kg, compared to 10kg for the 2-piece steel alternative. [10]
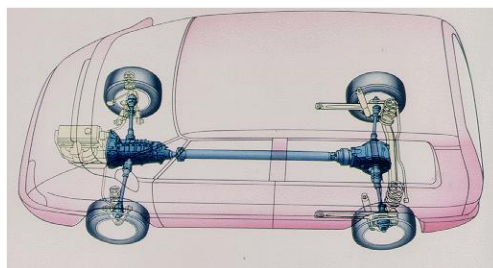
Figure 1.10: Renault Espace Quadra driveline [6].

Composite driveshafts were first introduced for Audi 80/90 Quattro applications in 1989, and production continued through model changes to Audi A4 and A8 Quattro's in 1998, by that time annual volume had reached 30,000 driveshafts per annum. 2-piece composite shafts (front composite/rear steel) were installed in preference to 2-piece steel shafts in order to meet a demanding crash performance requirement.

The Renault Safrane Quadra was introduced in 1992 with a 2-piece shaft (front steel/rear composite) in place of a three-piece steel alternative. The high bending mode frequency of the composite section (>200 Hz) improved the vehicle NVH, and there was an overall weight saving of 40%.

Development of the composite driveshaft for the Toyota Mark II is described in reference. The Renault applications described the use of a bonded connection, whereas an interference connection method was developed for the Toyota Mark II. The ends of the composite tube were reinforced by hoop-wound carbon fiber, with steel end parts inserted by force to overcome a designed interference. There was an improved NVH performance and crash behavior, and a weight saving of 6kg (50%). [6]

In a test started in August of 1994, a 1-piece carbon fiber driveshaft was installed in a garbage truck operating in Texas, which is shown in Figure 1.11. This shaft replaced a 2-piece steel shaft and a center bearing. The resultant weight savings was about 80lbs. The shaft had seen daily use for the last two years in what has been described as one of the most torturous commercial truck applications possible. Absolutely no problems have been recorded. [2]

Figure 1.11: Garbage truck with composite driveshaft [2].

Currently; composite driveshafts used in production vehicles, including the Mitsubishi Montero, the Nissan 350Z and the Mazda RX-8, weigh 40-50% less than comparable 2-piece steel designs. [10]

2. DESIGN OF THE DRIVESHAFT

Basic performance requirements for a driveshaft in automotive applications might be stated as: critical speed, torsional strength, torsional buckling strength and torsional fatigue life. [14]

When designing a driveshaft of metallic material, its cross-section can be determined for a specific design torque and allowable shear stress of the material. Since the external diameter of a shaft is mostly appointed by the space constraints, internal diameter is determined by design torque divided by allowable shear stress. [13] , [16] In essence, design parameters for a metallic driveshaft might be summarized as peak torque, allowable shear stress of the material and empty space under the car cabin.

In contrast with metallic ones, composite driveshafts are involved with more design parameters which are able to be altered. Shaft length and external diameter is still constrained by space but internal diameter, layer thickness, number of layers and their stacking sequence can be varied according to performance requirements. Tailorability of elastic constants by the variation of these parameters open up the way for many design possibilities. [3], [13] [17]

2.1 Design Methodology

In the present case, design studies are initiated with ply properties obtained from the literature. Classical laminate theory (CLT) is utilized in analytical domain to model the torque tube; it is duplicated on numerical domain with finite element analysis (FEA). After an initial glimpse of the situation, ply properties of production material would be determined by coupon manufacture and testing. The shaft is modelled with production material again and shaft characteristics are fully determined. A torsion test rig would then be utilized in order to verify the performance of the production shaft. Modal testing would be carried out to determine the dynamical characteristics. Final step would be the testing of the shaft onboard a production vehicle, in fully operational conditions. Design methodology of present study is visualized in Figure 2.1.
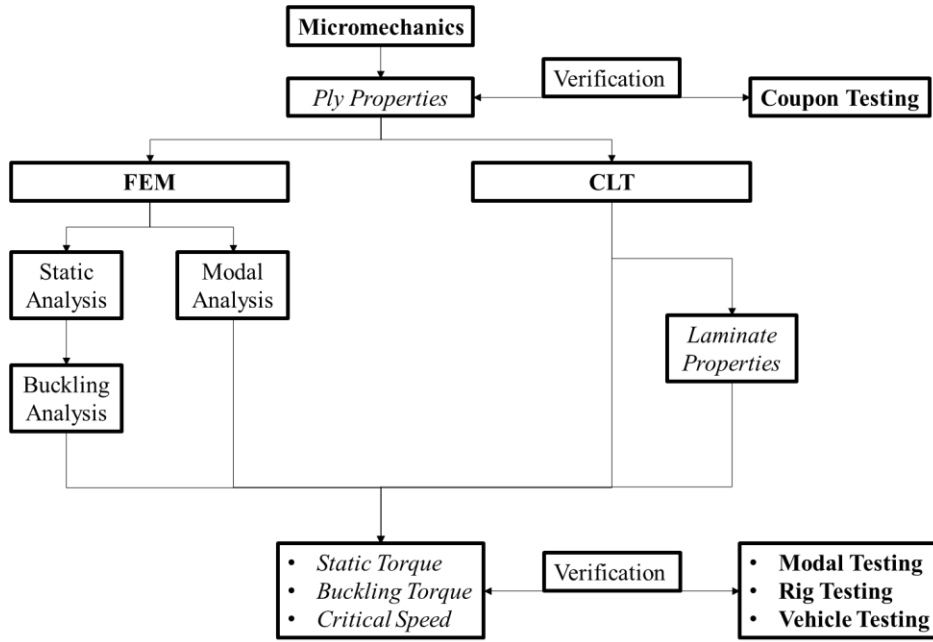
Figure 2.1: Design methodology.

The main design goal is to achieve the minimum weight while adjusting the parameters to meet a sufficient margin of safety; which is translated in a critical speed higher than the operating speed, a critical buckling torque higher than the ultimate transmitted torque and a strength ratio equal to the desired value after applying any of the failure criteria like the Tsai-Wu failure criterion. [13]

Static torque transmission, torsional buckling load factor and natural bending frequency are three basic design constraints that must be considered during the design phase of a driveshaft, as it is mentioned above. The design constraints are given as; the transmission of a 17000 Nm peak torque with a desired Tsai-Wu strength ratio of 2, a fatigue life of 300k cycles for a ±6800Nm fatigue torque, torsional stability (in other words, no torsional buckling) for the peak torque and a natural bending frequency of 130 Hz, respectively.

2.1.1 Parameters and constraints

Design parameters and constraints of the driveshaft is presented in Figure 2.2.

Geometrical constraints based on the distance between the transmission and rear axle together with the empty space under the chassis are provided as 1900mm for tube length and a maximum external diameter of 170mm by Ford Otosan.

A shaft of smaller diameter would have to meet larger shear loadings whereas a shaft of larger diameter would create problems in fitting a predefined area. As an initial approach, shafts of various internal diameters (A, B and later on C models) were investigated beforehand deciding on a final internal diameter of 130mm. As well as the internal diameter, different stacking sequences (Models 1 to 6) had been evaluated by their impact on design requirements.

Parameters	Constraints
Fiber Material - Carbon	l=1900mm, $r_{o_{max}}$ =170mm
Matrix Material - Epoxy	% Weight saving
Number of Plies - CLT / Tsai-Wu SR	Peak Torque - 17000Nm
Thickness of Plies - 0.3mm	Torsional Stability
Stacking Sequence – CLT / Tsai-Wu SR	Bending Frequency - 130Hz
	300k cycles @ 6800Nm
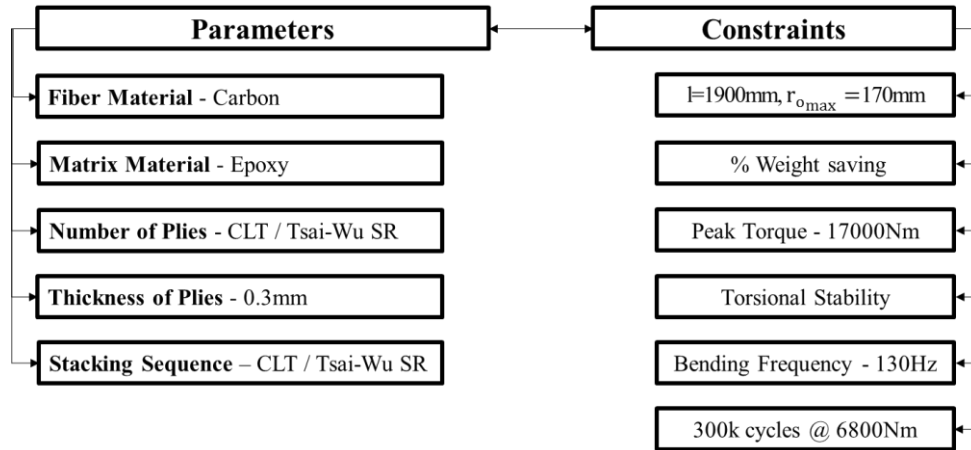
Figure 2.2: Design parameters and constraints.

2.1.1.1 Fiber material

For automotive driveshaft applications, either glass or carbon fibers are utilized as reinforcement in composite materials. Carbon fibers provide higher strength and stiffness beside a lower density than glass fibers; however, the price is considerably higher. Carbon fibers are selected as reinforcement material for the design of the shaft. [16]

2.1.1.2 Matrix material

The resin selected for most of the composite driveshafts are either epoxies or vinyl esters. In our case, epoxy resin is selected due to its high strength, good wetting of fibers, lower curing shrinkage and better dimensional stability. [16]

2.1.1.3 Layup selection

Thickness of a single carbon/epoxy layer produced by filament winding operation with a wet delivery system is specified to be around 0.3mm by various manufacturers.

Remaining design parameters of number of plies together with their stacking sequence might be referred as "layup". It is definitely the most important design parameter, paving the way for a great number of possible designs matching design constraints.

Layup selection for torsional and fatigue strength

Badie et al. [17] investigated the effects of fiber orientation and stacking sequence over torsional and fatigue strength of a torque tube.

The fiber orientation angle of 45° is the best in increasing the torsional stiffness. However, laminates containing fabric fibers placed at ±45° experience sudden failure whatever the material is; on the other hand, the stacking of 90°/0° experiences a progressive and gradual failure.

The stacking sequence has an effect on the fatigue strength. The torsional fatigue strength of ±45° carbon/epoxy specimens are approximately 3.7-3.8 times higher than that of the 0° specimens at an equivalent number of cycles. It is concluded that the layers of ±45° fiber orientation must be kept close to each other and have a location near to inner surface, not to be exposed at outer surface, from a fatigue point of view. Experiments indicated that the cracks are initiating in the zones free of fibers or in the outer skin of resin and increase with increasing number of cycles until the failure of specimen. The worst zone of the driveshaft from a fatigue point of view is the gripping zone of end connections.

Layup selection for torsional buckling

Mahmood et al. [18] observed that the stacking sequence has an important effect on the torsional buckling of a driveshaft. He concluded that; to increase the buckling torque, the modulus at hoop direction must be increased by orienting fibers to approach 90° angle. Changing the fiber orientation angle of one or more layers may not give a proportionality of buckling torque to the increase of angles. Result can be as best at 90°, good at 0° and worst at 40° angles; since the buckling strength is dependent on both axial moduli (E_x) and Hoop moduli (E_h).

Layup selection for critical speed

Badie et. al. [19] investigated the effect of fiber orientation angle on the natural frequency with a torque tube consisting of four layers stacked as [$\pm45_{glass}/0_{carbon}/0_{glass}$]. Various stacking sequences with different orientation angles for the carbon layer are evaluated. It has been clear that, the fibers must be oriented at 0° to increase the natural frequency by increasing the modulus of elasticity along the longitudinal axis of the shaft. The shaft loses 44.5% of its natural frequency when the carbon fibers are oriented in the hoop direction of 90° instead of 0°.

The stacking sequence has no effect on the natural frequency; because the matrix form of the dynamic equilibrium equation of elastic body only contain stiffness and mass matrices, when no damping and external forces applied.

2.2 Initial Design with Generic Material Properties

Design studies are initiated with generic material properties obtained from literature, which are provided in Table 2.1.

Table 2.1: Generic material properties [20].

ρ [kg/m^3]	1600
E_1 [GPa]	181
E_2 [GPa]	10.3
ν_{12}	0.28
G_{12} [GPa]	7.7
$(\sigma_1^T)_{ult}$ [MPa]	1500
$(\sigma_1^C)_{ult}$ [MPa]	1500
$(\sigma_2^T)_{ult}$ [MPa]	40
$(\sigma_2^C)_{ult}$ [MPa]	246
$(\tau_{12})_{ult}$ [MPa]	68

It has been provided that the fiber orientation angle dictates the maximum bending stiffness, in turn leading to the maximum natural frequency in bending. For that purpose, the fibers are arranged longitudinally at the 0° with respect to the shaft axis. On the other hand, the angles of ±45° are used to obtain the maximum shear strength, while 90° is the best for buckling strength. [3]

Based on the facts presented in layup selection sections together with regards to design constraints, 10 different models are appointed to be utilized on prototype driveshafts. "A" models have an internal diameter of 120mm whereas "B" models have 140mm. Number of layers are appointed by the iteration of stacking sequence of initial models A1 and B1 with respect to Tsai-Wu strength ratio. Remaining 10 models were iterated upon the initial model, each with aiming to provide different characteristics regarding design constraints. Shaft models are provided in Table 2.2.

Table 2.2: Initial models.

Model	Stacking Sequences	
	A	B
1	$[(\pm45)_2/45]_s$	$[(\pm45)_2/45]_s$
2	$[(\pm45)_8]_s$	$[(\pm45)_6]_s$
3	$[(\pm30)/30/(\pm45)_6/45]_s$	$[(\pm30)/30/(\pm45)_4/45]_s$
4	$[0_3/(\pm45)_6/45]_s$	$[0_3/(\pm45)_4/45]_s$
5	$[(\pm30)_3/(\pm45)_5]_s$	$[(\pm30)_3/(\pm45)_3]_s$
6	$[0_6/(\pm45)_5]_s$	$[0_6/(\pm45)_3]_s$

2.3 Analytical Model of the Driveshaft

An EXCEL document consisting of several worksheets is tabulated for the realization of analytical model of the driveshaft. Material properties are obtained from the literature at that point. In order to evaluate static torque transmission, CLT is applied and Tsai-Wu Strength Ratio of the torque tube is found. Natural bending frequency and critical buckling torque of the shaft is also calculated in analytical domain with the use of some formulas.

2.3.1 Static torque transmission

Safe transmission of peak torque in a static state is the first and most important design constraint to start with. It must be ensured that the shaft tube will not fail under given peak torque. Since composites are anisotropic and brittle type of materials, traditional approaches for material failure could not hold when designing a composite structure because most of these formulations were developed for isotropic and ductile type of materials. Classical lamination theory would have to be utilized when a "stacked" structure of fiber reinforced composites is being considered under a given design loading. In addition, special criteria must be utilized in order to determine the material would fail under design loading or not.

2.3.1.1 Classical laminate theory

Definition of laminated structures

A lamina is defined as a layer of a composite structure in which the fibers are all oriented in the same direction. A laminate is constructed by stacking a number of such lamina in the direction of the lamina thickness, which is illustrated in Figure 2.3.

The design and analysis of such laminated structures demands knowledge of the stresses and strains in the laminate. Also, design tools; such as failure theories, stiffness models, and optimization algorithms, need the values of these laminate stresses and strains. However, the building blocks of a laminate are single lamina, so understanding the mechanical analysis of a lamina precedes understanding that of a laminate. A lamina is unlike an isotropic homogeneous material. The contributions of a lamina to the properties in any other direction are also subject to calculation. The properties of the structure are then the sums of the contributions of each lamina. [20], [21]
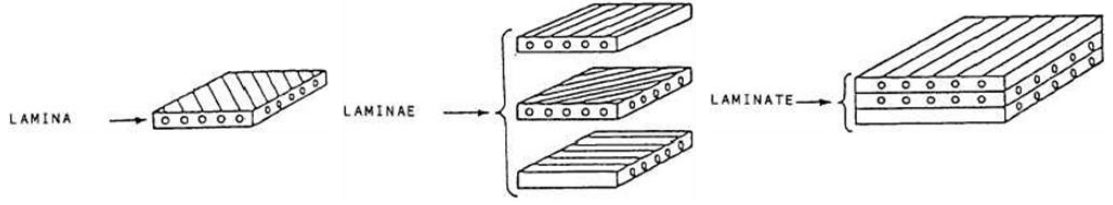
Figure 2.3: Lamina, laminae and laminate (Url-3).

Stress-strain relations in material coordinates

Stress-strain relations of a lamina in a 3-D case is expressed as (2.1).

$$\begin{bmatrix} \sigma_1 \\ \sigma_2 \\ \sigma_3 \\ \tau_{23} \\ \tau_{31} \\ \tau_{12} \end{bmatrix} = \begin{bmatrix} C_{11} & C_{12} & C_{13} & 0 & 0 & 0 \\ C_{12} & C_{22} & C_{23} & 0 & 0 & 0 \\ C_{13} & C_{23} & C_{33} & 0 & 0 & 0 \\ 0 & 0 & 0 & C_{44} & 0 & 0 \\ 0 & 0 & 0 & 0 & C_{55} & 0 \\ 0 & 0 & 0 & 0 & 0 & C_{66} \end{bmatrix} \begin{bmatrix} \varepsilon_1 \\ \varepsilon_2 \\ \varepsilon_3 \\ \gamma_{23} \\ \gamma_{31} \\ \gamma_{12} \end{bmatrix} \tag{2.1}$$

Where σ, τ represent stresses and γ, ε represent strains in material directions. [20], [21]

There is a possibility of reducing a 3-D problem into 2-D problem, if the lamina is very thin and no out-of-plane loads are applied. From the properties of the composite materials at fibers direction, the first step is the construction the reduced stiffness matrix. [6] The stress strain relationship of the unidirectional (UD) 2-D lamina in terms of its material directions are given in (2.2). [22]

$$\begin{bmatrix} \sigma_1 \\ \sigma_2 \\ \tau_{12} \end{bmatrix} = \begin{bmatrix} Q_{11} & Q_{12} & 0 \\ Q_{12} & Q_{22} & 0 \\ 0 & 0 & Q_{66} \end{bmatrix} \begin{bmatrix} \varepsilon_1 \\ \varepsilon_2 \\ \gamma_{12} \end{bmatrix} \tag{2.2}$$

$$Q_{11} = \frac{E_1}{1 - \nu_{21}\nu_{12}} \qquad (2.2a)$$

$$Q_{12} = \frac{\nu_{12}E_2}{1 - \nu_{21}\nu_{12}} \qquad (2.2b)$$

$$Q_{22} = \frac{E_2}{1 - \nu_{21}\nu_{12}} \qquad (2.2c)$$

$$Q_{66} = G_{12} \qquad (2.2d)$$

$$\nu_{21} = \frac{E_2}{E_1}\nu_{12} \qquad (2.2e)$$

E_1 is the modulus of elasticity in longitudinal direction whereas E_2 is the one in transverse direction, G_{12} is in-plane shear modulus, while ν_{12} and ν_{21} are major and minor Poisson's ratios, respectively.

Transformation to global coordinates

After the expression of stress-strain relations in material coordinate system of axes 1 and 2, it could be transformed into global coordinate system of axes x and y, which is visualized in Figure 2.4.
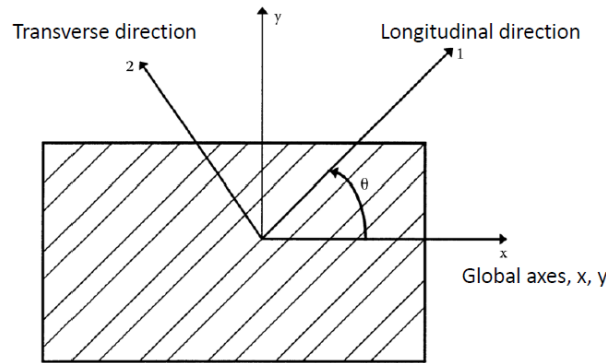
Figure 2.4: Material and global axes of a lamina with angle Ө [20], [21].

Stress-strain relations in global coordinates is expressed as (2.3). [20], [21]

$$\begin{bmatrix} \sigma_x \\ \sigma_y \\ \tau_{xy} \end{bmatrix} = \begin{bmatrix} \bar{Q}_{11} & \bar{Q}_{12} & \bar{Q}_{16} \\ \bar{Q}_{12} & \bar{Q}_{22} & \bar{Q}_{26} \\ \bar{Q}_{16} & \bar{Q}_{26} & \bar{Q}_{66} \end{bmatrix} \begin{bmatrix} \varepsilon_x \\ \varepsilon_y \\ \gamma_{xy} \end{bmatrix} \qquad (2.3)$$

18

$$\bar{Q}_{11} = Q_{11}c^4 + Q_{22}s^4 + 2(Q_{12} + 2Q_{66})s^2c^2 \tag{2.3a}$$

$$\bar{Q}_{12} = (Q_{11} + Q_{22} - 4Q_{66})s^2c^2 + Q_{12}(c^4 + s^4) \tag{2.3b}$$

$$\bar{Q}_{16} = (Q_{11} - Q_{12} - 2Q_{66})c^3s - (Q_{22} - Q_{12} - 2Q_{66})s^3c \tag{2.3c}$$

$$\bar{Q}_{22} = Q_{11}s^4 + Q_{22}c^4 + 2(Q_{12} + 2Q_{66})s^2c^2 \tag{2.3d}$$

$$\bar{Q}_{26} = (Q_{11} - Q_{12} - 2Q_{66})cs^3 - (Q_{22} - Q_{12} - 2Q_{66})c^3s \tag{2.3e}$$

$$\bar{Q}_{66} = (Q_{11} + Q_{22} - 2Q_{12} - 2Q_{66})s^2c^2 + Q_{66}(s^4 + c^4) \tag{2.3f}$$

$$s = \sin\theta, c = \cos\theta \tag{2.3g}$$

Construction of A, B & D matrices

In order to "assemble" the laminated structure consisting of different laminae, [ABD] matrix should be assembled. [ABD] is the stiffness matrix, yielding the general load-displacement relation of a laminated structure, which is presented in expression (2.4). [20], [21]

$$\begin{bmatrix} N_x \\ N_y \\ N_{xy} \\ M_x \\ M_y \\ M_{xy} \end{bmatrix} = \begin{bmatrix} A_{11} & A_{12} & A_{16} & B_{11} & B_{12} & B_{16} \\ A_{12} & A_{22} & A_{26} & B_{12} & B_{22} & B_{26} \\ A_{16} & A_{26} & A_{66} & B_{16} & B_{26} & B_{66} \\ B_{11} & B_{12} & B_{16} & D_{11} & D_{12} & D_{16} \\ B_{12} & B_{22} & B_{26} & D_{12} & D_{22} & D_{26} \\ B_{16} & B_{26} & B_{66} & D_{16} & D_{26} & D_{66} \end{bmatrix} \begin{bmatrix} \varepsilon_x^0 \\ \varepsilon_y^0 \\ \gamma_{xy}^0 \\ \kappa_x \\ \kappa_y \\ \kappa_{xy} \end{bmatrix} \tag{2.4}$$

$$A_{ij} = \sum_{k=1}^{n} [(\bar{Q}_{ij})]_k (h_k - h_{k-1}), i = 1,2,6, j = 1,2,6 \tag{2.4a}$$

$$B_{ij} = \frac{1}{2} \sum_{k=1}^{n} [(\bar{Q}_{ij})]_k (h_k^2 - h_{k-1}^2), i = 1,2,6, j = 1,2,6 \tag{2.4b}$$

$$D_{ij} = \frac{1}{3} \sum_{k=1}^{n} [(\bar{Q}_{ij})]_k (h_k^3 - h_{k-1}^3), i = 1,2,6, j = 1,2,6 \tag{2.4c}$$

[A] is the extensional stiffness matrix relating the resultant in-plane forces to the in-plane strains.

[B] is the coupling stiffness matrix coupling the force and moment terms to the mid-plane strains and mid-plane curvatures. When designing a composite part, symmetrical stacking sequences should be adopted so that the [B] matrix is zero. If [B] matrix is not equal to zero, the part will have a curvature under normal loading. When you stretch a metal part, you have two possible deformations; however, when you stretch a composite part, you could have up to 6 deformations in case of an asymmetrical and unbalanced laminate. If symmetrical sequences are not an option, the part should be designed so that the [B] matrix is kept at minimum.

[D] is the bending stiffness matrix relating the resultant bending moments to the plate curvatures. [4]

Exertion of the load on the laminate

Regarding the loads in load-displacement relations of a laminate; the axial force N_x is zero, the centrifugal force N_y is neglected and N_{xy} is the resultant shear force from torque loading in the case of an automotive driveshaft, visualized in Figure 2.5 and formulated in (2.5). The torque T is the peak torque if the design involves fatigue considerations. [13]

$$N_{xy} = \frac{T}{2\pi r_m{}^2} \qquad (2.5)$$
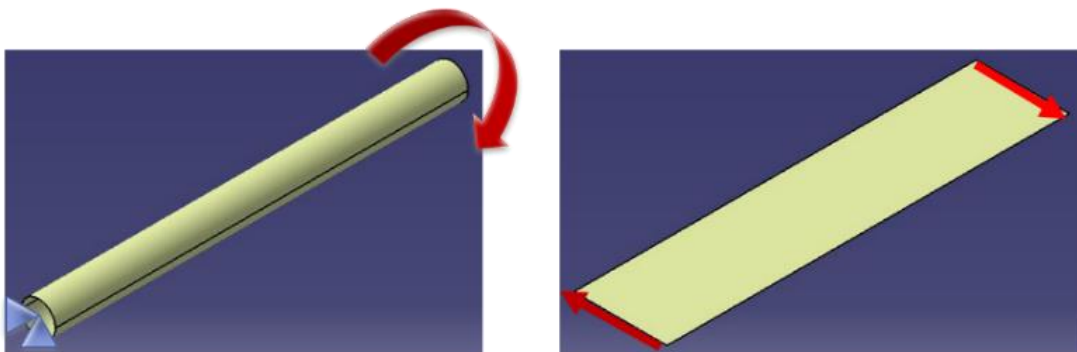
Figure 2.5: Exertion of torque loading in CLT.

20

2.3.1.2 Tsai-Wu failure criterion

Composite materials need special criteria to define failure due to their anisotropic and brittle nature. Literature is growing exponentially in that regard; however, there is no single widely accepted failure criteria yet. Tsai-Wu failure criterion is selected to be implemented in our case because; it is easy to implement in various situations, it distinguishes between the compressive and tensile strength of a lamina and it has been around for many years thus provides high degree of reliability.

A lamina is considered to be failed if the expression (2.6) is violated:

$$H_1\sigma_1 + H_2\sigma_2 + H_6\tau_{12} + H_{11}\sigma_1{}^2 + H_{22}\sigma_2{}^2 + H_{66}\tau_{12}{}^2 + 2H_{12}\sigma_1\sigma_2 < 1 \tag{2.6}$$

$$H_1 = \frac{1}{(\sigma_1{}^T)_{ult}} - \frac{1}{(\sigma_1{}^C)_{ult}} \tag{2.6a}$$

$$H_{11} = \frac{1}{(\sigma_1{}^T)_{ult}(\sigma_1{}^C)_{ult}} \tag{2.6b}$$

$$H_2 = \frac{1}{(\sigma_2{}^T)_{ult}} - \frac{1}{(\sigma_2{}^C)_{ult}} \tag{2.6c}$$

$$H_{22} = \frac{1}{(\sigma_2{}^T)_{ult}(\sigma_2{}^C)_{ult}} \tag{2.6d}$$

$$H_{66} = \frac{1}{(\tau_{12})^2{}_{ult}} \tag{2.6e}$$

$$H_{12} = -\frac{1}{2}\sqrt{\frac{1}{(\sigma_1{}^T)_{ult}(\sigma_1{}^C)_{ult}(\sigma_2{}^T)_{ult}(\sigma_2{}^C)_{ult}}} \tag{2.6f}$$

The components H_1-H_{66} of the failure theory are found using the five strength parameters of a UD lamina.

There are some different options to appoint H_{12}; Mises-Hencky approach is adopted here because it accounts the material properties of both directions (longitudinal-1, transverse-2) for tension and compression together. [20], [21]

Analysis steps with CLT might be compiled as following:

1) The reduced stiffness matrices [Q], using its four elastic moduli, E_1, E_2, v_{12}, and G_{12}, are calculated for each ply.

2) The transformed reduced stiffness matrices $[\bar{Q}]$ are calculated for each ply using the [Q] matrix obtained in step 1 and the angle of the ply.

3) The coordinates of the top and bottom surfaces, h_i, $i = 1...n$, are calculated, given the thickness, t_k, of each ply.

4) Three stiffness matrices [A], [B], and [D] are calculated using the $[\bar{Q}]$ matrices from step 2 and the location of each ply from step 3. Load-displacement relations of the lamina are constructed.

5) The applied forces and moments are substituted in load-displacement relations after the stiffness matrix values found in step 4.

6) The six simultaneous equations are solved to obtain the mid-plane strains and curvatures.

7) The global strains in each ply are found for their calculated location data.

8) To obtain the global stresses, the stress–strain relations are utilized.

9) Local stresses/strains are transformed from global stresses/strains.

10) The selected failure criterion is applied to each individual laminae using local stresses/strains found. [20], [21]

2.3.2 Bucking torque

An introduction to stress stiffness and buckling concepts, as given by Cook et al. [23], buckling means loss of the stability of an equilibrium configuration; without fracture or separation of the material or at least prior to it. It occurs when a member or structure converts membrane strain energy into bending strain energy with no change in externally applied load. Expression to find the critical buckling torque is given in (**2.7**).

$$T_{cr} = (2\pi r^2 t)(0.272)[E_x E_h^3]^{0.25}(t/r)^{1.5} \qquad\qquad \textbf{(2.7)}$$

Where t is the overall thickness, r is the mean radius and E_x and E_h are the average moduli in the axial and hoop directions, respectively. It is recommended that the critical buckling torque, T_{cr} be multiplied by 0.67 for use in an actual design.

The [A] matrix might be used to calculate and, which are the average moduli in the axial (2.8) and hoop (2.9) directions. [16]

$$E_x = \frac{1}{t}\left[A_{11} - \frac{A_{12}^2}{A_{22}}\right] \tag{2.8}$$

$$E_h = \frac{1}{t}\left[A_{22} - \frac{A_{12}^2}{A_{11}}\right] \tag{2.9}$$

2.3.3 Critical speed

Driveshaft can be idealized as a simply supported beam. The bending natural frequency of a composite tube is formulated in (2.10).

$$f_n = \frac{\pi}{2}\sqrt{\frac{E_x I}{mL^4}} \tag{2.10}$$

where m is the mass per unit length, L is the length and I is the moment of inertia of the torque tube. The lateral natural frequency directly related to the lateral stiffness $(E_x I)$ of the driveshaft and since I is only determined by the geometry (2.11), then the composite driveshaft can be designed to have higher lateral natural frequency by increasing the modulus, E_x. [17]

$$I_x = \frac{\pi}{4}(r_o^4 - r_i^4) \approx \pi r^3 t \tag{2.11}$$

where r is the mean radius and t is the wall thickness. To increase the natural frequency, carbon fibers are required to be oriented along the axial direction, as mentioned before.

As shown in equation (2.10), the lateral critical speed of a driveshaft is a function of its geometry and specific modulus, thus nearly constant for all metals currently used in driveshafts. As a result, for any given tube of fixed dimensions, the composite driveshaft can be designed to operate at higher speeds than comparable metal driveshafts. [12]

2.4 Numerical Model of the Shaft

Analysis of the composite driveshaft tube is carried out numerically by using FEA. It is a powerful numerical tool, which enables to discretize complex structures and obtain numerical results where no analytical solution is possible. Numerical model is developed using ANSYS® Composite PrepPost (ACP) in Workbench environment and ANSYS Parametric Design Language (APDL) in Mechanical.

Models in ACP and Mechanical APDL, which are given in Figure 2.6, both employ the same geometry whereas element structures are a little bit different. Shaft is fixed in one end and the torque is imposed on the central node placed on the other end. In Mechanical APDL, central node is a MASS21 element connected to circumference with "Dist F/M at Mstr" option. In Workbench environment, that is succeeded with a TARGET170 element in the center and CONTACT175 elements in circumference. Structure is meshed with SHELL181 elements of 10 mm edge sizing, 1650 in total.
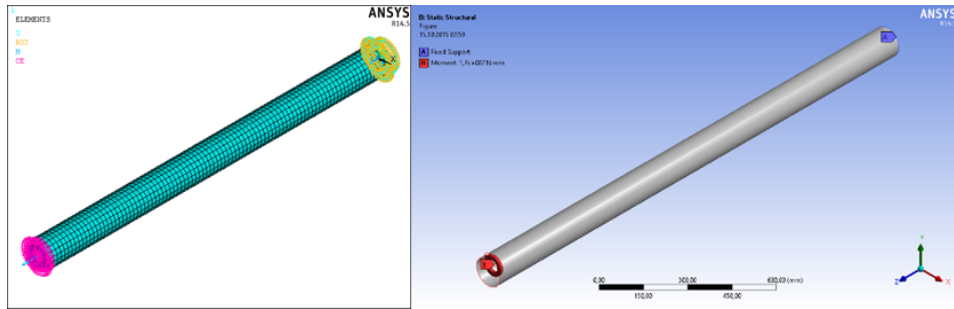
Figure 2.6: FEA models of the driveshaft.

SHELL181 is suitable for analyzing thin to moderately-thick shell structures, which is shown in Figure 2.7. It is a four-node element with six degrees of freedom at each node: translations in the x, y, and z directions, and rotations about the x, y, and z axes. The degenerate triangular option should only be used as filler elements in mesh generation. [24]
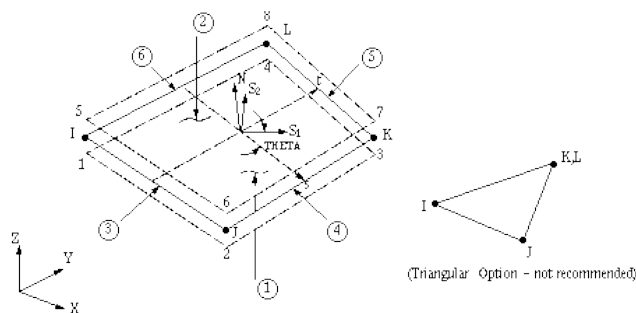
Figure 2.7: SHELL181 element (**Url-4**).

24

Driveshaft has a geometry of thin cylinder, which makes it susceptible to torsional buckling under shear loading. Buckling analysis is carried out in order to ensure torsional stability. Boundary conditions are the same with static analysis, since the software requires a static structural analysis to be performed beforehand and investigates the buckling possibility of that given case.

Resonance is a dangerous phenomenon for dynamic components and needs to be avoided. Modal analysis is carried out to investigate natural frequencies and mode shapes of the driveshaft. Shaft is analyzed in a free-free condition; in other words, no constraints are imposed. Meshing is the same as previous models.

In modal analysis, the model of the driveshaft does not need a fine meshing because the stress output is not required. Also there is no need to apply a load because the natural frequency is only function of mass and stiffness. It is apparent that, the contact area between the shaft tube and the yoke joint in addition to the type of joining were not considered in the calculations of the natural frequency. [17]

Results obtained from analytical model of the shaft with literature material is presented in Table 2.3.

Table 2.3: Analytical and numerical models.

Model	Tsai-Wu Strength Ratio		1st Bending Frequency [Hz]		Buckling Torque [Nm]	
	Analytical	Numerical	Analytical	Numerical	Analytical	Numerical
A1	0.79	0.84	72.05	173.66	4986	5301
A2	2.55	2.32	76.25	174.19	94122	85632
A3	2.59	2.38	89.20	202.45	105125	96601
A4	2.23	2.05	114.28	256.02	143746	132143
A5	2.34	2.22	100.45	227.09	108483	102920
A6	1.74	1.64	142.47	315.16	158830	149702
B1	1.07	1.01	83.75	190.95	5376	5074
B2	2.46	2.31	86.47	197.03	48865	45885
B3	2.50	2.37	105.38	238.00	55479	52594
B4	2.05	1.94	141.05	312.97	78547	74332
B5	2.20	2.14	121.12	272.30	55605	54088
B6	1.42	1.38	179.70	390.21	81452	79157

3. MANUFACTURING OF THE DRIVESHAFT

3.1 Composite Materials and Production Methods

3.1.1 Characteristics of composite materials

A composite is a structural material that consists of two or more constituents that are combined at a macroscopic level and are not soluble in each other. One constituent is called the reinforcing phase and the one in which it is embedded is called the matrix. The reinforcing phase material might be in the form of fibers, particles, or flakes. Matrix and reinforcement together create a product that has properties not achievable by the constituent materials alone. [4]

In composite structures, including driveshaft tubing, the mechanical properties are determined mainly by the mechanical properties of the fibers and the orientation of the fibers within the structure. The resin acts mainly as a binder, retains the fibers in the shape into which the composite materials were formed, and transfers stresses and strains from fiber to fiber. [2] Some advantages of using composites over metals might be summarized as; higher specific strength and modulus, higher fatigue strength and damage tolerance, anisotropic nature providing tailorability, production of both material and structure/component in a single operation, corrosion resistance and durability, damping, dimensional stability and lower CTE etc.

Composite materials offer some design benefits due to the characteristics mentioned; however, combining two or more materials together to make a composite is more work than just using traditional monolithic metals such as steel and aluminum. They are conducive to larger, more integrated designs which opens new design possibilities. Reduced corrosion and fatigue means less maintenance work and cost thus proven in-service durability. Recently, composite materials have been a trending topic so they have more potential for future development.

In addition to these, they provide some additional convenience for production. Composite structures usually consist of fewer parts, so quicker assemblies are possible which means efficient production through reduced flow times.

Composite materials are some sort of "engineering approach" for producing high performance materials. As for all engineering approaches, it is a trade-off between many parameters, so they come in with some inherent downsides.

- Fabrication of composites are usually higher in cost due to more expensive raw material and production equipment.
- Mechanical modelling of a composite structure is more complex than traditional approaches.
- Composites can be time consuming to repair and often require specialized equipment to ensure full strength repair.
- Composites don not have a combination of high strength and fracture toughness, unlike metallic materials.

Last but not least, it is important to keep in mind that composites do not necessarily give higher performance in all the properties; namely strength, toughness, formability, joinability, corrosion resistance, and affordability, used for material selection. [4]

3.1.2 Design of a composite structure

Design of a composite structure is multi-disciplinary. An integrated composite product is involved with many domains; ranging from mechanics, materials etc. to manufacturing and inspection, which is illustrated in Figure 3.1. [4]

Figure 3.1: Domains of composite design [4].

The design process for any composite involves both laminate design and component design and must also include considerations of manufacturing process and eventual environmental exposure. Designing a composite part involves designing of its materials and manufacturing methods. However, you cannot design composite parts in the same way you design metallic parts; you need to take advantage of properties and anisotropic nature of the material. Considerable savings in cost and weight can be achieved with a "proper" composite design. [25] Some advices in that regard might be given as:

- Fabrication requirements should have to be considered in all stages of composite design. No matter how technically brilliant a design is, it bears no meaning if the production could not be realized.

- "Net" parts should be designed so that machining is reduced to a minimum, if any is required. Whenever possible, co-curing of adhesively bonded assemblies should be considered. Incorporation of composite to metal joints are also a possibility.

- Simplicity should be the primary concern from design to manufacture of a composite structure. Ease of manufacturing should always be preferred over ease of analysis in the case of composites.

- Design of entire composite structures should be aimed rather than mere substitutions for metallic parts.

When weight, strength and stiffness are critical design factors, carbon epoxy outperforms steel and aluminum. Material properties can be conformed with loading requirements to meet design allowables while reducing overall weight. Properties of a composite material can be tailored by combining different percentages of $0°$, $\pm45°$ and $90°$ and plies of other angles. [4] Some design recommendations which involve taking advantage of the orthotropic nature of the fiber composite ply:

- Aligning fibers to carry in-plane tensile or compressive loads is a common design practice. For combined normal and in-plane shear loading, multiple ply angles should be provided for combined load capability. Interspersing of these angles, for example $[90_2/\pm45_2/0_2]_{4s}$ instead of a $[90_8/\pm45_8/0_8]_s$. Concentrating plies at nearly the same angle ($0°$ and $90°$ in the previous example) provides the opportunity for large matrix cracks to form. Same case would result with finer cracks in finer cracks for interspersed laminates rather than delaminations

which is generally a more dangerous phenomenon. These comments are valid for most composite applications regardless of the fabrication method.

- Extreme angle changes from ply to ply should be avoided. It is recommended to step from 15° to 45° to 60° to 85° rather than directly from 15° to 85°.

- If a design requires all 0° plies, some 90° plies (and perhaps some off-angle plies) should be interspersed in the laminate to provide some biaxial strength and stability and to accommodate unplanned loads. This improves handling characteristics and serves to prevent large matrix cracks from forming.

- Properties of the laminate and those of the adjoining structures should be matched, failing to do so could result in considerable shear loading in joining of metals and composites. CTE should also be considered in that regard; temperature changes can produce large interlaminar stresses if CTE of the laminate differs greatly from that of adjoining structure.

- Bonded layers should not have fibers perpendicular to the direction of loading. Composite should not be thickened in the joint area. The essential stiffness (EI, where E is modulus of elasticity and I is moment of inertia) of all elements of the joint should be in conjunction.

- Multiple ply angles should be utilized. They are usually oriented in at least two different angles, and possibly three or four ($\pm\theta°$, $0°/\pm\theta°$, or $0/\pm\theta°/90°$ covers most applications, with θ between 30° and 60°). Except the case when the load path is absolutely known, UD plies are rarely used. [26]

Cost is a strong driver in designing of any engineering system, so for composites. Composite materials are "front end loaded" which means that designing and fabricating of a composite material is costlier than conventional approaches in general. In order to be competitive, these front end costs should be either recovered or justified. In that case, a composite might be designed to provide reduced maintenance and lower costs to install. Additional benefits might be provided due to longer life, lower weight, higher performance and aesthetics etc. When looking at the life cycle cost of a composite product, it can be designed to be less expensive than one made of metals. [27] A comparative figure between composite and metal materials in a cost perspective is provided in Figure 3.2.
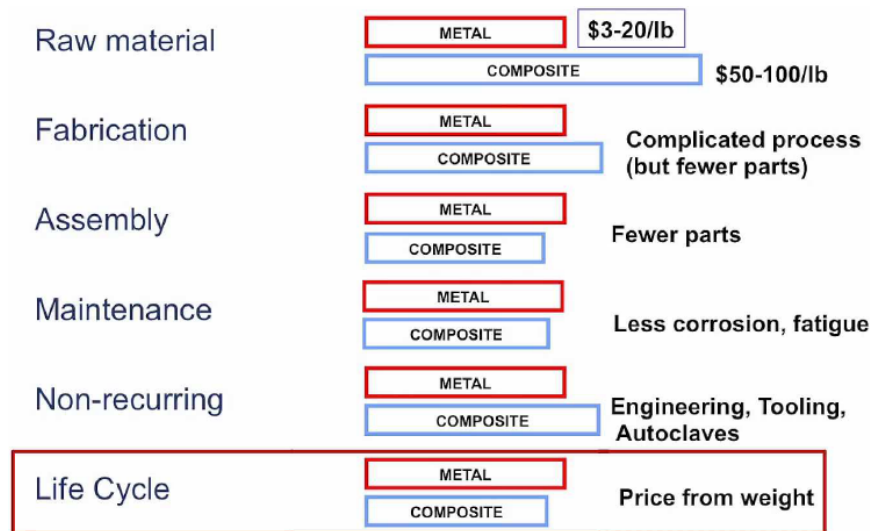
Figure 3.2: Cost comparison of metals and composites [4].

Provided that they have advantages through proper design, composites have only a narrow niche where they are cost-efficient. Composite materials still cannot compete in markets where there are good enough traditional solutions unless the cost is significantly lower. Thus to significantly broaden the composite market, costs must be reduced further.

Assumptions made during preliminary design may not be viable and should have to be reviewed often during the transition to full scale production. Manufacturing processes, especially scale-ups, joints, thickness changes, thermal stresses from adjacent metal parts, damage tolerance and provisions for repair are danger areas of composites that can create major deviations from assumptions on cost and weight. [4]

3.1.3 Production methods for a composite driveshaft

Kliger et al. [28] presented a review of composite shaft concepts in 1980 in which they examined the potential of alternative manufacture processes to yield a cost effective product. The potential processes considered were pultrusion, tape-wrapping, tube-rolling (or table-rolling) and filament winding. To these might now be added pullwinding and braiding or overbraiding, together with variations to suit thermoplastic matrices or introduction of the matrix by a resin injection process. The process identified to have greatest commercial potential was filament winding.

The process of filament winding can offer a number of significant advantages, chief amongst these being the ability to economically produce composite products if the production volume and level of automation is very high and the part is well designed.

Compared to many other composite manufacturing processes, filament winding often uses low cost facilities and tools and can reach production rates that are up to ten times that of its cousin, tape laying. For many applications, the reliance on the tension developed during the winding process to compact the fibers can remove the need for an autoclave cure, which often involves significant capital expense and restricts the size of structures produced. Tooling costs can be lower than for other processes and the ability to have multiple numbers of spindles (10 and 20-spindle machines are relatively common whilst 30-spindle machines are increasing in number) allows the production of multiple parts at the same time. [29]

This process scores highly because it allows accurate control of fiber orientations in the desired angle range, has flexibility to change product diameter or fiber orientation, is easy to automate and takes input materials in the lowest cost form. [28]

Disadvantages of filament-winding include the need for mandrel, which can be complex or expensive for some situations. Component shape should also be able to allow removal of the mandrel. Due to the mechanics of the operation, winding in reverse curvatures has always been a problem for filament winding operations. Change of the fiber orientation within a layer is not an easy task during the operation, which may require additional equipment such as winding pins or saw-tooth etc. External surfaces mostly have a poor surface finish in filament wound parts due to a lack of outer-mold.

Peters and McLarty [26] have explained the fundamentals of filament winding method; advantages/disadvantages, mandrels, filament winding machines, winding patterns, resin types, process parameters etc. Relevant parts of this paper will be given here on.

Filament winding is a process for fabricating a composite structure in which continuous reinforcements (filament, wire, yarn, tape, or other), either previously impregnated with a matrix material or impregnated during winding, are placed over a rotating form or mandrel in a prescribed way to meet certain stress conditions, which is visualized in Figure 3.3. When the required number of layers is applied, the wound form is cured and the mandrel can be removed or left as part of the structure.
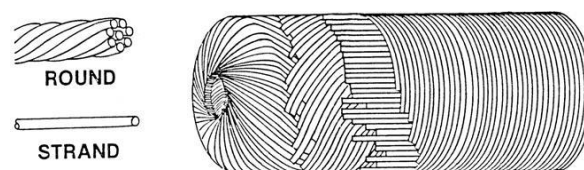
Figure 3.3: Raw materials and product of filament winding (**Url-5**).

High-speed, precise lay-down of continuous reinforcement in prescribed patterns is the basis of filament-winding. Correct use of fiber tension during winding is the only way to achieve straight fibers in a filament-wound structure, which is shown in Figure 3.4.
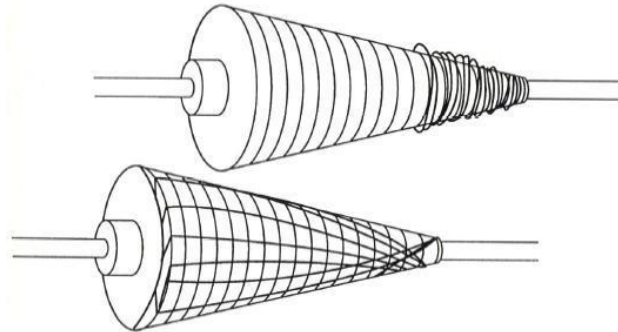
Figure 3.4: Effects of fiber tension on winding (**Url-5**).

One of the big advantages of filament-winding over other composite manufacturing methods is the simplicity of tooling. The mandrel, which provides the part with accurate internal geometry, is generally the only major tool. Equipment and facilities required are usually simple and often consist of just a winding machine and curing oven.

The mandrel can be cylindrical, spherical, or any other shape as long as it does not have re-entrant (concave) curvature. Large or thick-walled structures, particularly structures of revolution such as cylinders or pressure vessels, are most easily wound. Typical geometry which can be produced by filament winding is illustrated in Figure 3.5.
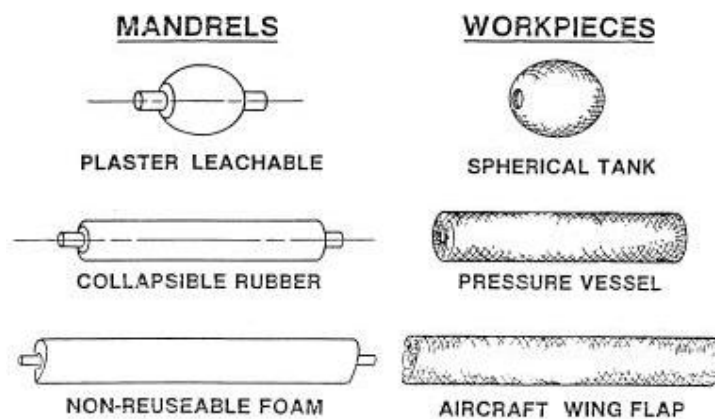
Figure 3.5: Typical mandrels and workpieces [26] .

Mandrel design can be as simple or as complex as the part requires. The factors that must be considered are production reusability, tolerances required, thermal expansion control, weight (equipment limitations), deflections (sagging), part removal from mandrel, and cost.

Low-cost mandrel materials such as cardboard or wood can often be used when winding routine parts. At the other end of the use spectrum, where critical parts require close tolerances, expensive steel mandrels designed for long-term use might be required. For high-temperature cure (315°C, or 600°F), graphite mandrels with low thermal expansion are advantageous. Gas-containment pressure vessels often require metal or plastic liners because composites are porous at high pressures; metal liners can also serve as mandrels.

The filament-winding machine, some examples of 2 and multiple axes are provided in Figure 3.6, traverses the wind eye at speeds that are synchronized with the mandrel rotation, controlling the winding angle of the reinforcement and the fiber lay-down rate. The deposition can be controlled either by computer numeric control (CNC) machines or by simple mechanically controlled winders. Usually, the mechanical machines are limited to three axes or less, whereas the CNC machines can accommodate up to seven axes.
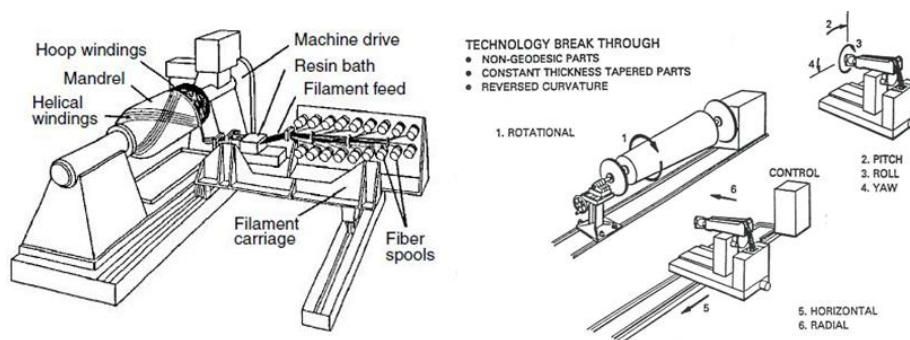
Figure 3.6: Filament winding machines [26] .

The reinforcement can be wrapped in adjacent bands or in repeating bands that are stepped the width of the band to eventually cover the mandrel surface. The fiber path cannot be changed easily, but it can be done by use of pins, saw-tooth, or slip of the tow. Fiber placement is the only fabrication method capable of "steering" the fiber.

The three basic filament-winding patterns are helical, polar (or planar) and hoop, shown in Figure 3.7.
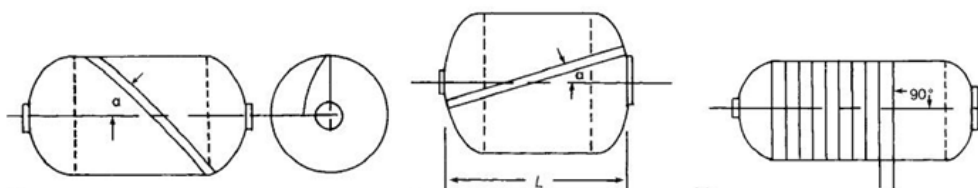
Figure 3.7: Winding patterns [26] .

34

In helical winding, the mandrel rotates more or less continuously while the fiber feed carriage traverses back and forth at a speed regulated to generate the desired helical angle. Winding of angle plies, if done with a helical program that does not completely cover the mandrel surface with each pass, results in a two-ply layer in which the two angles are interspersed. One of the major differences between filament-wound composite laminates and those manufactured by other methods is the presence of crossovers, which can be seen in Figure 3.8.
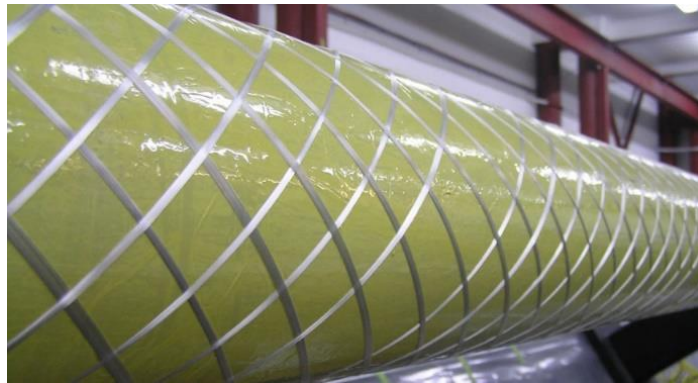
Figure 3.8: Crossovers of helical winding (**Url-6**).

In polar winding**,** the fiber passes tangentially to the polar opening at one end of the chamber, reverses direction, and passes tangentially to the opposite side of the polar opening at the other end.

Hoop patterns are also known as girth, 90°, or circumferential winding. Each full rotation of the mandrel advances the band delivery one full band width. The winding machine is much like a lathe in that the spindle speed is much more rapid than the carriage travel.

Thermoset resins, generally used as binders for reinforcements, can be applied to the dry roving at the time of winding, which is known as wet winding. They may also be applied prior to winding as a tow or tape pre-preg and used promptly or refrigerated.

Pre-impregnated rovings offer excellent quality control and reproducibility in resin content, uniformity, and band width control.

The commonly quoted disadvantages of pre-preg tow are:

- Requirement, generally, for refrigerated storage and control of out-time
- Higher cost
- No room-temperature cures are possible.

The lowest-cost materials for composite processing are those that are brought together at the process by the composite manufacturer. Thus, if the design requirements allow wet filament-winding, it will always be less expensive than winding with pre-preg, but the manufacturer must make some choices in terms of safety, cleanliness, and so on, before production.

The resin content is affected by several parameters (most of which are interrelated): resin viscosity, the doctor blade setting, the interface pressure at the mandrel surface, winding tension, the number of layers, and the mandrel diameter.

Often, the advantage of one delivery system over another is either lower cost or better resin content control. A major drawback of wet winding is that it is usually limited to horizontal winding operations.

It can also be seen that the typical fiber volumes are similar to those for composites made by other methods, and that the fiber volume for helical and hoop fibers can be different.

Void content for most wet-wound composites, unless special precautions are taken, are in the range of 3 to 6%. This has been of little concern to pressure vessel manufacturers who seek a composite that only experiences tension in the fibers at minimum weight, but it is of concern if the structure is to experience compression, bending, or shear.

Usually the cure of the filament-wound composite is conducted at elevated temperatures without vacuum bagging or autoclave compaction. Mandrel removal, trimming, and other finishing operations complete the process.

The technique can vary winding tension, reinforcement material, wind angle, or resin content, if wet wound, in each layer until the desired thickness and resin content of composite is achieved with the required orientation. Multiple composite components can be fabricated simultaneously in the same equipment, with accurate fiber angles and good resin control. For small items, such as golf shafts, it is possible to wind up to 20 components simultaneously.

Many new manufacturers have emerged, primarily in the commercial and sporting goods sectors, and the emphasis has shifted from filament-winding of rocket motors to that of golf shafts, driveshafts, or drill risers. [26]

3.2 Coupon Manufacture and Testing

Manufacturing of composite materials is a complex issue and material properties depend on many parameters. The properties of actual material may differ from catalogue values found in the literature. To address that issue, test plate production is carried out in accordance with ISO 1268. [30] Specimens are cut from test plates and mechanical properties are determined by testing per regarding ASTM standards.

At that point, question may arise as what properties to expect from our production material. Micromechanical analysis provides a viable reference point according to our fiber and matrix properties, which are provided in Table 3.1.

Table 3.1: Mechanical properties of fiber and resin.

	Fiber	Matrix
ρ [kg/m^3]	1800	1200
E_1 [GPa]	230	3.4
E_2 [GPa]	22	3.4
ν_L	0.30	0.3
ν_T	0.35	0.3
G_{12} [GPa]	22	1.3
$(\sigma_1^T)_{ult}$ [MPa]	2067	72
$(\sigma_1^C)_{ult}$ [MPa]	1999	102
$(\sigma_2^T)_{ult}$ [MPa]	77	72
$(\sigma_2^C)_{ult}$ [MPa]	42	102
$(\tau_{12})_{ult}$ [MPa]	36	34

Micromechanical analysis was carried out by tabulating relevant formulations in EXCEL, presented in Figure 3.9.

Figure 3.9: Micromechanical analysis.

The material properties obtained for different fiber volume ratios are given in Table 3.2. Values provided here are an average from the results of three different approaches; namely, strength of materials, elasticity and Halphin-Tsai.

Table 3.2: Mechanical properties for different fiber volume ratios.

	$V_f = 30\%$	$V_f = 50\%$	$V_f = 70\%$
ρ [kg/m^3]	1380	1500	1620
E_1 [GPa]	71.380	116.700	162.020
E_2 [GPa]	5.409	7.561	11.298
ν_{12}	0.316	0.326	0.336
G_{12} [GPa]	2.112	3.097	5.497
$(\sigma_1^T)_{ult}$ [MPa]	641.489	1048.778	1456.067
$(\sigma_1^C)_{ult}$ [MPa]	69.200	70.000	70.800
$(\sigma_2^T)_{ult}$ [MPa]	107.279	93.594	75.988
$(\sigma_2^C)_{ult}$ [MPa]	154.956	147.640	136.818
$(\tau_{12})_{ult}$ [MPa]	22.992	20.095	16.015

The possible maximum fiber volume ratio is around 70% for carbon fiber reinforced composites produced by filament winding method. [31] On the other hand, it is mostly an ideal figure and very hard to achieve in practical conditions. Furthermore, higher fiber volume ratios would cause the increase of the density and cost. Considering all these factors, a fiber volume ratio of 50% is accepted as an ideal value in the present study.

3.2.1 ISO 1268 Standard

Test plates are manufactured using the filament winding method per ISO 1268 standard. Relevant parts of the standard being utilized for the production of test plates are explained here.

3.2.1.1 Part 1: General conditions

- The various parts of ISO 1268 describe methods used to prepare reinforced-plastics plates from which test specimens can be cut.
- Since the mechanical properties of a reinforced plastic are known to be dependent on the process by which the plastic is produced, it is recommended that the test plates be prepared, if possible, by the same method that will be used to produce the plastic.
- The length, width and thickness of the plates produced will depend on the material being processed and the method used to produce them. The plate dimensions will also depend on the test, which will be conducted on the test

specimens cut from the plates. For example, a square plate of side at least 250mm is required to perform tensile tests in two perpendicular directions.

- Unless otherwise specified, the apparatus used to produce the plates shall be capable of maintaining the required temperatures and pressures to within the accuracy prescribed for the chosen plate production method.

- The laboratory/workshop shall be equipped with monitoring equipment, which will enable the production temperature and pressure to be recorded as a function of time.

- The plates obtained shall be inspected prior to cutting out test specimens. The criteria for acceptance or rejection of a plate shall be as defined in the materials specifications and in the plate production method, or as agreed between the interested parties.

- The fiber content shall be determined in accordance with ISO 1172 for glass-reinforced plastics and by a method agreed on between the interested parties for carbon-reinforced plastics.

- The degree of porosity, or void content, is a measure of the frequency of occurrence of open or closed cavities in the plate. Any of several methods might be used to determine it: visual examination, examination of a polished cross-section using a microscope (see ISO 7822), ultrasonic examination or X-ray examination.

- The density might be determined in accordance with the appropriate part of ISO 1183.

- The thickness of the plates shall be measured and, where necessary, the other dimensions.

- Each plate shall be marked to allow the identification of:
  - The mold or the mold cavity used
  - The side of the plate
  - The lay-up sequence, if required
  - The orientation of the plate with respect to the melt flow direction, or to any other direction specific to the material or the method of production

- In addition, plates shall have markings enabling the plate preparation report to be easily traced.

3.2.1.2 Part 5: Filament winding

- This part of ISO 1268 specifies a method of preparing reinforced-plastic test plates by the filament winding process, using textile glass rovings and thermoset resins (pre-impregnated fibers are excluded). To aid understanding of the method, the word "roving" is used throughout the text and is taken to include yarns, unless specifically mentioned to the contrary. A roving (or a number of rovings together) impregnated with resin is wound, in several successive layers, onto a former.

- It specifies the preparation, under optimum industrial conditions, of UD reinforced plates, from which test specimens for various static mechanical tests can be cut.

- This part of ISO 1268 has been established for glass-reinforced plastics made of polyester or epoxy resin, but it can be extended to other types of resin and reinforcement.

- It is intended to be read in conjunction with ISO 1268 Part 1.

- The required final thickness of the plates is obtained by strapping outer–mold pieces onto the former. Polymerization can be carried out either in a press with heated platens or in an oven.

- This method leads to the preparation of two similar plates simultaneously.

- This method applies to all rovings having a linear density between 200tex and 4800tex. For lower linear densities, use several rovings in combination to reach a linear density between 200tex and 4800tex (for example, 10 yarns of 22tex to obtain 220tex).

- It is recommended that the resin system used (polyester or epoxy resin + catalyst or hardener system) has the following characteristics:
    - Viscosity: Less than $0.4Pa \cdot s$ at the winding temperature.
    - Minimum pot life: The minimum pot life of the resin system at the operating temperature should be such that the increase in viscosity of the resin at the end of the winding operation is less than 40% of the initial value.

- If a resin system that does not have the above characteristics is chosen, the viscosity and minimum pot life of the resin system used shall be stated in the test plate preparation report.

- The minimum dimensions of the plates produced are 300mm in length and 220mm in width.

- The glass content shall be specified by the person requesting the plate. The glass content of this type of laminate is typically 70% by mass. A glass content of 70% by mass corresponds to 52% by volume.

- The reel shall be fitted with a tension-regulating system permitting adjustment of the roving tension between 0N and 15N (tension measured before the roving enters the impregnating bath).

- The winding machine shall have the following characteristics:
  - Speed of Spindle: Continuously variable from 0 to 70RPM
  - Pitch: Adjustable from 0.5mm to 5mm (the pitch is equal to the travel of the thread guide when the former makes a complete revolution)
  - When necessary, a radiant panel permitting winding of the roving on to the former at a nearly constant temperature.

- The temperature of the resin system in the bath shall be monitored to maintain its viscosity as nearly constant as possible in order to ensure uniform and complete impregnation of the roving.

- It is therefore recommended that the impregnating bath should have a double wall permitting the circulation of a temperature-regulating liquid and that the dimensions of the bath allow an impregnation length of at least and provide a resin capacity of about 1 litre.

- The type of bath shown in Figure 3.10 is given as an example. It is recommended that the bath have the following characteristics:
  - An eye-type thread guide at the entrance to prevent abrasion (made of e.g. polytetrafluoroethylene or chromium plated metal)
  - A thread guide at the exit, ensuring complete impregnation without drying
  - Devices for retaining resin foam
  - Guide rods under the resin surface (alternating sets of flat and grooved)

Key

1. Exit guide
2. Foam-retaining devices
3. Entrance guide (eye-type)
4. Roving
5. Impregnating bath with double wall
6. Grooved guide rod
7. Flat guide rod
8. Radiant panel
9. Former
10. Impregnating bath
11. Movable arm
12. Winding machine
13. Tension-regulating system
14. Roving bobbin or package
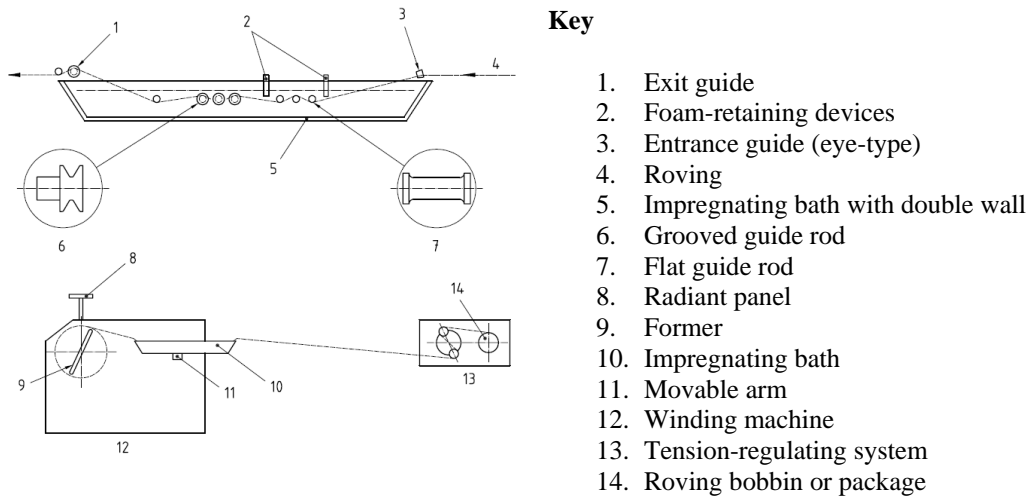
Figure 3.10: Resin bath with flat-type guide rods [30] .

- The roller, which is shown in Figure 3.11 as an example, shall be corrosion-
  and wear-resistant. It shall be freewheeling and have a minimum diameter of
  120mm. The length of the area of contact between the roving and the roller
  shall be not less than 20% of the roller circumference, and the roller shall be
  immersed in the resin to a depth of approximately 20% to 30% of its diameter.
  A doctor blade shall be used to control the amount of resin on the roller. The
  distance between this blade and the roller shall be variable between 0mm and
  30mm. The setting of this blade shall be determined by preliminary tests. A
  scraper blade shall be used to remove the resin the roving does not pick up.

Key

1. Roving
2. Roller
3. Resin
4. Guide
5. Doctor blade
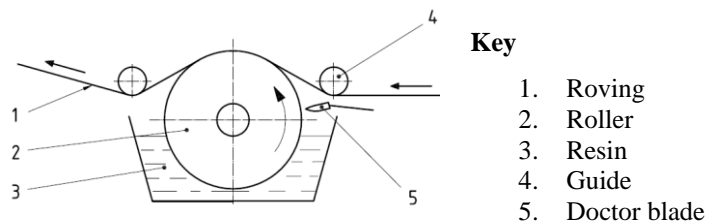
Figure 3.11: Resin bath with roller device [30] .

- A former frame, ground flat on both sides, onto which the roving is wound and
  outer-mold pieces designed to be placed over both faces of the winding and
  press onto the sides of the former, thus accurately defining the thickness of the
  winding. The faces of the outer-mold pieces shall be perfectly flat, and parallel
  to the former faces. An example is provided in Figure 3.12.
- Rod-shaped silicone-rubber end pieces are required to seal the gap between the
  former and the outer-mold pieces and prevent resin loss during curing.

42

Key

1. Former frame
2. Outer-mold pieces
3. Spindle mounting
4. Notch
5. Thickness of winding
6. Silicone-rubber end piece
7. Roving
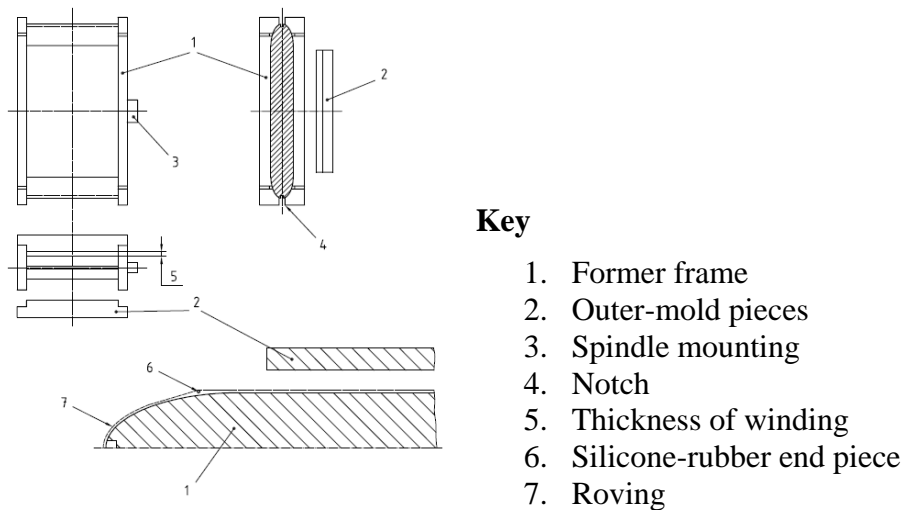
Figure 3.12: Former [30] .

Winding procedure

1) Unless otherwise specified, the rovings shall be processed without previous conditioning.

2) Mount the former on the spindle of the winding machine. When the impregnating bath has to be kept at a temperature higher than 50℃ , it is recommended that the former be maintained at as nearly constant a temperature as possible (by means of a radiant panel for example).

3) Adjust the speed of rotation of the spindle to obtain a roving speed of between 5m/min and 15m/min; the speed shall be selected such that the winding operation can be completed during the pot life of the resin.

4) Choose the winding parameters as follows:

   - Winding pitch: $0.5mm < p < 4mm$

   - Number of layers: $2 \leq n \leq 12$

5) See Annex A for examples of convenient winding parameters and Annex B for calculation if needed.

6) Place the roving bobbin(s) on the unwinding reel, if applicable.

7) Unwind a suitable length of roving by tangential or overhead take-off, feed it through the tension-regulating system, the guide rods in the bath and the thread guide, and attach it to the former.

8) By means of the tension-regulating system, adjust the tension in the roving to ensure the roving will be wound uniformly on the former.

9) Pour the resin system into the impregnating bath.

43

10) Maintain the temperature of the bath at the chosen temperature.

11) Coat the outer-mold pieces with a release agent, which is stable at the operating temperature, or cover with a heat resistant film.

12) If using a former without the notches that permit the winding to be cut off, fix to each end of the former a plastic rod to facilitate removal of the plates and to prevent damage to the former when cutting the winding.

13) Place the silicone-rubber end pieces at each end of the two sides of the former as shown in Figure 3.12. These rods are intended to keep the roving in tension during winding and to avoid any loss of resin at the mold closure. Their position and diameter shall be such that the part of the winding between them is flat.

14) Coat the outer-mold pieces with a thin layer of the resin system.

15) Wind a layer of roving. If necessary, remove the resin appearing on the surface with a flexible spatula or a roller.

16) Repeat for each layer of winding.

17) When winding has been completed, fix the outer-mold pieces on the former.

18) Place the assembly either between the hot platens of a press, or in an oven with the outer-mold pieces clamped in place.

19) Cure the molding under the time and temperature conditions that are recommended for the resin system used.

20) Proceed to post-curing of the molding (this might be done with or without the outer-mold pieces).

21) Allow to cool to room temperature.

22) Separate the plates by means of a saw.

23) Trim the plates to length and width. To avoid edge damage, a diamond saw is recommended.

24) Test specimens intended for mechanical tests shall be taken from these plates and cut to the dimensions given in the appropriate test standards.

Verification of the characteristics of the plates obtained

- The fiber content shall not differ by more than 2% from the specified value.

- After molding, the visual appearance and quality of impregnation of the plates shall be investigated to confirm that the laminate is of suitable quality.

- Measure the thickness, width and length of the plates.

- The test plate preparation report shall include the following information:

- A reference to this part of ISO 1268
- The place and date of production of the test plates
- Details of the number of layers and the winding pitch, in mm
- A description of the materials used (including type of reinforcement, type of resin, type of filler, if applicable, catalyst curing system, etc.)
- A description of the impregnating device used (bath, roller or other)
- The operating conditions (resin system temperature, in, and the roving speed, in m/min)
- Whether a press or an oven was used
- The dimensions of the plates produced
- The fiber content and filler content, if applicable
- The quality of the test plates (appearance, impregnation);
- Any other information needed to reproduce the plates exactly;
- Any deviations from this part of ISO 1268.

Annex A-Examples of convenient winding parameters

Table 3.3 gives parameters that lead to 3mm-thick UD plates having a final glass content near 70% by mass when a resin of density $1,2 \text{g/cm}^3$ is used.

Table 3.3: Examples of convenient winding parameters [30] .

Linear density of roving [tex]	Number of rovings	Overall linear density [tex]	Calculated Parameters		Alternative parameters for even number of layers	
			Number of layers	Winding Pitch [mm]	Number of layers	Winding Pitch [mm]
210	2	420	11	1,14	6	0,56
210	3	630	9	1,40	6	0,68
300	1	300	13	0,97	8	0,47
300	2	600	9	1,33	6	0,67
300	3	900	7	1,56	4	0,82
800	1	800	8	1,59	4	0,77
1200	1	1200	6	1,79	4	0,94
1600	1	1600	6	2,38	4	1,09
2000	1	2000	5	2,47	4	1,22
2400	1	2400	5	2,98	4	1,33
2400	2	4800	3	3,57	2	1,89

Annex B-Calculation of winding parameters

$$n = \sqrt{\frac{h^2 \cdot \rho \cdot \varphi \cdot 10}{\rho_l}} \tag{3.1}$$

$$p = \frac{n \cdot \rho_l}{h \cdot 10 \cdot \rho \cdot \varphi} \tag{3.2}$$

In expressions (3.1) and (3.2), p is winding pitch [mm], n is the number of layers, ρ_l is the linear density of fibers [gr/km], h is the plate thickness [mm], ρ is the volumetric density of fibers [gr/cm^3], and φ is the fiber volume ratio.

Equations (3.1) and (3.2) indicate that the number of layers and winding pitch would differ for each specific fiber volume ratio chosen. Interpreting it from another angle, winding pitch and the number of layers are important parameters for controlling the fiber volume ratio during the filament winding process.

An Excel table was tabulated in order to provide convenience in calculating parameters for winding test plates of different properties, which is presented in Figure 3.13.

ISO 1268 Winding Parameters				Winding Time		
Glass Fibers (as Specified in the Document)				**Mandrel Measurements**		
Ply Count		**Winding Pitch**		Width [mm]		1000
h [mm]	3	n [-]	8	Length [mm]		260
ρ [gr/cm³]	2,540	ρₗ [gr/km]	800	Thickness [mm]		24
ρₗ [gr/km]	800	h [mm]	3	Pitch [mm]		2,384
φ [%]	52	ρ [gr / cm³]	1,790	Length of a Single Pitch [mm]		595
n [-]	4	φ [%]	52	Number of Pitches in a Layer [-]		420
		p [mm]	2,750	Fiber Length of a Layer [mm]		249788
Carbon Fibers (to be Used in Our Winding)				Number of Layers [-]		8
Ply Count		**Winding Pitch**		Total Length [m]		1998
h [mm]	3	n [-]	8	Chuck Speed	[deg/min]	10000
ρ [gr/cm³]	1,790	ρₗ [gr/km]	800		[RPM]	27,778
ρₗ [gr/km]	800	h [mm]	3	Winding Speed [m/min]		17
φ [%]	50	ρ [gr / cm³]	1,790	Winding Time [min]		121
n [-]	3	φ [%]	50			
		p [mm]	2,384			

Figure 3.13: ISO 1268 winding parameters calculated.

Using the tabulated EXCEL file, it is possible to obtain winding parameters of test plates with any material. For convenience, winding time is also calculated together with material count to be spent during the winding operation.

3.2.2 Test Plate preparation report

Test plates were manufactured according to ISO 1268 "Fiber Reinforced Plastics-Methods of Producing Test Plates" as mentioned before.

Test plate production was carried out in cooperation with MAKSAV Inc. based in Kırıkkale, utilizing their workshop and production equipment. Test plates were manufactured on 21.01.2015 Wednesday and transported to ITU following day. Temperature was 7/-4°C and relative humidity was around 40-50% on that day.

Winding was planned as 8 layers of 0.375mm, 3mm thickness in total. Planned winding pitch was 1.6mm, however actual winding pitch was around 3mm.

Aksa A-49 of 12K tow size (Figure 3.14) was used for fibers, which has a linear density of 800tex.

Figure 3.14: Aksa A-49 12K carbon roving.

Voraforce^{TM} Filament Winding System comprising of Voraforce^{TM} TW100 epoxy resin and TW156 hardener was used in manufacturing of test plates (Figure 3.15). Viscosity of the resin system is 1000-1500mPa·s or 1-1,5Pa·s @ 25℃ which is higher than the value specified in the standard. ISO 1268 has no strict rules on resin viscosity, however resin system fully complies with the standard as long as the bath temperature is above 40°C. As per minimum pot life condition, winding process must be completed in 100 minutes, assuming winding conditions in room temperature.

Resin and hardener is mixed on 1:1 basis regarding mass with 2kg of each and a mixture of 4kg was obtained. Later on, it had been assumed that mixture would begin to precure so an additional mixture of 4kg was poured into the bath. The total amount of resin system expended is around 8kg whilst roughly the half of that amount was drained without wetting any fibers. A considerable amount of resin to wet the fibers is also wasted on the stand, limiting the amount of resin present in the winding to a much lower value.

Figure 3.15: Resin and hardener.

Environmental conditions (cold and dry weather) had made it hard to get a good mixture of resin and hardener, primary cause being the extremely high viscosity of resin. A bath of evaporating water was prepared in order to lower resin viscosity and an improvised mixer was used in order to better mix the resin and hardener, which can be seen in Figure 3.16.

Figure 3.16: Mixing of resin and hardener.

Viscosity of resin-hardener mixture had been observed to be low enough to flow easily even in an adversely cold environment, thus no problems were encountered when filling and draining the bath, shown in Figure 3.17. Winding process had been started with a bath temperature of 25°C, which was progressively increased to 65°C in later stages.

Figure 3.17: Mixture and its pouring into the bath.

Filament winding stand, shown in Figure 3.18, is stated as the firm's own construction and it has two axes of motion (rotation of the mandrel and translation of the carriage). It is able to wind five workpieces simultaneously. The stand did not have a reel system to control fiber tensioning during winding operation. It was observed that the stand is able to wind up to speeds of 20-30RPM.

A bath type impregnation device, which can be seen in Figure 3.18, which has a liquid volume more than 4 liters, was used. An eye-type thread guide is present; however, it is in the exit side, not the entrance as stated in ISO 1268. Flat-type guide rods are present as submerged in the resin, there are no devices for retaining resin foam in the setup though. Resin bath has a temperature regulating resistance. It is fixed on its legs and does not translate with the motion of carriage.

Figure 3.18: Filament-winding stand and resin bath.

Mandrel (Figure 3.19) is designed and manufactured per ISO 1268 standard. It is roughly a plate of 24mm thickness with a width of 500mm, length of 1150mm and fully rounded edges. Winding on the mandrel would produce 2 pieces of test plates, which are 1000mm in length and 500mm in width. Outer-molds and notches were excluded in order to provide manufacturing convenience. It was manufactured of AISI 304 steel material and has a total weight of 113.450kg with spindle mountings.
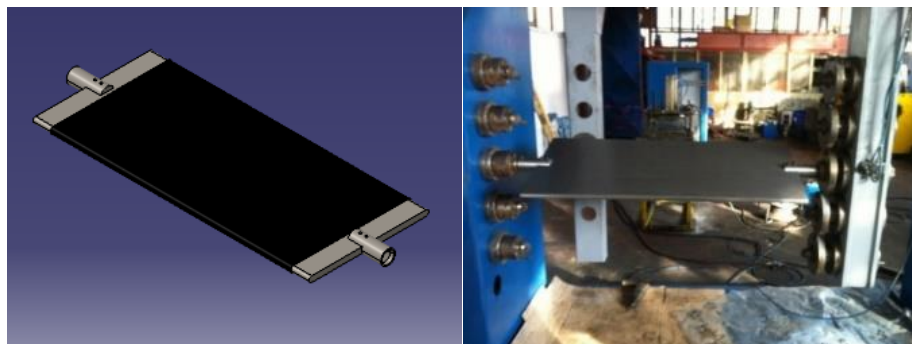

Figure 3.19: Mandrel.

49

NC program of the winding had been compiled by using CADFill® 7.61 for 3mm tow width and 0.375mm ply thickness. It is calculated that the winding of 8 plies with 1.6mm pitch would take nearly 1h for a winding speed of 10000DPM, consuming 1.5km of fiber and 1.2kg of resin in total.

A trial winding of glass fibers without the use of resin had been initiated in order to verify winding program, which can be seen in Figure 3.20. Winding was continued with resin later on, on the purpose of observing the behavior of resin system during the winding operation in our particular environment.
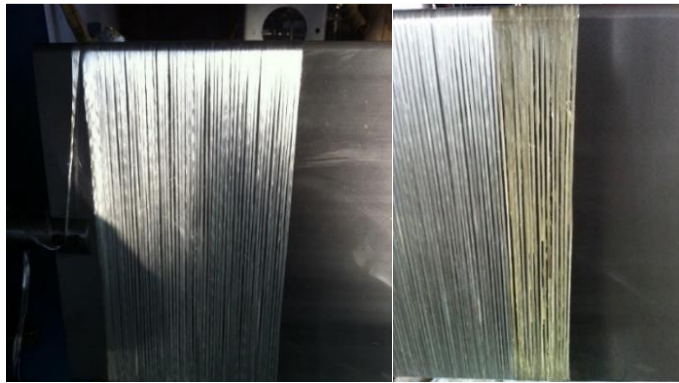
Figure 3.20: Glass fibers wound for trial.

As the first problem encountered, stand tended to break the tow at higher winding speeds. Winding speed was reduced to 1500DPM for a better observation of winding characteristics.

It had been observed that fiber tow would develop gaps on flat surfaces of the mandrel, which was still able to consolidate in rounded regions with the help of curved geometry. Trial winding was continued with resin and tow width was updated to 5mm in order to close the ranks between successive tows; however, gaps would still continue to build up and the remnants resulting from the piling of the tow would stick on to tow and winding due to resin viscosity.

After trial winding, mandrel surfaces were cleaned with cellulosic thinner.

Due to the oven being used in another process, mandrel surfaces were heated by the use of a welding torch, which is seen in Figure 3.21. It is assumed that temperatures of 30-40°C were obtained on mandrel surface, however it only endured for a brief moment of time, approximately 10-15min.

Figure 3.21: Heating of the mandrel.

After the heat was applied, mandrel surface was covered with the mold release agent to ensure the separation of winding and mandrel after curing process, aftermath can be seen in Figure 3.22. Its performance is stated to be better than that of other release agents in the market and no problems had been encountered during the removal phase.

Figure 3.22: Release agent on surface of the mandrel.

Tow broke off for the first time towards the end of the first ply, which is seen in Figure 3.23. Winding was continued by tying the tow to the nearest surface on the mandrel. Braking of the tow persisted to continue in later stages of winding, in an irregular fashion. High speed of winding had been assumed to be the reason of the problem, so the winding speed was reduced to 3000DPM. Permanency of the winding is greatly affected; variety of the resin content could be observed visually. Braking points of the tow constitute a source of irregularity, reducing homogenous properties of the winding.
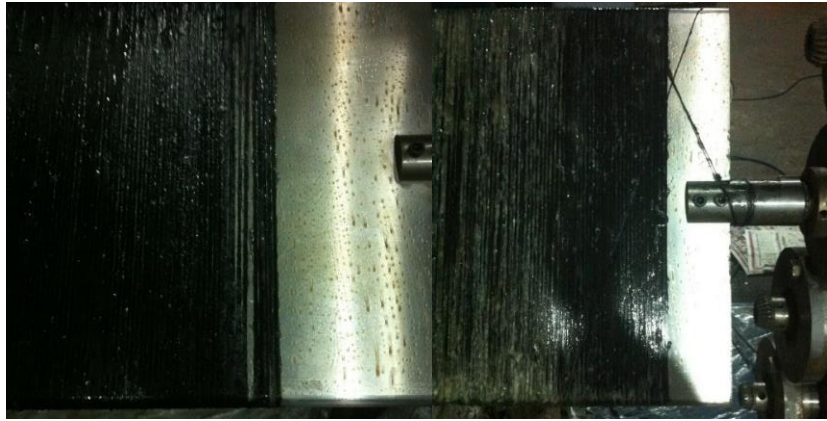
Figure 3.23: The first breaking point of the tow.

Another reason for the breaking of the tow was assumed that it is forced to slide on the rough surfaces of a zig-zag path, which can be seen in Figure 3.24. Tension of the tow had been observed to increase overtly when forced to slide on the surfaces of guide eyes of the bath and the carriage, thus the tow would break off with higher winding speeds due to increasing tension.

Figure 3.24: Path of the tow.

Improper contact of the tow with guide eyes of bath and carriage is thought to be another reason of pilling. Relatively rough surfaces of eyes would pile the tow of carbon fibers, which are of brittle and fragile nature. Adverse environmental conditions could also be assumed to worsen the situation; most of the materials get more and more brittle with decreasing temperature. Zig-zag path on which the tow travels from roving to mandrel is likely to increase fiber tension in an uncontrolled fashion, resulting in more pilling.

Figure 3.25: Tow and the carriage.

Residues of the tow being wound can be seen on the Figure 3.25. Remnants of the tow which has been pilled elsewhere might stick on various surfaces on its path, however the remnants of the tow which is pilled on the carriage directly sticks into the winding on the mandrel. Due to closer proximity to the winding, it is more important to provide smoother contact surfaces on the carriage.

In order to provide the tow a linear path, bath was moved laterally together with the motion of the carriage to ensure that they remain in the same position relative to each other. Guide eye of the bath was also removed from the setup in order to reduce frictional surfaces. Without the use of an eye, excess resin was removed by the use of some cardboard pieces, handheld in position. Rollers on the carriage were also bypassed, in order to further reduce the sources of friction. In the latest configuration, which is seen in Figure 3.26, a winding speed of 10000DPM was achieved. Maximum winding speed has been observed as 12000DPM but tow persisted to brake off in that conditions. It is understood that a winding speed of 10000DPM was an optimal speed concerning our setup.
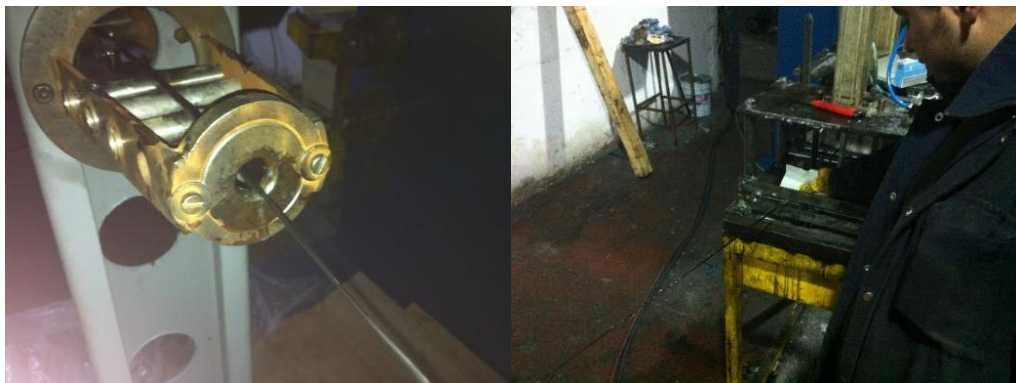
Figure 3.26: Measures taken to reduce friction.

After eight plies had been wound, a thickness of 3mm was achieved and winding was terminated. Finished winding is seen Figure 3.27. Winding had been calculated to take around 1h; however, practice it approximately took 3h.

Figure 3.27: Finished winding.

It had been observed that there was some excess resin present in the winding, visible on the outer plies of the winding. It constituted a translucent crust on the top surface, tended to drip from bottom surface of the winding, which can be seen in Figure 3.28.

Figure 3.28: Excess resin in the winding.

Residues from pilling of the tow had been stuck and flaked on the surfaces of the winding. They were easily noticeable due to their size and irregular shapes, given in Figure 3.29. It is evaluated that residues of equal sizes might also exist inside the winding, between various plies.

Figure 3.29: Residues stuck in the winding.

54

An oven (Figure 3.30) was used for curing operation. It has 1.2x5m dimensions and covered in thermal cloth. An improvised carriage was assembled to be used on rail mechanism.

Figure 3.30: Oven.

Curing cycle is specified as 2h at 90°C + 4h at 150°C. Heating and cooling would take 1h each so the winding would spend 8h in the oven in total.

A carriage of square frames, which is seen in Figure 3.31, was constructed in order to provide support for spindle mountings of the mandrel. Mandrel and the winding would be rotated from outside the oven with the help of an extending arm. Mandrel was rotated 45° per 10 minutes throughout the curing cycle in order to provide more uniform distribution of resin across the structure.

Figure 3.31: Improvised carriage for the oven.

A fishplate had been present on the bottom surface of oven. The amount of resin on it could give a good idea of excess resin present in the winding before curing. Outer surfaces of the winding that had just come out of the oven would look rather matt and rougher than previously thought, which are all presented in Figure 3.32.

Figure 3.32: Cured winding and fishplate.

It had been planned to produce two identical test plates, measuring 1000mm in length and 500mm in width; however, due to improper grinding operation during the removal from mandrel, 5 plates of different dimensions were obtained. Plate dimensions are provided in Figure 3.33.

Sample No	Measurements		Area [cm^2]	Weight [gr]	Areal Density [gr/cm^2]
	Width [cm]	Length [cm]			
1	48	24	1152	390	0,339
2	48	29	1392	460	0,330
3	48	47	2256	750	0,332
4	48	47	2256	744	0,330
5	48	53	2544	850	0,334
			9600	3194	0,333
			Total Area	Total Weight	Average Areal Density

Figure 3.33: List of produced test plates.

Fiber volume ratio of the production material was calculated as 37% by making the use of an EXCEL tabulation, which is presented in Figure 3.34, based on the material expense during the process, which is nearly one thirds shorter than the value of 52% specified in ISO 1268.

Linear Density of Fiber [gr / km]	800
Total Winding Length [km]	1,890
Fiber Weight [gr]	1512
Fiber Density [gr / cm^3]	1,790
Fiber Volume [cm^3]	845
Matrix Weight [gr]	1682
Resin Density [gr / cm^3]	1,15
Hardener Density [gr / cm^3]	1,18
Matrix Density [gr / cm^3]	1,165
Matrix Volume [cm^3]	1444
Fiber Volume Ratio [%]	36,907

Figure 3.34: Fiber volume ratio based on the material expense.

Plates have very rough outer surfaces with a matt outlook. Inner surfaces are a little bit smoother and shiny, visual quality of the plates are not so well in accordance with expectations in general though.

Fibers were well impregnated during the winding operation; excess resin is present in the winding for that reason. Resin system was able to wet fibers successfully throughout the operation, as bath temperature was raised to around 65°C towards the end of winding operation.

Winding surfaces could be seen as they had just come out of the oven in Figure 3.35. Photos are taken in a darker environment, giving no idea of surface gloss. In a brighter environment, matt surfaces are more easily recognizable. It is thought to be the result of excess resin being present on winding surface.

Figure 3.35: Surface roughness of the winding.

Roughness of the plates could most likely be the result of the excessive presence of residues from tow pilling on the outer surfaces.

It had been evaluated that surface roughness and excess resin on the surface could be removed by grinding with a fine grade of finishing stone. The material removed from the surface was mostly a white dust with fine powder, which could only be from the grinding of the resin, can be observed in Figure 3.36.

Figure 3.36: Grinding outer surfaces of the winding.

Winding was mostly grinded in the direction of fibers; it had been, for a brief moment, grinded in transverse direction and cracked all along, which is seen in Figure 3.37. Both top and bottom plates are extracted from mandrel in two pieces.

Figure 3.37: Sawdust from grinding.

In order to preserve actual plies of winding and their thickness, grinding operation was cut short without eliminating all of rough features present, seen in Figure 3.38. Winding was field stoned on fully rounded edges for the purpose of removing the winding from it. Dark powder from the grinding of fibers was observed.

Figure 3.38: Surface roughness after grinding.

Test plates, which had been removed from mandrel, were cleaned with cellulosic thinner and packed. It can be observed in Figure 3.39 that plates would warp immediately after removal from mandrel. Bottom surfaces of the plates are a lot finer than rough surfaces on top.

Figure 3.39: Test plates after removal from the mandrel.

All of the winding parameters and relevant parts of plate production is carried out per ISO 1268 standard, no further specific information is required to reproduce the plates exactly.

Deviations from ISO 1268 might be listed as below:

- Workshop was not conditioned regarding heat, dust and humidity.
- Tow broke off many times during the winding process.
- Pilling of the tow was unavoidable and residues were often stuck on the winding.
- An exact control on the amount of resin wetting fibers could not be achieved.
- Tension of the tow was not controlled.
- Resin-hardener mix had stayed in the bath for more than 6h, it showed no visual signs of pre-curing. However, visual inspections of the samples in microscope clearly indicates otherwise.
- There was clearly more resin on the winding than required and together with residues of pilled tows, these are critical factors lowering fiber volume ratio, thus mechanical properties.
- Due to the breaking of the tow randomly, a uniform winding could not be achieved. Mechanical properties and densities of different samples could disperse in that case.

3.2.3 Coupon tests

Specimens were cut from plates 4 and 5 because they could offer the largest and flattest area for machining operations. A special type of cutting insert was procured for high speed cutting, in order not to damage coupons during the operation. A CNC milling machine with 3 axes was utilized for this process.

Coupon tests were performed to obtain the mechanical properties, using an MTS322.21 universal testing machine; per ASTM D3039 [32] for tension, D6641 [33] for compression and D3518 [34] for shear properties. Strain gages were utilized to obtain moduli and Poisson Ratio data. Test specimens are shown in Figure 3.40. Each of the tests are repeated for three specimens and the average of these values are presented as the mechanical properties of our production material.
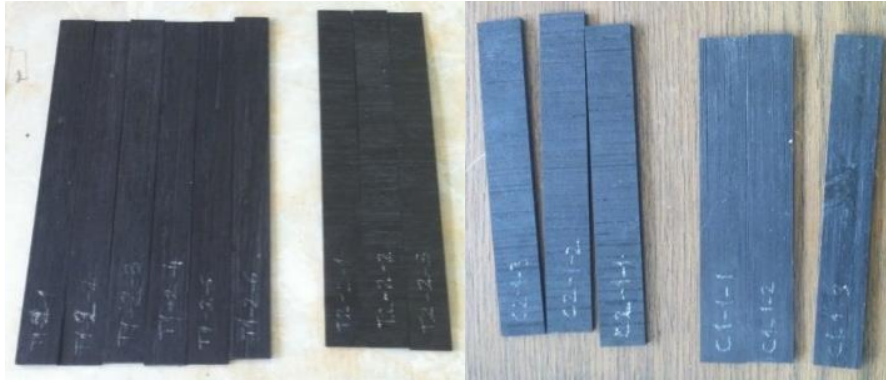
Figure 3.40: Specimens cut from test plates.

Technical drawing of specimens per regarding ASTM standards is provided in Figure 3.41. Specimens of compression testing have different dimensions than ones intended for tension/shear testing. Dimensions are provided in a Table 3.4; "L" denotes length, "w" is for width and thickness is denoted with a "t", of a specimen.
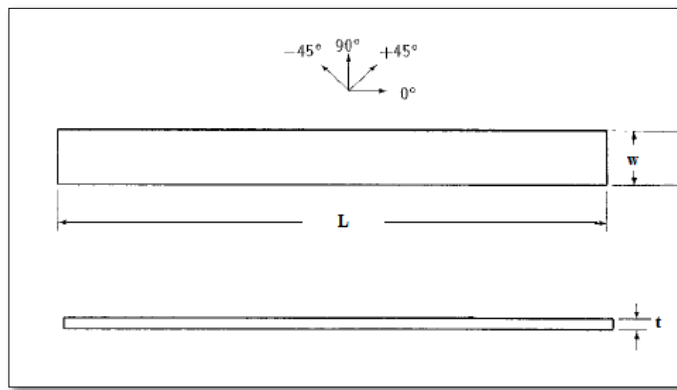

Figure 3.41: Drafting of a specimen [31] -[33] .

Table 3.4: Dimensions of specimens [31] -[33] .

Specimen	w [mm]	L [mm]	t [mm]
Tension	25	250	3
Compression	20	140	3
Shear	25	250	3

3.2.3.1 Tension test

Tension tests were carried out per ASTM D3039. Specimens of 0° and 90°, without tabs, were loaded in tensile direction to the point of failure, Figure 3.42 presented as an example.

Figure 3.42: Specimens after failure on MTS322.21.

Some tension specimens after failure are shown in Figure 3.43.

Figure 3.43: Tension specimens after failure.

Specimens tested for tensile stress and according results are presented in Table 3.5.

Table 3.5: Results of tension test.

Ply Type	Specimen	Strength [MPa]
UD (0°)	T1-2-5	692.04
UD (0°)	T1-2-6	625.82
UD (90°)	T2-2-1	11.92
UD (90°)	T2-2-2	8.91
UD (90°)	T2-2-3	13.73

3.2.3.2 Compression test

Compression tests were carried out per ASTM D6641. Specimens of 0° and 90°, without tabs (Figure 3.40), were loaded in compressive direction to the point of failure. An apparatus for preventing specimens from buckling is used per testing standard, which is shown in Figure 3.44.
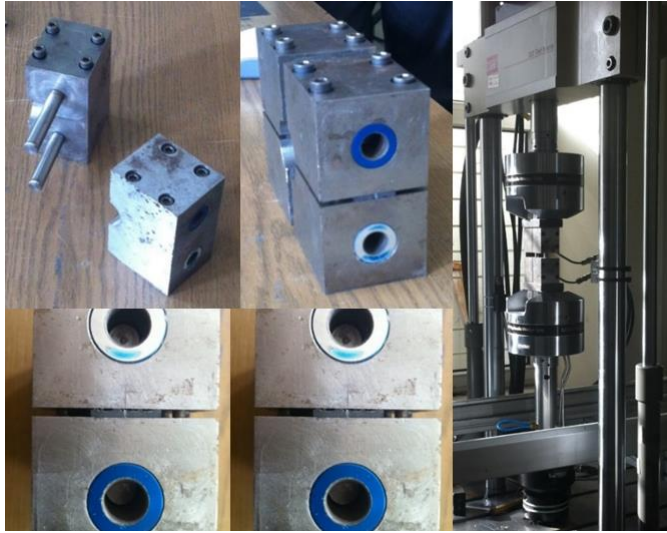
Figure 3.44: Compression specimens in apparatus.

Some compression specimens after failure are shown in Figure 3.45.

Figure 3.45: Failed compression specimens.

Specimens tested for tensile stress and according results are presented in Table 3.6.

Table 3.6: Results of compression test.

Ply Type	Specimen	Strength [MPa]
UD (0°)	C1-2-4	338.85
UD (0°)	C1-2-5	321.20
UD (90°)	C2-1-2	43.17
UD (90°)	C2-1-3	40.50

3.2.3.3 Shear test

Shear tests were carried out per ASTM D3518. It is a similar process with tension test, in which 45º angled specimen is loaded in tension to the point of failure. Shear strength of the specimen is then determined from tensile strength, within a certain strain limit. More definitive standards and test methods for determination of shear properties also exist, such as a v-notched specimen per ASTM D5379. Specimens tested for shear strength and according results are presented in Table 3.7.

Table 3.7: Results of shear test.

Ply Type	Specimen	Strength [MPa]
UD (45°)	S1-1-1	10.80
UD (45°)	S1-1-2	7.49
UD (45°)	S1-1-3	6.76
UD (45°)	S1-1-4	8.34
UD (45°)	S1-1-5	8.05

3.2.3.4 Determination of elastic moduli

Stress-strain curves of a material should be evaluated in order to determine tension, compression and shear moduli.

Strain gages are placed over specimens, which can be seen in Figure 3.46, for this purpose. Midpoints of the specimen in width and height is established and marked in the first step. Marked midpoint is cleaned by the use of some clothing and isopropyl alcohol. Epoxy adhesive is applied on the cleaned surface and the strain gage is placed. Sellotape is applied to fix the strain gage; it might be removed after the epoxy had been cured. Specimen is ready to be tested as strain gage is properly placed onto position.

Figure 3.46: Placement of a strain gage over a specimen.

Specimens tested for elastic moduli and according results are presented in Table 3.8.

Table 3.8: Determination of moduli.

Modulus	Ply Type	Specimen	Value [GPa]	ν_{12}
Tension	UD (0°)	T1-2-1	64.871	0.3252
Tension	UD (90°)	T2-2-3	3.998	0.0135
Compression	UD (0°)	C1-1-1	57.392	0.2784
Compression	UD (90°)	C2-1-1	3.776	0.0069
Shear	UD (45°)	S1-1-1	1.489	-

3.2.3.5 Density test

Density of the specimens are determined per ASTM D792. [35] A specimen of known weight is taken at room temperature. It is submerged into water, by using an apparatus if floatable, and weighed again. Ratio of submerged weight and dry weight yields the relative density. Relative density is multiplied by the density of water at room temperature and density of the specimen is found. Measuring displacement might be difficult for specimens of smaller size; determining relative density is a more convenient way to find the density of a specimen.

Specimens and utilized equipment for density test can be seen in the Figure 3.47. During testing, room temperature was measured as 20.7°C and the density of water at that temperature is 998.06kg/m^3.
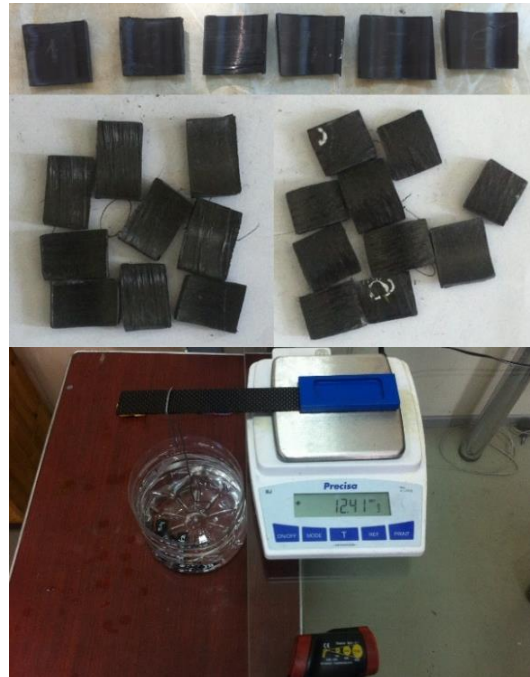

Figure 3.47: Specimens and equipment for density tests.

Eight specimens are tested in total and densities between 1200 and 1270kg/m^3 are recorded. Results would provide an average density of 1243kg/m^3. Based on a calculation using fiber and resin densities, assuming no voids present, a fiber volume ratio of 12,5% is obtained.

Fiber volume ratio calculation based on the results of the density tests are considerably lower than those calculated from material expense during the winding. The most probable cause of this situation would be the high percentage of voids present in the microstructure of the production material. Dispersion of specimen densities are also remarkable, which puts the repeatability of the process in question.

Some sample driveshafts has been purchased in order to have an understanding of current composite driveshaft applications and their properties. One of them is brand-new and the other two are second-hand. Although duration of use was not known, second-hand shafts have no sign of damage except the corrosion over the joints etc.

In the next stage, specimens had been cut from sample shafts for density testing. Purpose of implementing density test on sample shafts is prediction of fiber volume ratios assuming some generic fiber and resin densities.

Ten specimens had been taken from each of the sample shafts procured. First one has an average density of 1465kg/m^3, a fiber volume ratio of 48% is predicted assuming the same densities with our fiber and matrix. Second and third shafts have average densities of 1448 and 1474 kg/m^3 from which fiber volume ratios of 45% and 47% are predicted respectively.

Evidently, densities and fiber volume ratios of sample shafts are considerably higher than our production material. Difference between sample densities are much lower. Void content, based upon visual and cross-sectional inspection of the samples, seem to be much lower than our coupon material.

3.2.3.6 Investigation with optical devices

Specimens of production material are evaluated with optical devices after density testing. Maximum magnification of microscope is x100; however, most of the images were captured in x50 magnification.
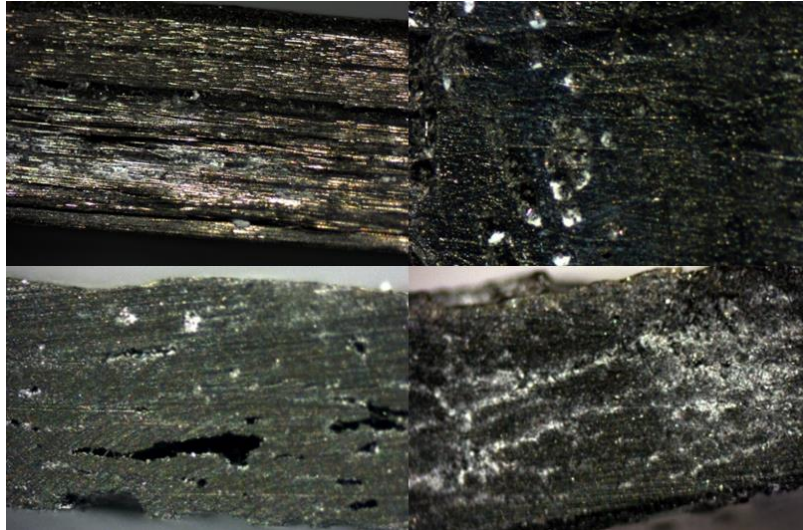
Figure 3.48: Investigation of samples with optical devices.

A section of longitudinal direction can be seen in the top left section of Figure 3.48. Fibers across the section are shining as bright yellow dots, concentrated in some areas. Residues of pre-cured resin may also be seen, of matt white color. Distribution of fibers does not seem to be uniform as bright pixels are mostly concentrated around first plies at the bottom. Fibers get sparser in the plies above, in a more uniform fashion nonetheless. There are some darker strips than the resin itself concentrated around the middle, which might be commented as big voids or delaminations.

Sections of transverse direction can be seen for various samples in bottom left and right sections of Figure 3.48 that verifies the existence of voids. There are hardly any yellow dots as fibers, which points out a lower fiber volume ratio. Residues of pre-cured resins might be observed as matt white regions, together with cracks/voids as darker areas. Voids are greater in scale and more or less distributed towards the bottom plies, pointing out very poor handling of manufacturing process. Some other regions are also present, which bear no cracks/voids, however with excessive residues of pre-cured resin. Some white dots exist in the upper plies, which are evaluated to be prematurely cured resin blobs. Inferior microstructure might be a good explanation for lower mechanical properties in transverse direction.

Top right section of Figure 3.48 presents a glimpse of outer surface of a specimen. Fibers may again be recognized of bright yellow color together with matt white details of pre-cured resin. Random orientation of fibers along with the presence of pre-cured resin blobs even on the surface explain poor visual quality of the outer surfaces of the test plates, even on a microstructural level.

3.2.4 Evaluation of coupon material properties

The material properties are found to be lower than desired values. The reasons are found to be mostly related to the poor handling of the winding process, which are listed below:

- A controlled environment could not be achieved during manufacturing (regarding temperature, humidity and dust in the production environment). That could be a probable cause for the formation of voids.

- Proper and constant mandrel temperature could not be maintained. It would contribute to the formation and consolidation of voids.

- Winding parameters could not be maintained as planned due to various reasons. Winding pitch was close to 3mm in practice, which means a lower fiber volume ratio than planned.

- Resin content had variations throughout the whole structure, due to various reasons. Fiber tow broke off many times nearly in all plies of winding. These would cause the variation of material properties.

- Process took longer time to complete than planned. Resin gel time could probably be exceeded and pre-curing of the resin is started on the stand. That might have reduced mechanical properties of resin system, so the whole composite material.

- Pilling of the tow. It would contribute to the formation of voids in addition to the roughness of external surfaces, which are not molded directly by mandrel.

- Tension creel was not present in the winding device and the shape of the mandrel was not suitable for fiber to get tension over flat plate areas. That is a highly probable cause for inferior material properties in fiber direction.

Overall, fiber volume ratio of the test plates would be calculated around 37% for consumed amount of materials in the process. However slightly lower mechanical properties and density would be credited to the existence of a high amount of voids/cracks/delaminations in the material, due to improper manufacturing conditions.

3.2.5 Updating of analytical and numerical models

After the determination of moduli and Poisson Ratio data, mechanical properties of our production material is fully revealed together with its strength. Mechanical properties of the coupon material are presented in Table 3.9.

Table 3.9: Mechanical properties obtained from coupon testing.

E_1 [GPa]	61.1315
E_2 [GPa]	3.887
ν_{12}	0.3018
G_{12} [GPa]	1.489
$(\sigma_1^T)_{ult}$ [MPa]	658.930
$(\sigma_1^C)_{ult}$ [MPa]	330.025
$(\sigma_2^T)_{ult}$ [MPa]	11.520
$(\sigma_2^C)_{ult}$ [MPa]	41.835
$(\tau_{12})_{ult}$ [MPa]	8.288

After the evaluation of our production material by coupon testing, the need arose to update the analysis of driveshaft with production material properties. Upon updating the analysis, "A" models have been dropped due to lower values of design constraints. A new type is introduced as "C" models, having an internal diameter of 130mm. Number of layers and stacking sequences are also updated per new material data, as provided in Table 3.10.

Table 3.10: Updated models.

Model	Stacking Sequences	
	B	C
1	[(±45)$_2$/45]$_s$	[(±45)$_2$/45]$_s$
2	[(±45)$_{14}$/45]$_s$	[(±45)$_{17}$]$_s$
3	[(±30)/30/(±45)$_{13}$]$_s$	[(±30)/30/(±45)$_{15}$/45]$_s$
4	[0$_3$/(±45)$_{13}$]$_s$	[0$_3$/(±45)$_{15}$/45]$_s$
5	[(±30)$_3$/(±45)$_{11}$/45]$_s$	[(±30)$_3$/(±45)$_{14}$]$_s$
6	[0$_6$/(±45)$_{11}$/45]$_s$	[0$_6$/(±45)$_{14}$]$_s$

Analytical and numerical models of the shaft have been updated after coupon manufacture and testing with production material properties results are presented in Table 3.11.

Table 3.11: Updated analytical and numerical models.

Model	Tsai-Wu Strength Ratio		1st Bending Frequency [Hz]		Buckling Torque [Nm]	
	Analytical	Numerical	Analytical	Numerical	Analytical	Numerical
B1	0.34	0.23	38.20	101.44	1118	756
B2	2.25	1.52	42.34	112.43	95260	64353
B3	2.11	1.43	48.86	128.31	112742	76408
B4	1.99	1.37	62.68	161.39	166546	114657
B5	2.07	1.40	54.56	142.22	125019	84554
B6	1.83	1.27	77.86	197.71	209672	145510
C1	0.29	0.21	35.53	94.29	1078	781
C2	2.35	1.71	40.58	107.69	138600	100854
C3	2.30	1.90	45.97	120.85	160871	132893
C4	2.21	1.62	57.63	148.84	230037	168624
C5	2.20	1.60	50.77	132.60	177449	129054
C6	1.98	1.48	70.66	180.24	289946	216727

3.3 End Connections of the Composite Driveshaft

End connections constitute, perhaps the most interesting and challenging issue about designing and producing a composite driveshaft. It is referred to with different words, such as "joint", "coupling", "end-link" etc. Throughout this study, the term of "end connection" will be used because the word "joint" is mostly used referring to universal joints of a driveshaft. "Coupling" also implies a physical connection between components, which may not always be the case. The term "end connection" is found to be the most general reference on the topic.

There are currently two different type of applications regarding the end connections of a composite shaft with its universal joints, press fitting or adhesive bonding.

Advantage of using a lightweight composite material is that it can be used to form a press-fit molded joint with its yokes (joints that connect the shaft to the axle), rather than using an adhesive that can axially constrain the yokes during crashes, according to "Design News for Mechanical and Design Engineers". The steel or aluminum end part is inserted into the composite tube using a press to overcome a designed interference. In order for this to work, the composite tube requires additional hoop-wound reinforcement to its ends. Torques are transmitted during normal operation of the driveshaft by friction alone, but axial loads cause slip of the connection at a known load. Other design features can be introduced to make the axial load progressively increase, stay constant, or progressively decrease with extended displacements. In this way, it is possible to devise solutions, which meet virtually any OEM requirement. [11]

Aside from crash behavior, a press-fit connection would damage the plies of the torque tube in vicinity. Interference pressure to transmit a torque loading of 17000Nm could be dangerously high to the inner layers of the composite shaft. Another thing to note is crash behavior is a minor concern at that stage since serial production of the shaft in current configuration is not intended. Thus, there is no point in using a press-fitted connection solely based on a crash behavior advantage.

It has been decided to utilize an adhesive co-bonding with end connection parts, during the curing stage. Since additional bonding processes would not be required, it provides ease in manufacturing. In addition to that, a coupling may still be formed between end connection parts and composite shaft.

3.3.1 Review of current applications

70% of the overall driveshaft weight is accounted for in a conventional driveshaft by the mass of the end connections and joints or couplings. When the steel tube is replaced by composite, it is the minor share of the driveshaft weight that is reduced. To achieve the ultimate lean-weight driveshaft, it is necessary to develop low weight end fittings. [6] Existing designs are investigated prior starting to develop our own.

3.3.1.1 Commercial applications

GKN have published work in this area, which has led to the ultra-low weight driveshaft proposal shown in Figure 3.49. This system has an overall weight of 2.5kg, replacing a conventional 2-piece steel driveshaft system weighing 10kg. [6]
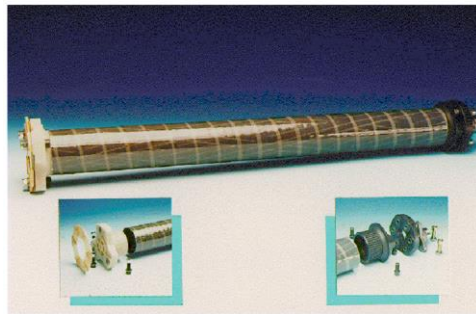
Figure 3.49: Ultra-low weight composite driveshaft [6].

A "hybrid" connection is developed by Teufelberger GmbH, based in Germany, dubbed T-IGEL, which is provided in Figure 3.50. A pin arrangement specifically designed for the application load is calculated and is automatically transferred to the metal base body. Through material accumulation different pin structures can be realized. Because of the reliable and tight connection, T-IGEL$^®$ is especially suited for the application in highly strained shafts, beams, struts, different structural and crash components. (Url-7)
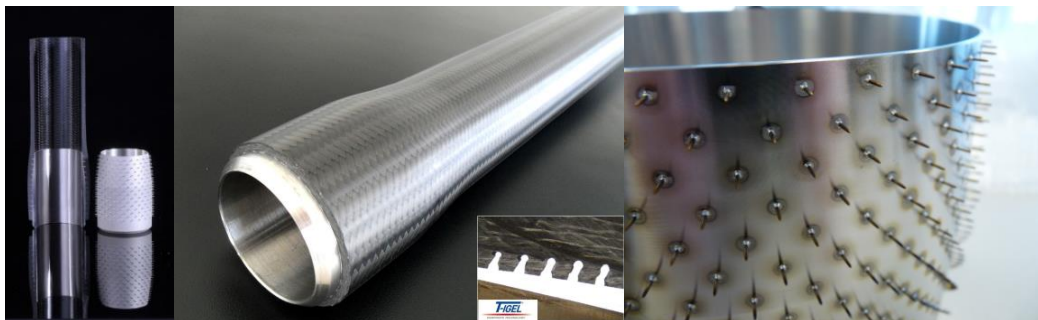
Figure 3.50: T-IGEL from Teufelberger GmbH (Url-7).

Sample shafts

Sample shaft end connections, which are shown in Figure 3.51, were investigated by destructive testing. Despite belonging to three different models of vehicles belonging to three different manufacturers, all of the sample shafts employ the same type of connection. A splined profile is press-fit into composite section and it is axially fixed by a channel of additional adhesive.

Figure 3.51: End connections of sample shafts.

3.3.1.2 Patents

A patent search, involving some 111 patents belonging to various dates, is conducted. They might be categorized as:

- Couplings (5)
- Adhesive channels and connector sleeves (6)
- Key and clamp connections (4)
- Yoke members (7)
- Spline connections (5)

Regarding the categories, couplings may provide most useful solutions fit for our purpose. Although it may prove otherwise in real-life applications, solutions such as adhesive channels and key connections are not evaluated as useful. Different solutions for yoke members and spline connections may yield interesting designs at a later stage since the basic requirement is to "connect" composite shafts to the metal joints for the moment. Bear in mind that, all the ideas presented here are "patented" so they could only inspire for some ideas at best. Some of the inspiring solutions are presented:

- Flange design for filament wound composite shaft, provided in Figure 3.52. [36]
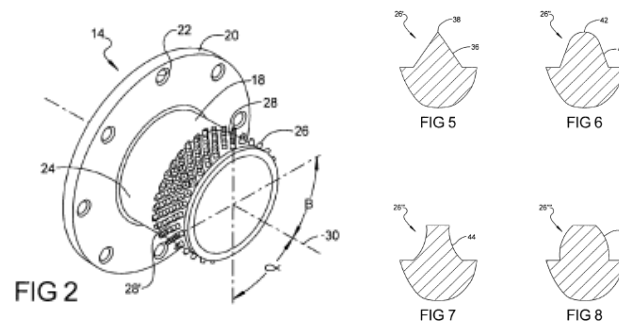
Figure 3.52: Flange design for filament wound composite shaft [36] .

- High torque density flexible composite driveshaft, given in Figure 3.53. [37]
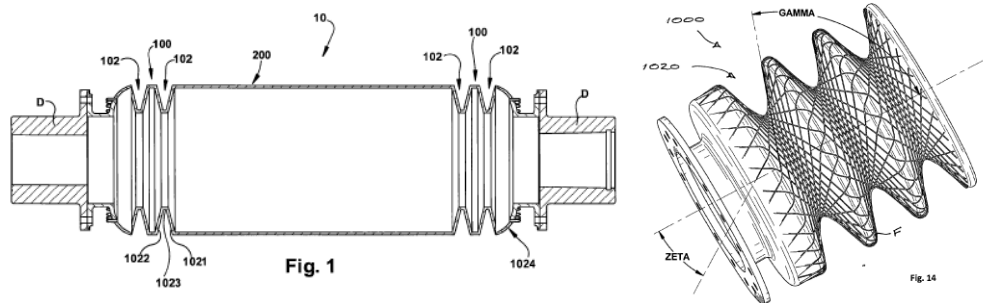
Figure 3.53: High torque density flexible composite driveshaft [37] .

- Composite torque tube captured end fitting, shown in Figure 3.54. [38]
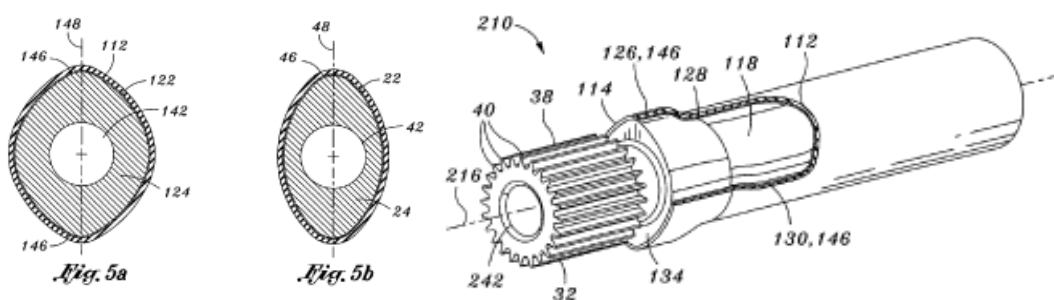
Figure 3.54: Composite torque tube captured end fitting [38] .

- Fiber reinforced composite shaft with metallic connector sleeves mounted by a polygonal surface interlock [39] , Fiber reinforced composite shaft with metallic connector sleeves mounted by longitudinal groove interlock [40] , Fiber reinforced composite shaft with metallic connector sleeves mounted by connector ring interlock [41] , which are all provided in Figure 3.55.

72
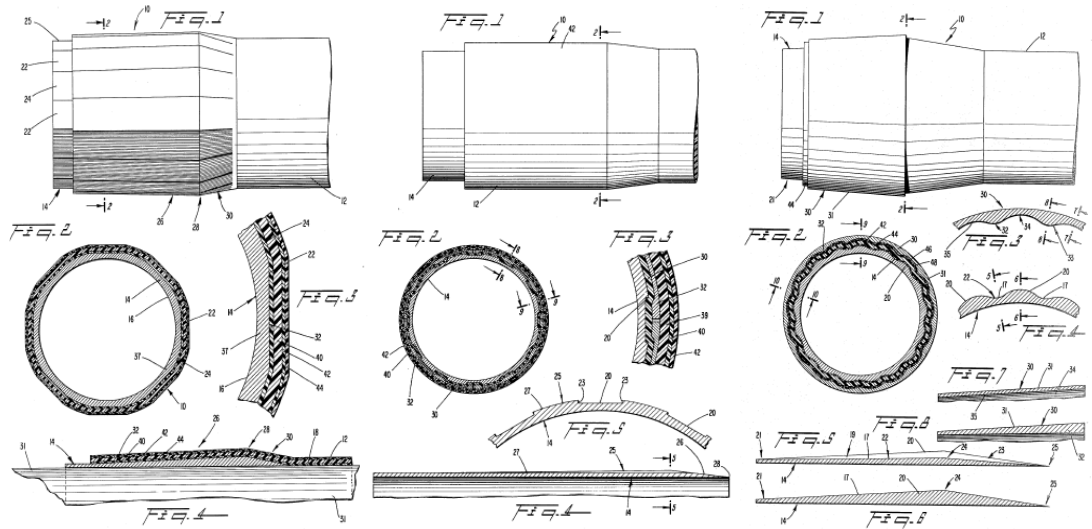
Figure 3.55: Metallic connector sleeves [39] -[**41**] .

- Production of driveshafts from reinforced plastics pipes, which can be seen in Figure 3.56. [42]
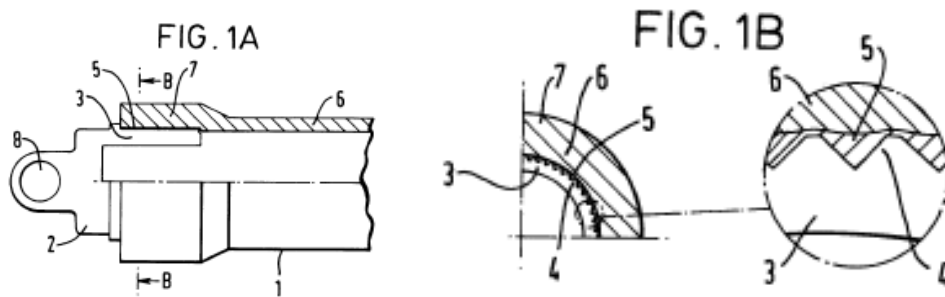
Figure 3.56: Production of driveshafts from reinforced plastics pipes [42] .

- End fitting having adhesive channels for driveshaft assembly [43] , End fitting for driveshaft assembly and method of manufacturing same [44] , which are both provided in Figure 3.57.
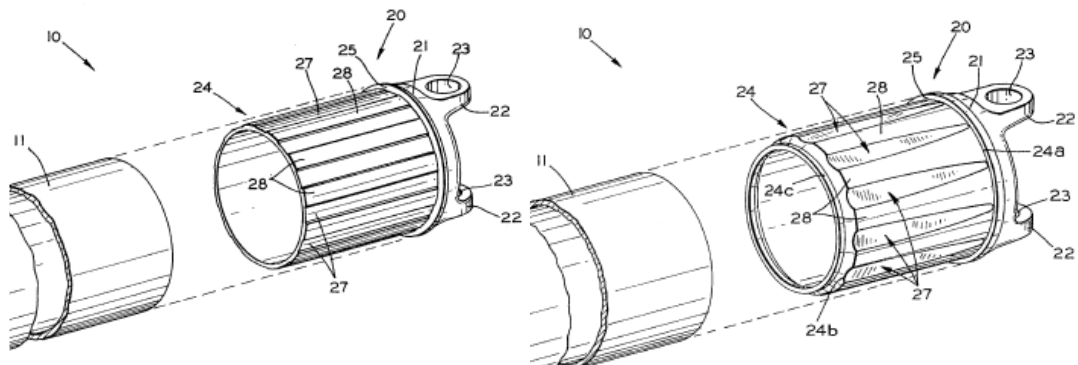
Figure 3.57: Adhesive channels [43] [**44**] .

73

- Braided composite shaft with yoke member, which is shown in Figure 3.58. [45]
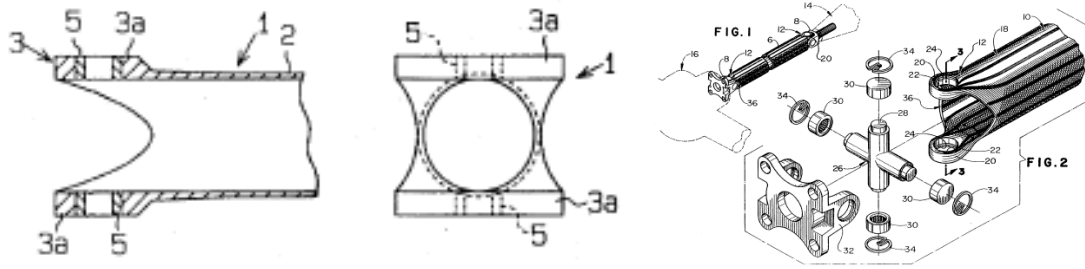
Figure 3.58: Braided composite shaft with yoke member [45] .

3.3.2 Preliminary design tool for adhesively bonded tubular joints

In the past, a variety of analyses tools have been developed to analyze adhesively bonded joints. These analytical methods are based on various approaches such as continuum mechanics, plane strain/stress closed form solutions, 2-D and 3-D finite element analyses, and 2-D and 3-D variational approach based solutions. Rastogi, et. al. presented comprehensive review of the stress analyses codes available for bonded composite joints. In addition, the text by Adams, Comyn and Wake presents a comprehensive treatise on the design of various adhesively bonded joints used as primary load carrying members. [14]

End connections, which are machined from blocks of C50 material, are planned to be co-cured with filament wound carbon/epoxy shaft tube. An adhesive layer of epoxy would develop between them and its strength should be investigated in order to transmit the design torque safely. The situation could be modelled as adhesively bonded concentric tubes, which are illustrated in Figure 3.59. Theoretical expression of shear stress that would develop in adhesive layer is expressed as (3.3). [14]
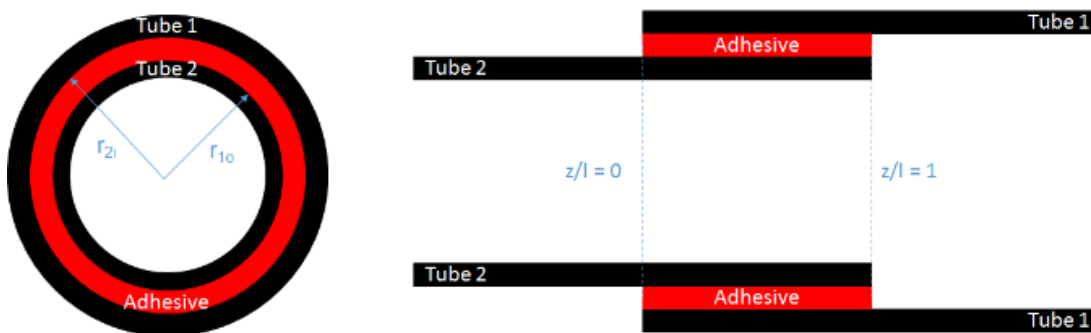
Figure 3.59: Adhesively bonded concentric tubes.

$$\tau_a = \frac{T\alpha}{2\pi r_m{}^2} \left[\left(\frac{1 - \Psi(1 - \cosh \alpha l)}{\sinh \alpha l} \right) \cosh \alpha z - \Psi \sinh \alpha z \right] \tag{3.3}$$

$$\alpha = \sqrt{\frac{\delta}{\Psi}} \tag{3.3a}$$

$$\delta = \frac{2\pi r_m^2 r_{1o} G_a}{G_1 J_1 \eta} \tag{3.3b}$$

$$\Psi = \frac{G_2 J_2 r_{1o}}{r_{2i} G_1 J_1 + r_{1o} G_2 J_2} \tag{3.3c}$$

$$r_m = \frac{r_{1o} + r_{2i}}{2} \tag{3.3d}$$

In expression (3.3), T is the torque, r_m is the mean radius of the adhesive ring, l is the adhesion length, z is the axial position along the adhesion length. The equation employs various parameters, which are given below:

In the expressions above; r_{1o} is the outer radius of the inner tube, r_{2i} is the inner radius of the outer tube, G_1, G_2, and G_a are shear moduli of tubes and adhesive, J_1 and J_2 are polar moment of inertias of tubes, and η is the adhesive thickness.

The mean (average) shear stress in the adhesive layer is given by:

$$\tau_{mean} = \frac{T}{2\pi r_m{}^2 l} \tag{3.4}$$

The expression (3.3) yields the distribution of shear stress along the adhesion length, which should be checked for maximum shear strength of the adhesive, in our case epoxy matrix of the composite.

By varying the key design parameters such as adhesive shear modulus, adhesive thickness and bond length, one can quickly create comparison curves for shear stress distribution across the bond line in the joint, and get a preliminary estimate of optimal joint design parameters.

In our case, the most critical parameters to be employed in the expression (3.3) are adhesion length (l) and adhesive thickness (η). Adhesion length could be tailored according to the distribution of shear stress; however adhesive thickness should be

appointed beforehand. Ply thickness is predicted as 0.3 mm in coupon production, 0.2 mm would be a fair prediction for adhesive thickness at this point. Rest of the parameters employed are $r_{1o} = 64.8$mm, $r_{2i} = 65$mm, $G_1 = 80$GPa, $G_2 = 1489$MPa, $G_a = 1300$MPa.

Shear stress distribution is calculated and presented in Figure 3.60, for adhesion lengths of 10mm, 25mm, 50mm and 100mm respectively. Distribution of shear stresses are roughly starting from the same point and asymmetrical up to adhesion lengths of 50mm, giving a higher spike towards z/l = 1. The last case is asymmetrical too, however without the higher spike in the end that looks like a favorable solution. Further increment of adhesion length does not considerably decrease the shear stress where z/l is zero, thus the adhesion length is decided to be l = 100mm.
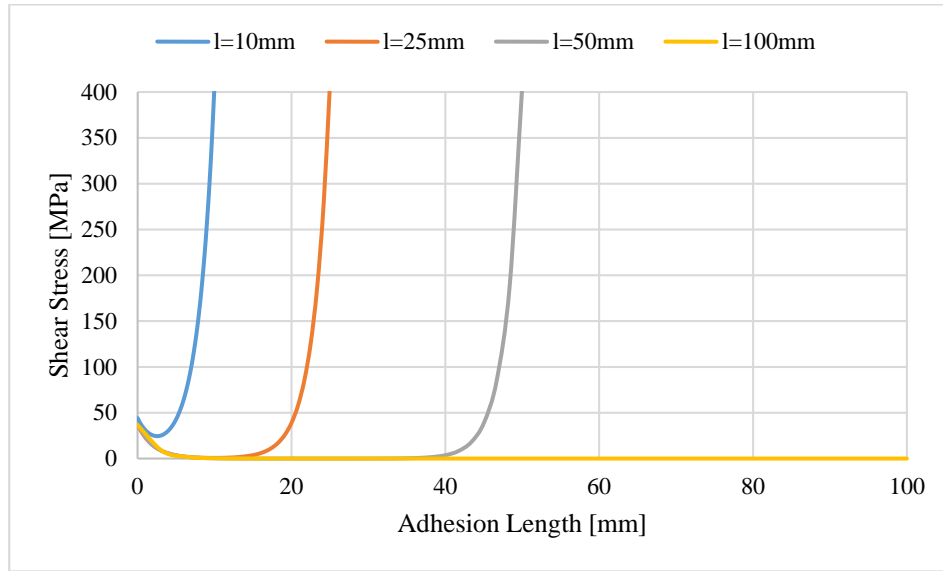
Figure 3.60: Distribution of shear stress along the adhesion length.

Torque transmission capability of the joint is defined by τ_{mean}, however failure of the joint would start from the spikes in the end regions thus these should be the points of attention in a structural point of view. The peak adhesive shear stress can be compared with the ultimate adhesive shear strength to get a preliminary estimate of torque load required for failure initiation in the yoke-to-tube adhesive bonded tubular lap joint.

In order to ensure safer transmission, hexagonal shape for the joint is chosen to provide coupling between the shaft and joint. An appropriate amount of taper is given to provide a smooth inner bore and continuous layers, hexagonal cross-section would provide coupling to the joint. Baseline shape of the end connection is shown in Figure 3.61.
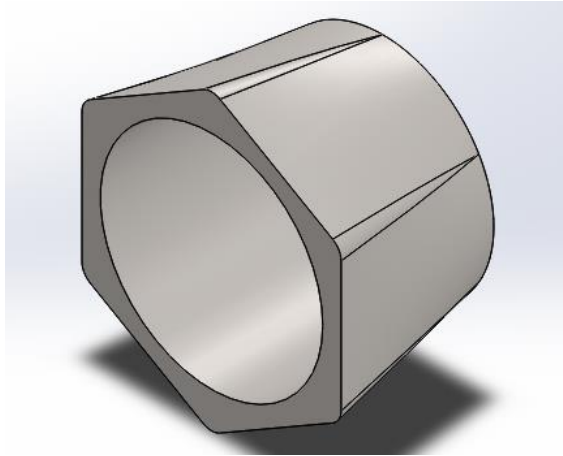
Figure 3.61: Conic hexagonal end connection geometry.

Baseline calculations are about appointing a proper adhesion length, so that the design would stay in shear strength limits of the adhesive. Besides, adhesion length is an important parameter on defining end connection part geometry. Conicity is employed for the purpose of improving shear stress distribution in addition that it would increase the area of adhesion to some extent. Since our torque is rather high for an automotive application, all aspects of the connection parts are shaped to increase torque transmission capability, hoping that it could provide a greater factor of safety in operation.

An actual production shaft to be utilized on a vehicle would have a different design of joints than the one intended for rig testing, which can be compared in Figure 3.62. Thus, there are two different configurations of the prototype shaft, a rig configuration and a vehicle configuration. Vehicle configuration parts are the same with Figure 3.61, welded with a spline and universal joint by an addition of a ring; however, test configuration involves two parts of different geometries, one of them has a housing for rig shaft while the other is a flanged part.

Figure 3.62: Rig and vehicle configurations of proposed driveshaft.

It was decided that a mandrel of steel material would be removed from flanged side after curing so that the flanged coupling part provides the space for removal process.

During the design process of end connections, evaluation and approval of Adalar Machinery Inc. was provided in order to verify that designed end connections are eligible for shaft production by filament winding method.

End pieces are manufactured from blocks of C50 material by machining to desired geometry. One of the pieces has a housing to couple with the shaft of test rig and the other one is flanged to be able to fixed on a bracket. CAD configuration of connection parts, which has been created in SolidWorks 2013, is shown in Figure 3.63.

Figure 3.63: End connections in rig configuration.

3.3.3 Finite Element Analysis of end-connection parts

End pieces of appointed geometry are evaluated by FEA and their strength regarding design torque is investigated. Pieces are fixed in housing and flange regions and a torque of 35000Nm is applied over hexagonal geometry. An iterative selection of refining mesh was applied so that convergence of models could be ensured. Material properties are provided in Table 3.12.

Table 3.12: C50 material properties (**Url-8**).

Modulus of Elasticity [GPa]	200
Poisson Ratio	0,3
Yield Strength [MPa]	250
Ultimate Strength [MPa]	460
Tangent Modulus [MPa]	1450
Fracture Strain [%]	15

3.3.3.1 Part with Housing

Initial and final meshing of the model is provided in Figure 3.64.
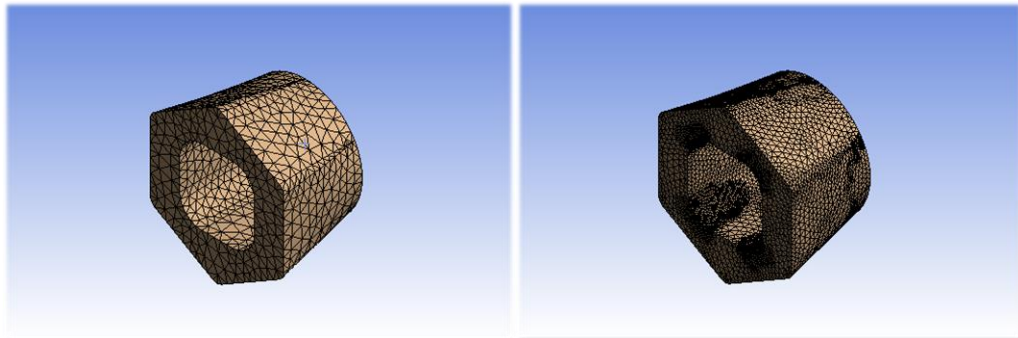
Figure 3.64: Initial and final meshing of the part with housing.

Deformation of the part with housing in circumferential direction is provided in Figure 3.65.
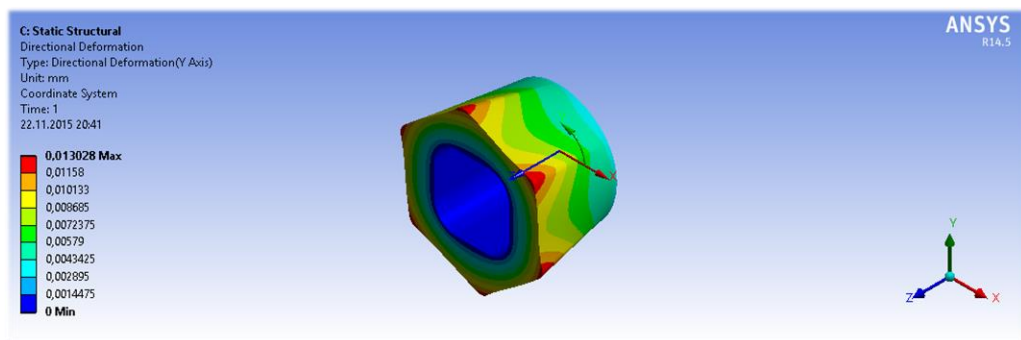
Figure 3.65: Deformation of part with housing in circumferential direction.

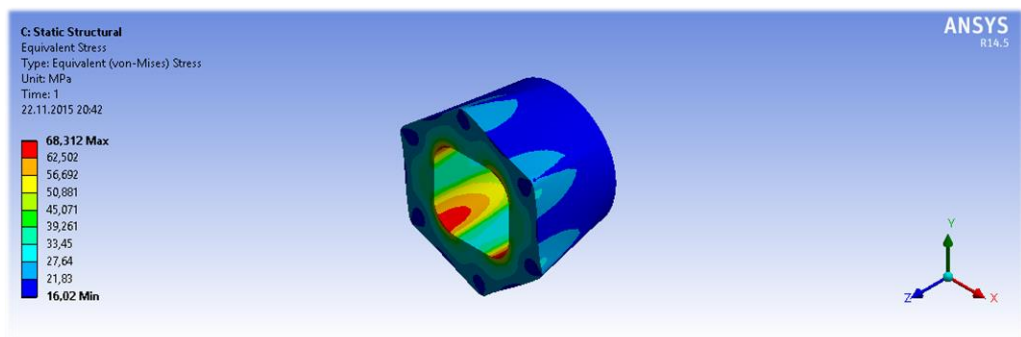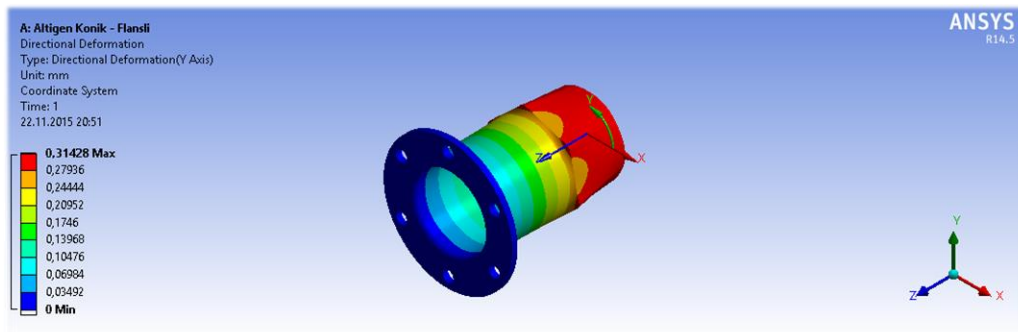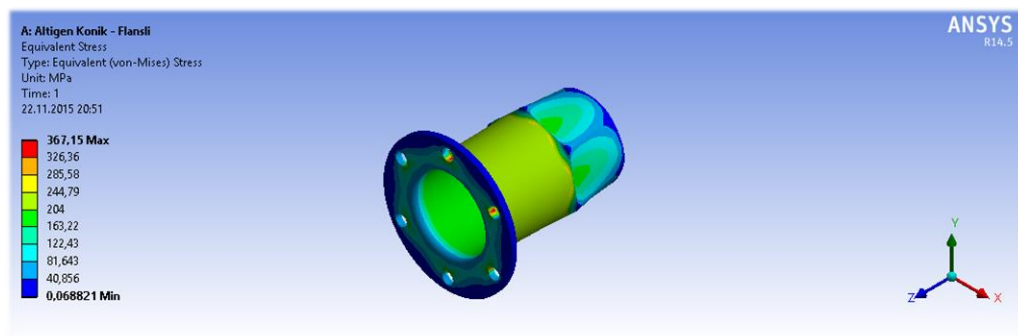Distribution of von Mises stress on the body is shown in Figure 3.66.

Figure 3.66: Distribution of von Mises stress on the part with housing.

Convergence steps of the part is given in Figure 3.67.
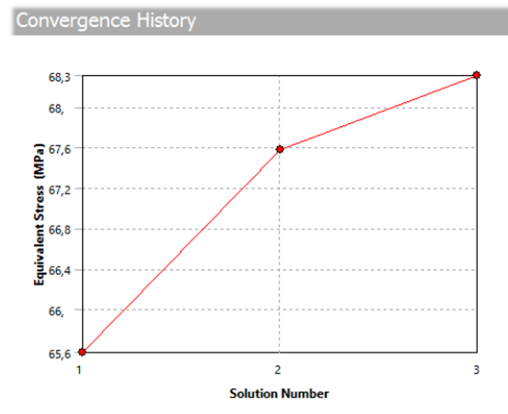
Figure 3.67: Convergence history of part with housing.

3.3.3.2 Flanged Part

Element structure of the part was iterated so that the convergence of the model is ensured, same as the part with housing.

Deformation of the flanged part in circumferential direction is provided in Figure 3.68.

Figure 3.68: Deformation of flanged part in circumferential direction.

Distribution of von Mises stress over the body is shown in Figure 3.69.

Figure 3.69: Distribution of von Mises stress on flanged part.

Convergence steps of the part is given in Figure 3.70.
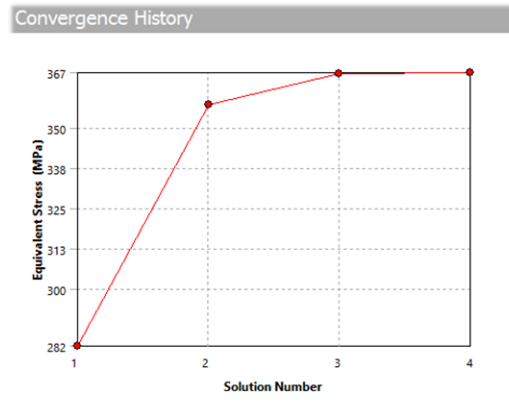
Figure 3.70: Convergence history of flanged part.

Maximum stress region is seen in Figure 3.71.
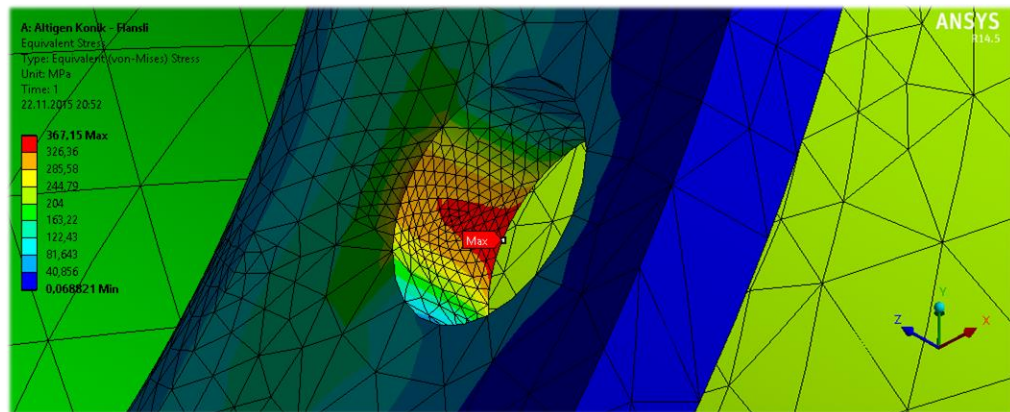
Figure 3.71: Maximum stress region on flanged part.

Finite element model of flanged part has converged, with higher von Mises stresses than anticipated nonetheless. Design torque imposed over models is 35000Nm and considered with safety factor of composite tube, the part may never reach this loading. Even if it did, some plastic behavior of the material might be allowed because end connections are useless with a failed composite tube. For these reasons, flanged part is modelled again, with a nonlinear material model this time.

von Mises stresses over the flanged part are higher than yield point but lower than ultimate strength of the material. Since this is a part of testing configuration, the part may never reach the design torque of 35000Nm fully imposed on it. Even if it did, some degree of plasticity may still be allowed since the part will already undergo destructive testing. On that purpose, a nonlinear material model is employed with bilinear isotropic hardening.

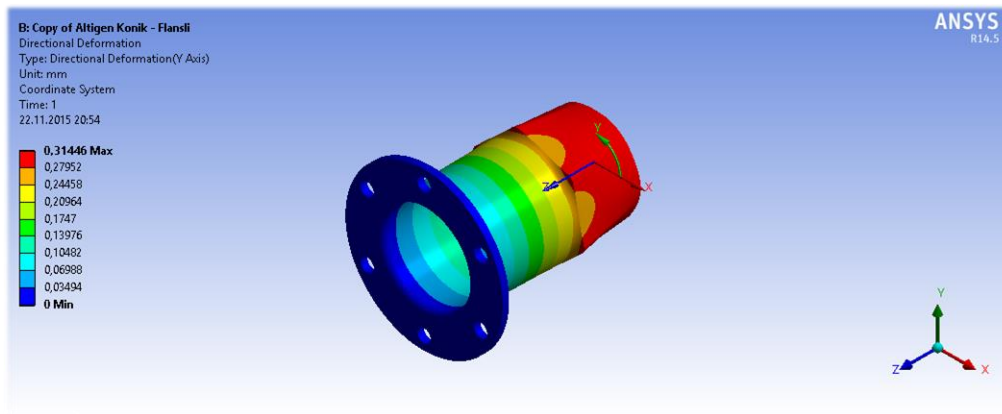Deformation of the model is provided in Figure 3.72 for the nonlinear case.

Figure 3.72: Deformation of flanged part in nonlinear case.

Distribution of von Mises stress are provided in Figure 3.73 for the nonlinear case.
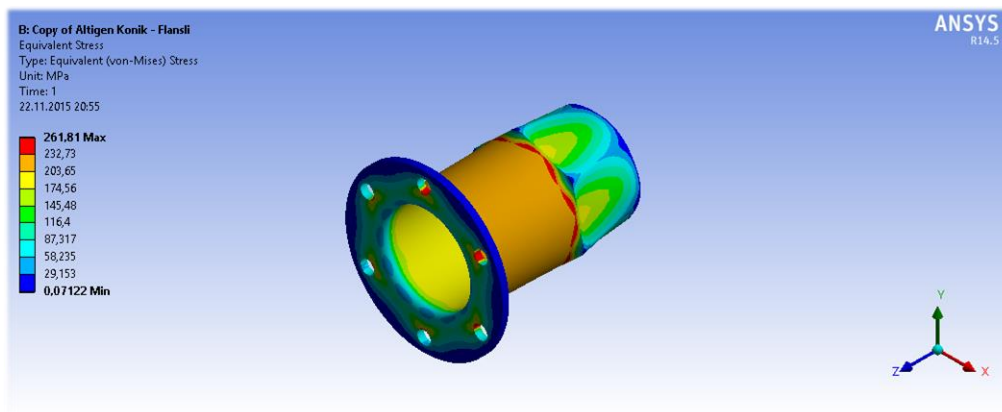

Figure 3.73: Distribution of von Mises stress in nonlinear case.

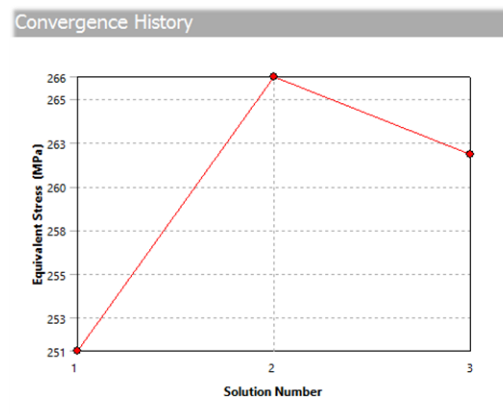Convergence steps are given in Figure 3.74.

Figure 3.74: Convergence history of flanged part in nonlinear case.

Flanged part model with nonlinear material has also converged. Distribution of von Mises stresses are more or less the same, however there is a maximum plastic strain of 0.18596% is present (Figure 3.75), which is way below the fracture strain of 15%. Both stresses and displacements are deemed to be in acceptable margin, so that flanged part might stay intact for a while after composite tube had failed.
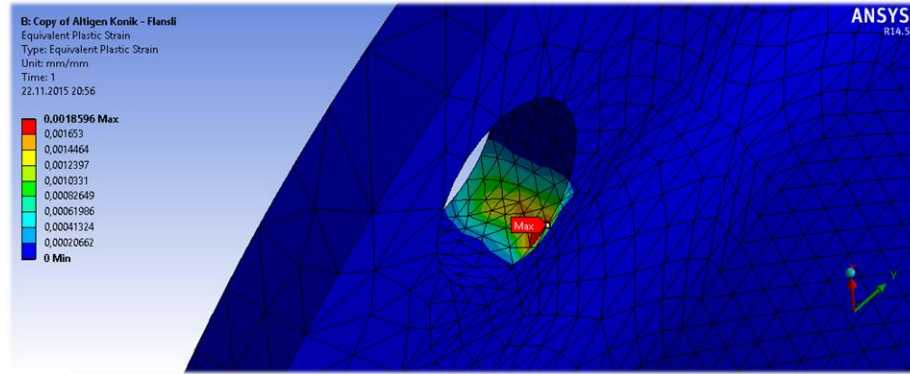

Figure 3.75: Equivalent plastic strains in nonlinear case.

3.3.3.3 Thermal-stress study

After investigation of strength, contact status of composite tube and parts are investigated for the conditions of curing cycle.

Curing cycle is specified as 2h at 90°C + 4h at 150°C, as mentioned before. It has to be ensured that composite tube and end connections would stay in contact when the temperature is raised to 150°C in the oven. If the parts expand considerably relative to each other, the contact over hexagonal regions might be lost and adhesion would not be achieved.

End pieces and composite tube could not be modelled together in ANSYS Composite Pre-Post, due to a glitch in the installed version of software. In order to overcome this problem, parts had been separately analyzed and deformations in radial direction of hexagonal region are investigated. CTE for steel is provided as $\alpha = 12 \times 10^{-6}$. CTEs for the composite material of our production are calculated as $\alpha_l = -0,695 \times 10^{-7}$ in longitudinal, and $\alpha_t = 31,5 \times 10^{-5}$ for transverse direction.

Deformations in the radial direction of hexagonal geometry, which are provided in Figure 3.76 and Figure 3.77, are evaluated; maximum deformation on the outer surface of end piece is 0.13202mm and it is 0.13198mm for the inner bore of composite tube. Difference is evaluated to be marginal and it was concluded that surfaces would not separate during curing cycle.
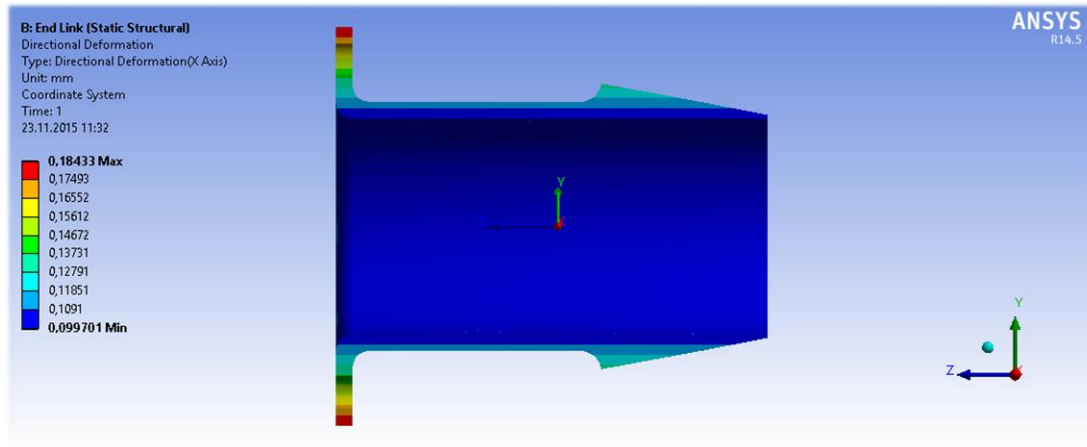
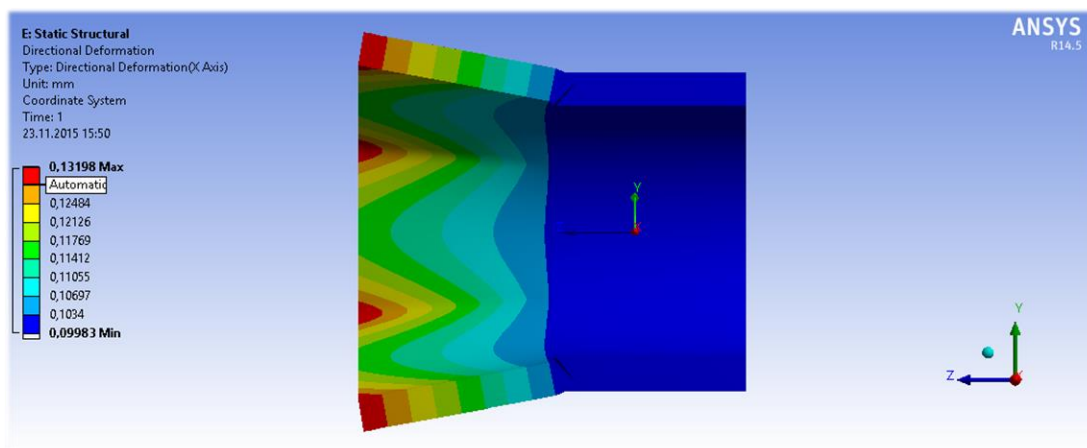**Figure 3.76:** Deformation of end connection in radial direction.

Figure 3.77: Deformation of composite tube in radial direction.

3.4 Manufacture of Composite Shaft and End Connections

3.4.1 Manufacturing of the prototype driveshaft

3.4.1.1 Winding configuration and trials

Winding configuration consists of the mandrel body, which is shown in Figure 3.78, and end connections mounted onto it. Masking tape is applied on all of the winding surface, in order to protect winding surfaces. Release agent is also applied, bar the conic hexagonal adhesion regions on the end connections. Carbon fibers, which are impregnated with epoxy resin system, would be wound on this setup, which is shown in Figure 3.78. After curing cycle, the mandrel would be removed from the bore of flanged end connection part; leaving a composite cylinder adhered to the end connections, which is our composite driveshaft in test rig configuration.
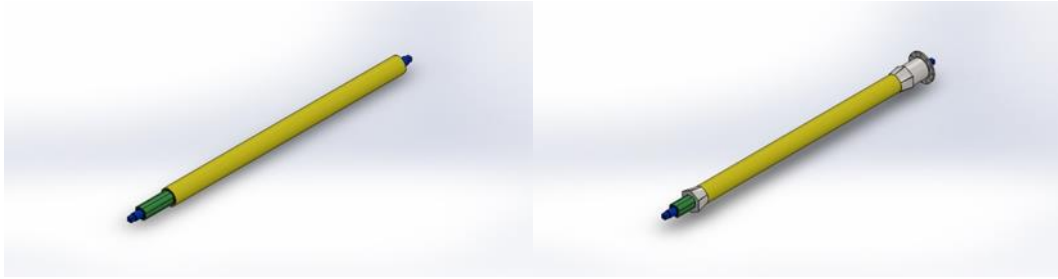
Figure 3.78: Mandrel body and winding configuration.

A trial winding was initiated in order to verify winding program and setup. Glass fibers without resin and masking tape had been wound in the first step, which is shown in Figure 3.79.

Figure 3.79: The first trial winding with glass fibers.

In the following step, winding in the same conditions was repeated with carbon fibers, presented in Figure 3.80.

Figure 3.80: Trial winding with carbon fibers.

A tow, measuring 20-30mm in width, was bundled by using 6 rovings together, which is seen in Figure 3.81.

Figure 3.81: Bundling of the tow.

It was observed that fibers had been able to wound in a uniform fashion, especially on the cylindrical sections of the mandrel; however, the tow would separate on the hexagonal surfaces of end pieces by slipping in separate directions, which can be observed in Figure 3.82.

Figure 3.82: Separation of bundles over end pieces.

In order to solve that problem, pins were decided to be placed in the end of hexagonal regions, supporting and holding fibers in desired place. Flanged end piece has enough space to facilitate pins, however a new interfacing part was machined for the part with housing, which is given in Figure 3.83.
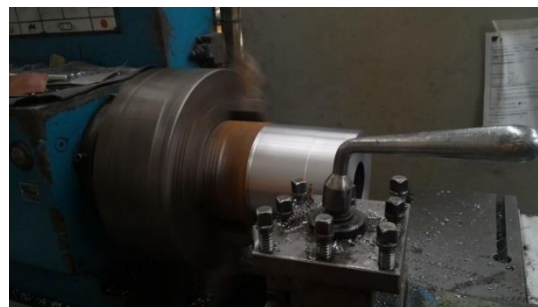
Figure 3.83: Turning of a new interface part.

Interfacing part was machined by turning, onto which the winding pins were placed, in Figure 3.84. It was aimed that pin surfaces could hold and support the fibers which would try to separate and slip so that the problems created by the conic hexagonal connection geometry are eliminated.

Figure 3.84: Winding pins in place.

Pins tended to bend in circumferential direction with the influence of fiber tension, even some of them had broken, which can be observed in Figure 3.85. There was no controlling mechanism for fiber tension on the stand so no sounding proof on the issue could be collected.

Figure 3.85: Bent and broken pins.

As long as the problem stood ground, winding on cylindrical region would stand in the same uniform fashion too. ±30° layers were observed to be able to cover cylindrical space of the mandrel perfectly, forming a very uniform winding, presented in Figure 3.86.

Figure 3.86: A complete layer wound for trial.

In the following steps, pins were fixed with a steel wire, fixing them, in a more rigid fashion, seen in Figure 3.87. Fiber tow had no difficulty in bending the pins again, however none of them have broken.

Figure 3.87: Bending of pins fixed with steel wire.

Cylindrical region in the middle of the mandrel was again underwhelmed from the problems on the connecting geometry, which can be observed Figure 3.88.

Figure 3.88: Winding on the cylindrical region of mandrel.

In the following steps, pins were nailed and weld around a ring, fixing them, in the most rigid way. Tow was again able to bend the pins slightly, bundles would still separate, which can be evaluated in Figure 3.89. It was evaluated that the space between the pins need to be reduced, in a denser and more uniform distribution, however it was deemed to be impossible in current conditions.

Figure 3.89: Bending of pins fixed on a ring.

At this step, it was clearly concluded that cylindrical surface of the mandrel is completely relieved from the problems encountered on the surfaces of end pieces. No matter how bad the winding was in the end regions, it was always able to preserve uniformity, a fact which is grasped from Figure 3.90. In the later steps, it is evaluated that a lower angled winding than ±30° might be applied in order to further increase axial modulus of the driveshaft.

Figure 3.90: Winding with pins fixed on a ring.

Following that, pins had been removed and winding was repeated with masking tape applied on the mandrel and fibers impregnated with the resin system, for which the setup is seen in Figure 3.91. Uniformity of the winding was preserved on cylindrical regions. Tow was able to hold together in a brief extent; however, the problem is still present. Separation of the tow would still leave some blank regions without fibers, which could create weaker resin rich regions in the adhesive layer.

Figure 3.91: Winding with resin and masking tape.

Following that, pins were again introduced into the setup, worsening the situation, which could be seen in Figure 3.92. Previously, pins had been able improve winding quality to a marginal extent. However, the outcome was exactly the opposite this time. Depending on the distribution of pins, tow could also be separated by them. It is observed that each and every parameter on a winding setup has to be evaluated together in order to improve production quality. A winding setup has to be evaluated as a whole, together with all depending parameters.

Figure 3.92: Separation of the tow between the pins.

In a last attempt, hexagonal edges of flanged end piece were trimmed. Ending edges of hexagon was milled in order liken it to a cylindrical geometry, which is presented in Figure 3.93. End piece surfaces had been covered hoop windings of 90°, on the possibility that fiber tow might behave more stable on a composite layer rather than steel.
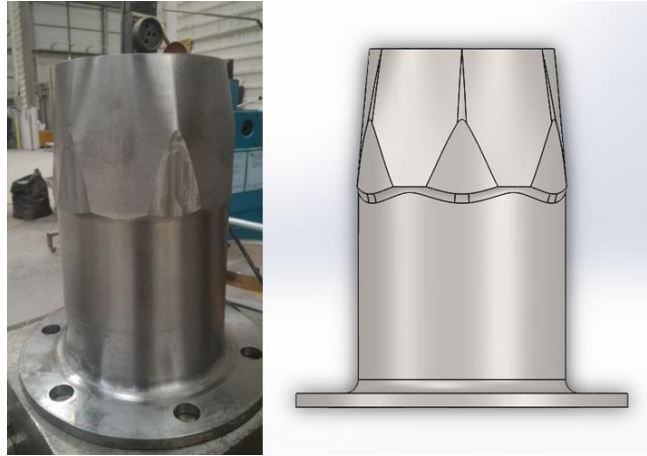
Figure 3.93: Trimmed end piece.

Unfortunately, no improvement was achieved over previous attempts as tow still tended to separate over conic hexagonal surfaces, which can be observed in Figure 3.94.

Figure 3.94: Winding on trimmed end piece.

At this stage, desired winding was not possible on the connection geometry of mandrel ends, even if various parameter changes and different setups are applied. Some partial improvement in the winding was noted in the setup with ringed pins without resin and masking tape similar to the one without pins where the resin and masking tape was present. It is interesting to note that winding is uniform and perfectly able to cover cylindrical surfaces in all winding conditions. That leads to the conclusion of the essence of our problem being the geometry of our coupling.

3.4.1.2 Draping analysis with ACP

In trial windings, circular sections were perfectly able to be wound upon whereas conic hexagonal end geometry was a problematic area. That points out the geometry as a source of the problem itself.

Layered composite structures are typically formed by placing reinforced plies against a mold surface in desired orientations. In the case of flat and singly curved surfaces, the orientation of the ply stays practically unchanged over the whole application area. When it comes to doubly curved surfaces, a ply can follow the surface only by deforming. In particular, dry and pre-impregnated woven fabrics can adapt to the shape of a doubly curved surface without use of excessive force. Deformation occurs with in-plane shear and up to certain deformation level, the shear stiffness of the fabric is insignificantly small. [46]

When a ply deforms by shearing to follow the surface, the fiber orientation changes. Different approaches have been developed for the simulation of the so-called draping process. [47] The need for draping simulation is twofold. Firstly, the manufacturability of the composite product can be assessed. Areas where the reinforcement cannot follow the surface are indicated and hence measures can be taken in design to avoid this. Secondly, the draping simulation gives the actual fiber orientations at any location in the model. This information is needed for accurate FEA of the structure.

The draping effect highly dependents on the manufacturing process. A few process relevant values can be defined in the ACP draping algorithm.

The draping algorithm minimizes the shear energy dissipation where an internal "Draping Mesh" is used for the evaluation. This mesh is independent from the structural mesh and has its own size. Analog to the structural mesh, the optimal "Draping Mesh size" is derived from the balance between the precision of the draping evaluation and the computational cost.

The result of the draping evaluation can be visualized on "Production Ply" and "Analysis Ply" level. The flat wrap and the draping mesh can be visualized. The contour plot of the draping shows the average shear (distortion) angle of each element (in degree). The last result of the draping are the draped fiber directions which are considered in the analysis. These directions can be visualized with the button "Show Draped Fiber Directions". This visualization combined with "Show Fiber Directions" highlights the influence of the draping, which can be seen in Figure 3.95. [46]
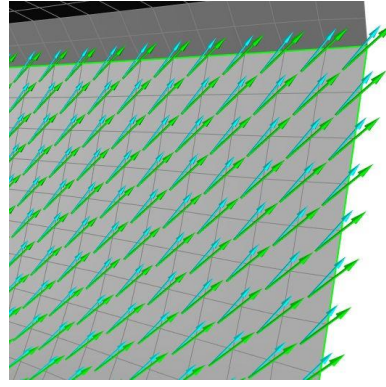
Figure 3.95: Defined and draped angle vectors [46] .

The draping tool indicates the shear stress in every element. In a case where a certain amount of shear stress leads to wrinkles or other undesired effects is strongly dependent of the fabric used. Therefore, the user (or the manufacturer of the fabric) must have knowledge about shear-limits for a specific fabric that still allows for reasonable draping. The final fiber angle can be nicely visualized and is of course considered in the analysis-model.

Draping procedure

The draping simulation in ACP uses an energy algorithm. In this approach, a reinforced ply is idealized with a pin joint net model. [48] [49] The net consists of unit cells, which are constructed of inextensible bi-directional fibers that are pinned together at crossover node points. The deformation of the fabric takes place by pure rotation of the fibers around the pins as illustrated in Figure 3.96.
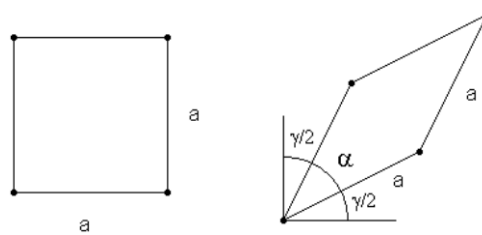
Figure 3.96: Deformation of the draping unit cell [46] .

In the draping simulation, draping unit cells are laid one by one on the surface of the model so that they are fully in contact with the surface. The draping procedure involves the search for two types of draping cells: those with two or three known node points as shown in Figure 3.97. In case of three known node points, the search algorithm seeks the fourth node point from the surface so that the distances along the surface to the adjacent node points are equal to the unit cell side lengths.
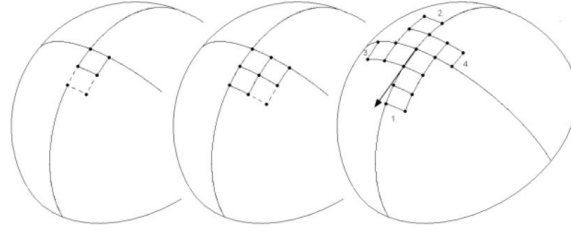
Figure 3.97: Draping scheme [46] .

Draping of a cell that has two or three known node points (left/middle) and propagation scheme using orthogonal directions (right).

When two node points are known and the locations of the other two must be determined, the search algorithm is based on the minimization of the shear strain energy [50]

$$minE = \frac{1}{2} G \gamma^2 \tag{3.5}$$

where G is the elastic shear modulus of the uncured reinforcement. The shear deformation is related to the angle α between the originally orthogonal fibers [47]

$$\gamma \approx \cos \alpha \tag{3.6}$$

The total shear strain energy of the draping cell is defined as the sum of energy computed at the four corners. The two constants can be excluded and the minimization problem becomes:

$$minE' = \sum_{i=1}^{4} \cos^2 \alpha_i \tag{3.7}$$

From this, the locations of the two node points can be determined with an iterative minimization algorithm.

The draping simulation starts from a given seed point and progresses in the given draping direction. In this phase each draping cell has initially two known node points. Draping cells are laid until the model edge is reached. Then, the procedure is repeated in the opposite direction (if applicable) and in the orthogonal directions, which is shown in Figure 3.97. After the main draping paths have been determined, the cells with three known nodes are populated. The algorithm resolves if the whole model is draped or if there are areas where the draping simulation needs to be restarted.

The simulation determines fiber principal directions 1. These directions are mapped to the finite element model to correct laminate lay-ups accordingly. The shearing angle β is defined as:

$$\beta = 90° - \alpha \tag{3.8}$$

It expresses the deviation from the ideal non-sheared case. The visualization of β values over the model surface is useful for depicting problem areas. For most fabric reinforcements, the maximum deformation angle alpha is 30-40 degrees. [51] When a fabric is sheared to a specific deformation level, the shear force starts to increase radically with only little increase in the shear deformation. This limit is called the locking angle. Beyond this limit buckling can be observed. The locking angle of a reinforcement can be determined experimentally. [52]

The pin joint net model is specifically developed for woven fabrics, but it has been proven to work for cross ply pre-preg stacks and also for single UD plies when the deformation is moderate. [53]

Implemented energy algorithm

In the adopted software implementation, the material draping behavior is controlled by draping coefficients *d0*, *d1* and *d2*. The coefficients are considered as weighting factors for the different draping modes. The three modes are: (Figure 3.98)

- Pure shear deformation of a regular woven fabric (mode 0).
- Parallel sliding in the fiber direction of a UD ply (mode 1).
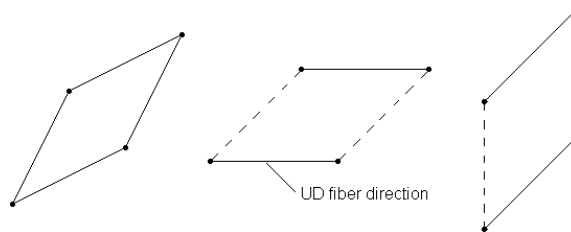- Parallel sliding orthogonal to the fiber direction of a UD ply (mode 2).

Figure 3.98: Draping modes: mode 0, mode 1 and mode 2 [46] .

A shear energy minimization routine is used to determine the draping mesh when the shear energy used in the minimization routine is the sum of the shear energy of every mode with the respective weighting:

$$E = d_0 \cdot E_0 + d_1 \cdot E_1 + d_2 \cdot E_2 \tag{3.9}$$

$$E_0 = \sum_{i=1}^{4} cos^2 \alpha_i \tag{3.9a}$$

$$E_1 = [\cos(\alpha_1) + \cos(\alpha_2)]^2 + [\cos(\alpha_3) + \cos(\alpha_4)]^2 \tag{3.9b}$$

$$E_2 = [\cos(\alpha_1) + \cos(\alpha_3)]^2 + [\cos(\alpha_2) + \cos(\alpha_4)]^2 \tag{3.9c}$$

The shear energy for the pure shear mode, *E0*, uses the expression in (3.9). The energy formulations for the parallel sliding modes, *E1* and *E2* are a derivation of this expression. They introduce a directional bias into the draping algorithm:
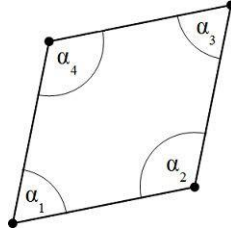
Figure 3.99: Angle notation for the draping energy algorithm [46] .

The pure shear mode is active by default. It is recommended to use the default coefficient values (1, 0, 0) for regular woven fabrics. For UD fabrics or an irregular woven fabric, it is recommended to set the drapability by adjusting *d1* and *d2* in combination and setting *d0* to zero. The draping coefficients can be any positive real number or zero.

Limitations of draping simulations

The draping simulation approach has the following limitations:

- The surfaces to be draped must be smooth. No sharp edges are allowed.
- The draping procedure does not change mechanical properties and the thickness of the ply.
- It is assumed that fabric transverse direction is perpendicular to the principal direction 1.
- The fiber slippage is a phenomenon that takes place after the locking limit and is noticeable only at relatively high deformation levels. The fiber slippage is not considered in this draping approach.

Investigation of end connection geometries

Draping analysis is carried out to investigate the effects of part geometry over winding characteristics. Based on the curvature of input geometry, outer surfaces are covered with a quad type mesh and draping angle is determined by the distortion of elements.

Various possibilities are investigated for current end connections. Half of the winding geometry of each part is modelled for convenience. Green arrows indicate the desired fiber orientation whereas blue ones indicate the result of draping analysis.

The first geometry to be investigated (Figure 3.100) was the conic hexagonal part which had been produced. It can be observed that fibers tend to drape in left to right and upwards. A fiber tow is evaluated to break apart when forced to be placed on surfaces which has different draping angles since tow is also a sum of fibers provided from different rovings. A narrower tow, made up from a single roving would be easier to place on production surfaces, however it could spiral up winding times. That might exceed gel time of our resin, decreasing tow width is still evaluated to be a solution though.
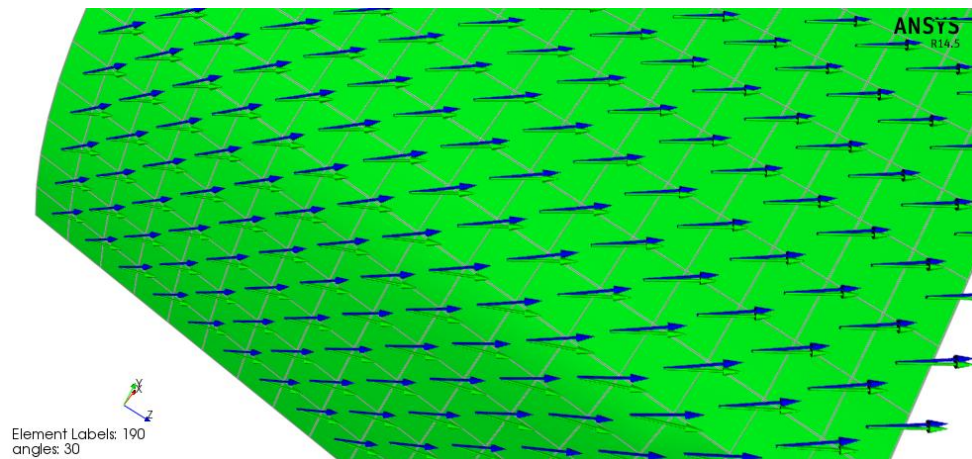
Figure 3.100: Draping distribution on conic hexagonal geometry.

Another reason for the spreading of the tow might evaluated to be conic peaks of hexagonal geometry. Sharp edges on that region were eliminated with a relatively large radius, which is visualized in Figure 3.101. There is a rather uniform distribution on the surfaces of hexagon whereas large angles of draping in an arbitrary fashion is observed over the radii. Changes on the geometry had no effect on the solution of the problem, in fact worsened it.
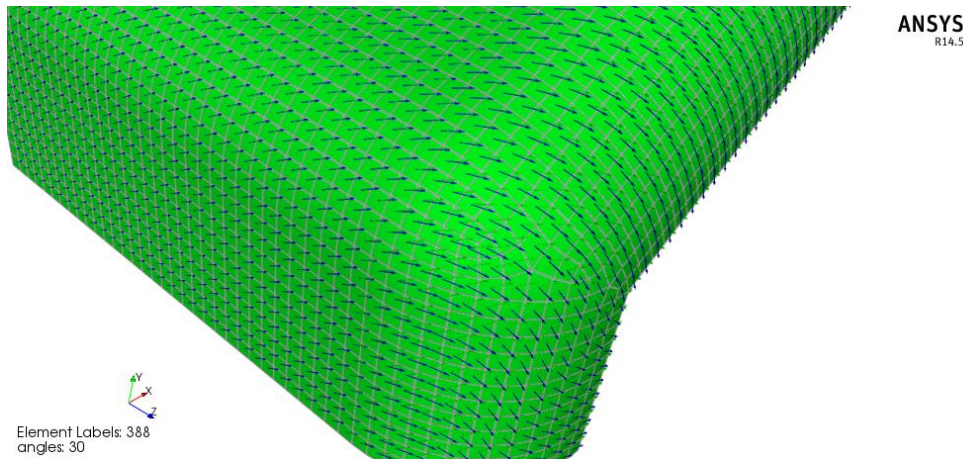
Figure 3.101: Hexagonal geometry with a large ending radius.

In order to provide a smoother transition, a part with hexagonal flange is investigated in the next step. Flange has a uniform distribution of draping, especially around the bottom right corner, a fact which can be evaluated in Figure 3.102. However, there has been no change over conic hexagonal, draping angles are decreasing going from left to downright nonetheless.
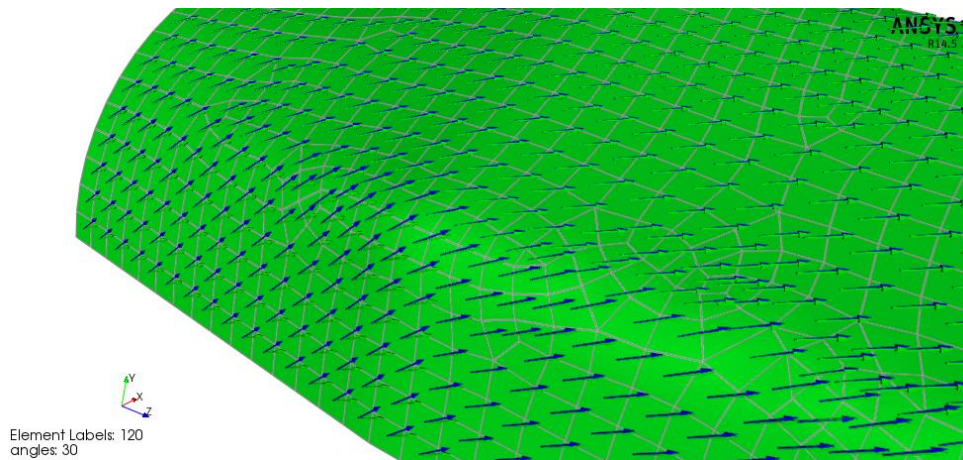

Figure 3.102: Conic hexagonal geometry with its flange.

It had been observed that uniform winding of the tow was achieved in all phases of trial winding over the cylindrical geometry in the middle of the mandrel. At that point, it is thought to provide a good benchmark point for draping analysis. A cylinder with a large radius on the end, which is given in Figure 3.103, is evaluated in the following step. There's a perfect uniform distribution and hardly any draping over the cylindrical geometry. However, radii regions continue to pose problems in keeping fiber orientations in desired direction.
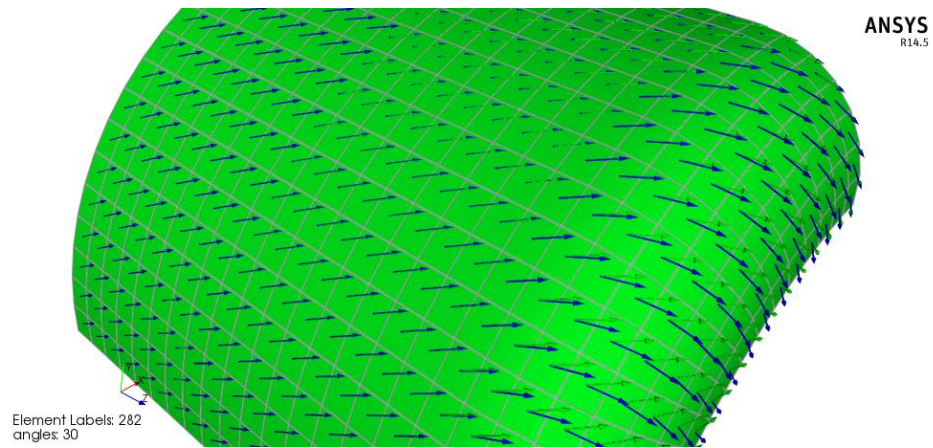
Figure 3.103: Cylinder with a large ending radius.

In the next model, a conical cylinder (Figure 3.104) is investigated for comparison purposes. Fibers started a tendency to drape over conical parts of cylindrical geometry. Moreover, distribution of draping angle is changing in the radial direction, which would force the tow again to spread into different parts. Judging from previous models, conicity and large values of radii are adverse factors when draping of the fibers is considered.
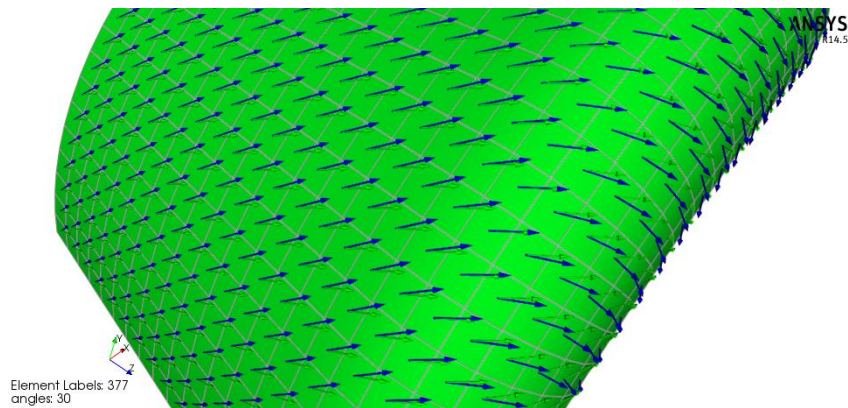

Figure 3.104: Conic cylinder with a large ending radius.

Some geometries involving symmetry (Figure 3.105) are evaluated in order to highlight its effect on draping.
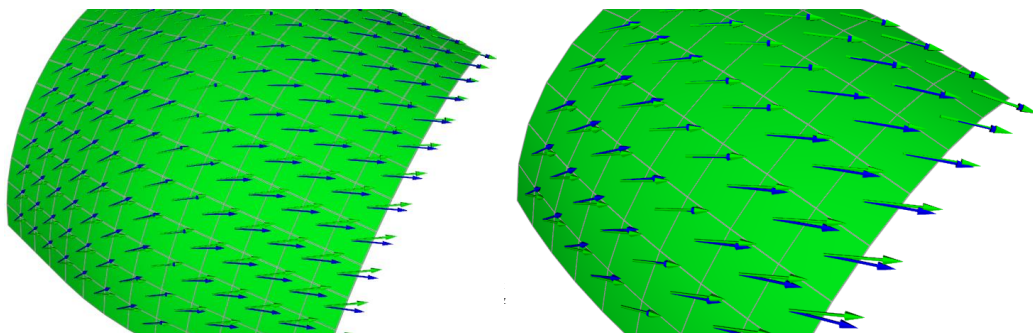
Figure 3.105: Symmetrical geometries.

99

As it can be seen in the figures; transitions in the radial direction, whether symmetrical or not, result in irregularities in draping angle of the fibers. It has to be realized that the important point is to have a uniform distribution of draping rather than eliminating it. In the case of a uniform distribution of draping, fibers in the tow would stay in the same orientation even if they had slightly been deviated from desired orientation. It is the most ideal situation to have a perfectly uniform distribution with little or no draping. Since we are attempting to create a coupling between composite tubing and interface part, draping of the fibers might be allowed to some extent due to the deviations from cylindrical geometry.

Current geometry of conic hexagonal is investigated again with restricting the conical transition to a limited length of the part and increasing the number of edges in order liken it to a cylinder, which is provided in Figure 3.106.
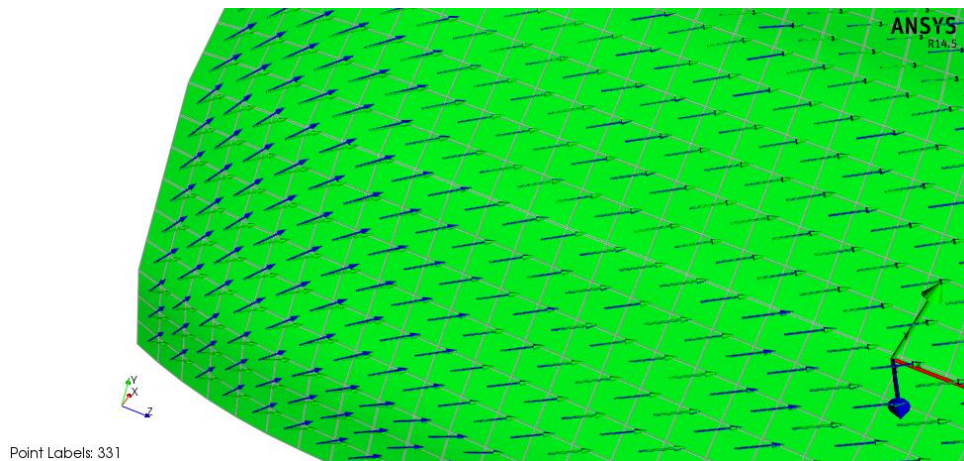
Figure 3.106: Polygon with 18 edges.

Conicity was removed and edge count is increased to 18 in the latest configuration. It was observed that there is little or no draping with a perfect distribution over polygonal geometry, however problems continued to persist over transitional region.

Another polygonal section comprising of three eccentric circles (Figure 3.107) is constructed. They are connected with tangent lines in order to avoid bridging between them. Polygonal geometry yielded similar results to the previous step. As a side note, draping happens to a lesser extent in the current part than previous one, when carefully examined. It might be explained that current geometry behaves more likely as a cylinder than the previous one.
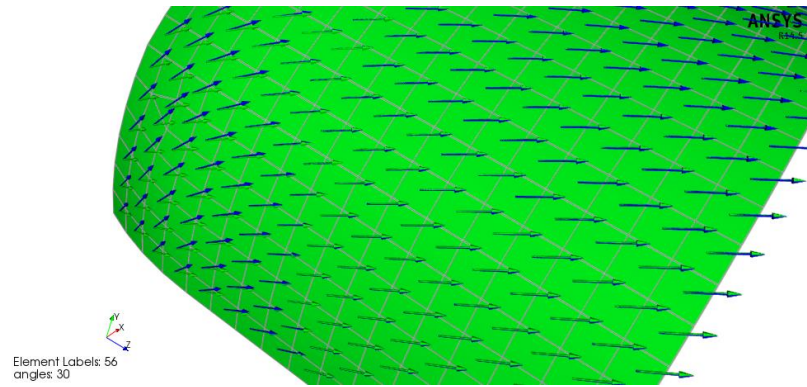
Figure 3.107: The other polygonal geometry.

Conic hexagonal part was trimmed in order to eliminate sharper edges during trial windings. Some complex geometries had been obtained further coarsening the mesh over the part, which can be seen in Figure 3.108. It would be noted that there is little or no considerable change over hexagonal region, however the transition after conic hexagonal is greatly improved. Since draping of the fibers continue to vary from left to the up right direction of the part, it might be predicted that draping problem would continue to persist with a trimmed configuration of conic hexagonal part.
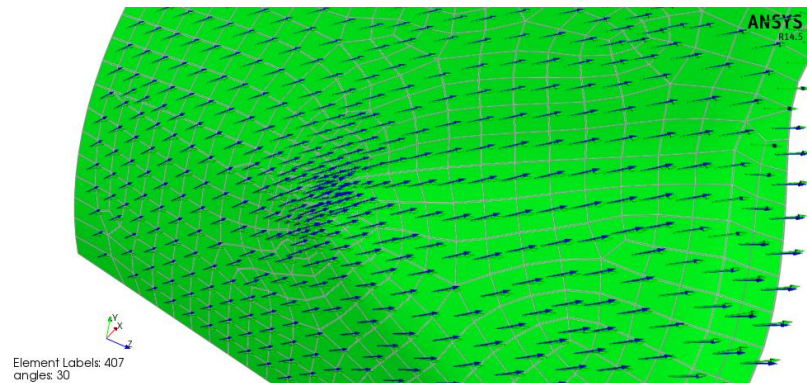
Figure 3.108: Trimmed conic hexagonal geometry.

3.4.1.3 Trial windings with 3-D end connection with polygonal section

After the problems encountered with connection geometry during trial windings and evaluation of it by draping analysis, a new connection part with a polygonal section is designed. A sample was manufactured by 3-D printing for trial windings, which is shown in Figure 3.109.

Figure 3.109: 3-D print part for trial winding.

At a point, extending mandrel length was also discussed, thinking that a longer path of return would better allow the fiber tow to follow the connection geometry. For that purpose, flanged connection part was utilized as an addition to the mandrel, posing as an extended part of the mandrel. A better quality of winding has been achieved over the new section of connection geometry, results can be seen in Figure 3.110.
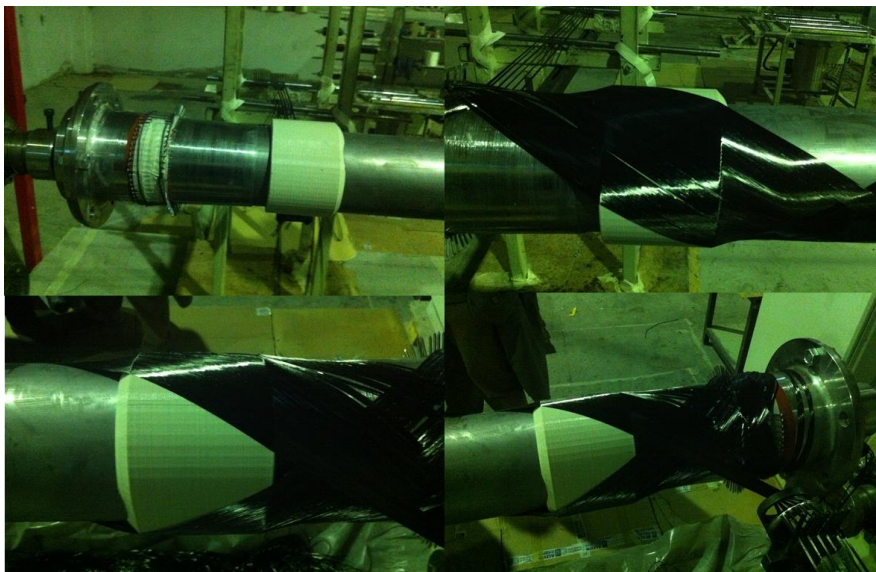

Figure 3.110: Trial winding with 3-D print part.

3.4.1.4 Winding of the prototype driveshaft

In the beginning conic hexagonal geometry was deemed suitable for production of the shaft with filament winding method, however all the attempts have proven otherwise. Existing connection parts had been decided to be machined into conic cylinders so that the production for the first shaft would be possible. It is thought to be a "rehearsal" for winding and removal operations together with the calibration of the test rig. Latest mandrel configuration is seen in Figure 3.111

Figure 3.111: Latest configuration of mandrel and end connection parts.

Winding of the first prototype driveshaft was carried out in order to avoid problems encountered during trial windings. Cylindrical and end sections of the mandrel can be seen during the winding of the first ply in Figure 3.112.

Figure 3.112: Trial winding in latest configuration.

Prototype shaft can be seen, just after the completion of winding process, in Figure 3.113.

Figure 3.113: Prototype driveshaft after winding operation.

Upon completion of the winding process, curing cycle has been initiated in oven. Winding has spent 2h at 90°C + 4h at 150°C in addition to a 4h of heating up and cooling down times. Curing took a total of 10h, resulting in a properly cured composite which has good visual appearance, especially around cylindrical regions of the torque tube. After mandrel removal and some trimming operations, the first prototype driveshaft is presented in Figure 3.114.

Figure 3.114: Prototype driveshaft after mandrel removal and trimming.

4. TESTING OF THE DRIVESHAFT

Static and fatigue testing of the driveshafts are planned, as mentioned before. A torsion test rig is to be employed on the MTS322.21 universal testing system, which is present in Composite Structures Lab. / Faculty of Aeronautics and Astronautics of ITU, for this purpose.

MTS322.21 is a testing device which is able to produce an axial force of ±100kN maximum. An axial force alone is not useful for torsion testing of a shaft, for which a torque arm thought to be utilized for that purpose, which is shown as a schematic in Figure 4.1. Test rig and related components are designed and modelled in CATIA V5 environment. FEA to prove its strength of design torque was carried out in ANSYS Workbench environment.

Key
1. Shaft
2. Universal Joint
3. Connecting Plate
4. Bearing Unit
5. Bearing Billet
6. Torque Arm
7. Universal Joint Bolt
8. Bracket Bolt
9. Bearing Billet Bolt
10. Bearing Unit Bolt
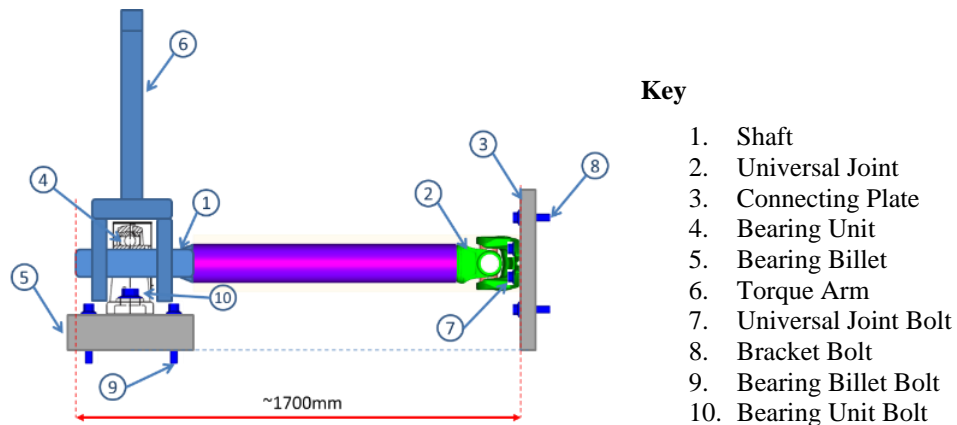
Figure 4.1: Initial schematic proposed for the setup.

An initial design for the proposed setup was devised, which is shown in Figure 4.2. It is based on the utilization of a torque arm in order to obtain a torque loading from an axial force, which had been mentioned before. In order for this idea to work, shaft and related components should be properly joined and supported, utilizing bearing units and other joints.
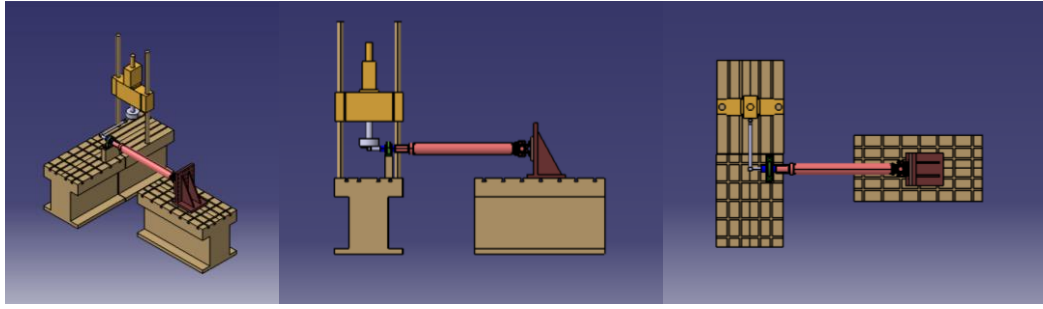
Figure 4.2: Initial model of the test rig on MTS322.21.

4.1 Design of a Torsion Test Rig

4.1.1 Theoretical calculations

Bending of the torque arm is a fundamental problem due to a very high value of testing torque, which requires very large cross-sections to be employed by traditional approaches. However, that would pose another problem, since supporting and joining large sections with bearings is not an easy task.

A preliminary calculation was carried out in order to have an idea about selection of cross-section for the torque arm. Deformation and stresses of various cross-sections; a circular, rectangular and I-beam, were calculated and compared. A rectangular section is evaluated to provide a favorable solution, regarding lower values of stress/strain in addition to the ease of manufacture and assembly with other components.

Theoretical calculations had been carried out in EXCEL software, which were compared with FEA results obtained in ANSYS Workbench environment. Comparison of these two solutions are provided in Table 4.1 which shows that stress and deformations are generally in conjunction.

Table 4.1: Sections evaluated for torque arm.

	Circular Section		Rectangular Section		I-Beam		
	Theoretical	FEA	Theoretical	FEA	Theoretical	FEA	
W_b	2,66E+05		2,44E+05		3,23E+05		[mm^3]
I	1,99E+07		2,79E+07		2,83E+07		[mm^4]
y	1,045	1,171	0,747	0,726	0,737	1,191	[mm]
σ_b	188	188	205	139	155	167	[N/mm^2]

In Table 4.1, W_e is the bending moment of inertia, I is the moment of inertia, y is deflection and σ_b is bending stress.

106

A rectangular section has been decided to be employed as a torque arm, due to its decent strength and ease of support/joinability with other components. An I-Beam would create problems in that regard and a circular cross-section would not provide adequate strength.

In addition to the clevis-pin assembly and torque arm, bearing unit and its billet is an important component of the setup. A self-aligning bearing unit had been thought to be utilized, however the idea is abandoned due to the lead times specified. A bronze bushing mounted in a steel slab is utilized instead. Test shaft is raised to the position by bearing billet mounted below. Test rig components and its assembly on MTS322.21 are presented in Figure 4.3.
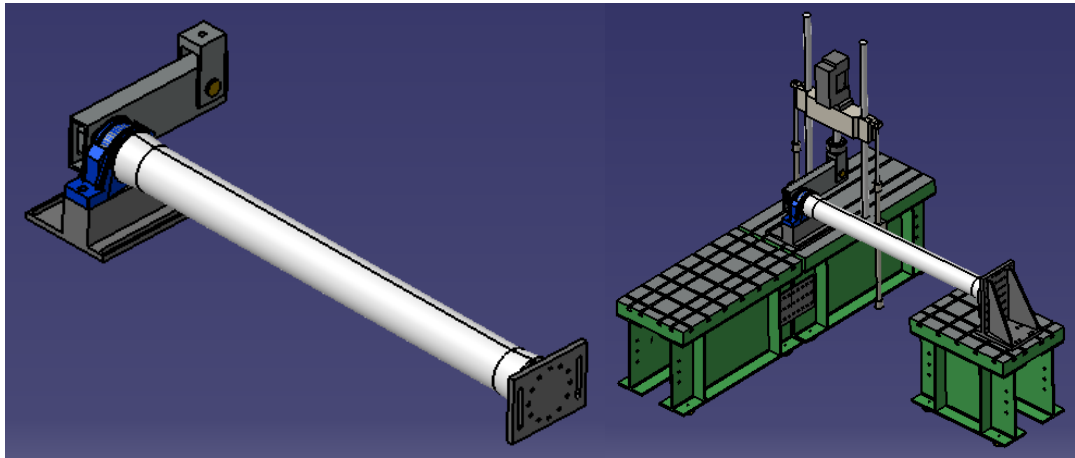
Figure 4.3: Components of test rig and assembly on MTS322.21.

4.1.2 Finite element analysis of test rig components

Submodeling technique is implemented in FEA of test rig elements. Modelling of all components in a single file would require a lot of time and processor power and most likely to include singularities due to complexities in geometry and contact status. Each component of the structure is modelled separately predicting the boundary and loading conditions. In that way, a more detailed analysis of parts would be provided in addition to saving valuable time.

Models are meshed with default options in the beginning and the software is configured to refine meshing structure according to convergence history, same as previous analysis of end connection parts. By that way, denser meshes would be created exactly where they are needed and it also provides a chance to investigate convergence status of the model.

4.1.2.1 Clevis and pin

Clevis and its pin is investigated as a start. Clevis-pin assembly is connected to load cell and MTS322.21 by a stud. Model is fixed on the hole and loading is applied on pin surface as a bearing load.

Clevis and its pin are investigated as a first case. Clevis is connected to the load cell, so to the MTS322.21 via a bolt. Pin is secured inside clevis hole. Situation has been modelled that clevis is fixed around the hole where it is connected to the load cell and force is applied around pin as a distributed bearing load. A quarter part of the structure is modelled utilizing symmetry in two planes.

As mentioned before, meshing structure is rather coarse in the beginning. In latest step of convergence, it could be seen that a lot finer mesh than the initial one is created by the software.

Contact between clevis and pin is modelled as bonded in the first step. Deformations in x and y axes, provided in Figure 4.4 and Figure 4.5, are rather small. In contrast, maximum von Mises stresses in the model continuously increases with increasing element count. Stresses tend to build up around circle in contact with pin, reading a maximum stress of 201MPa in latest step. It looks like the stresses yielded by analysis around that region is not in contact with reality. Distribution of von Mises stress are given in Figure 4.6.
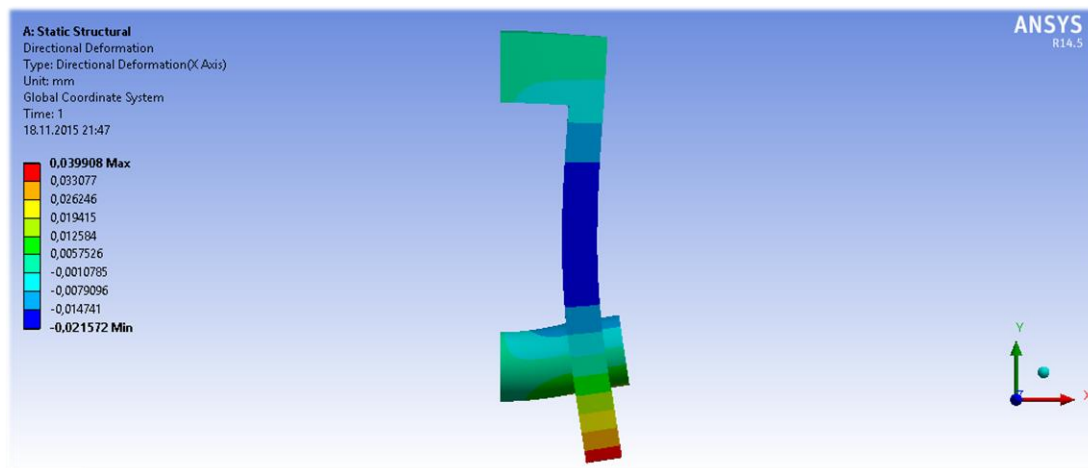
Figure 4.4: Deformation of clevis and pin in x-axis.
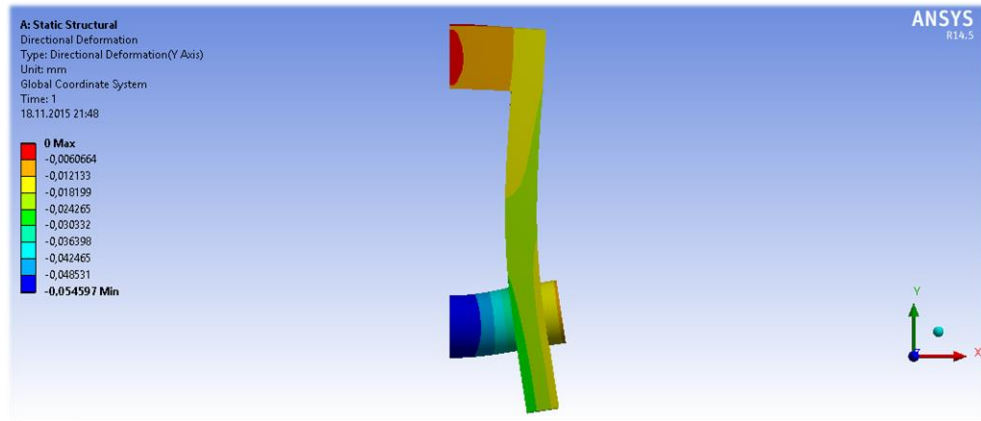
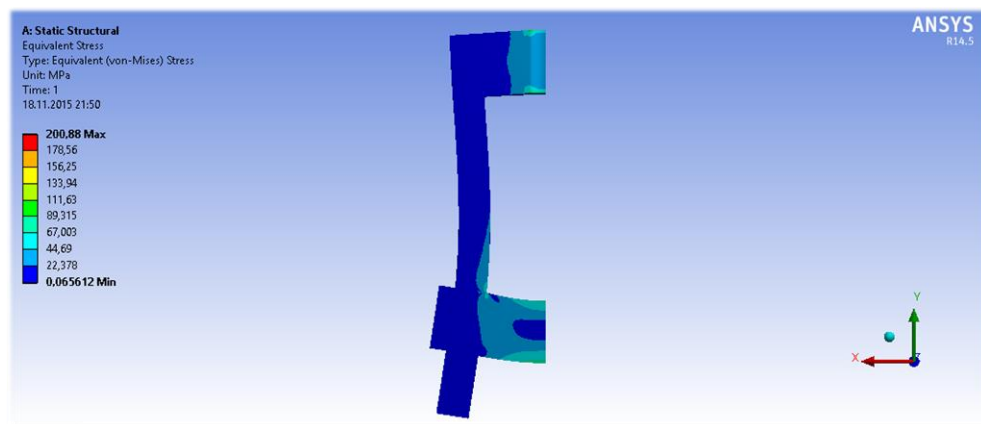**Figure 4.5:** Deformation of clevis and pin in y-axis.

Figure 4.6: Distribution of von Mises stress on clevis and pin.

Stresses build up around the pin housing on clevis (Figure 4.7), FEA is trying to converge to infinite stress due to a very sharp edge (Figure 4.8). This is a singularity situation due to geometry. A frictional contact with a coefficient of 0.16 is defined in a new model. Bonded contact might have further increased stresses around contact edge, constraining relative motion of pin and clevis.
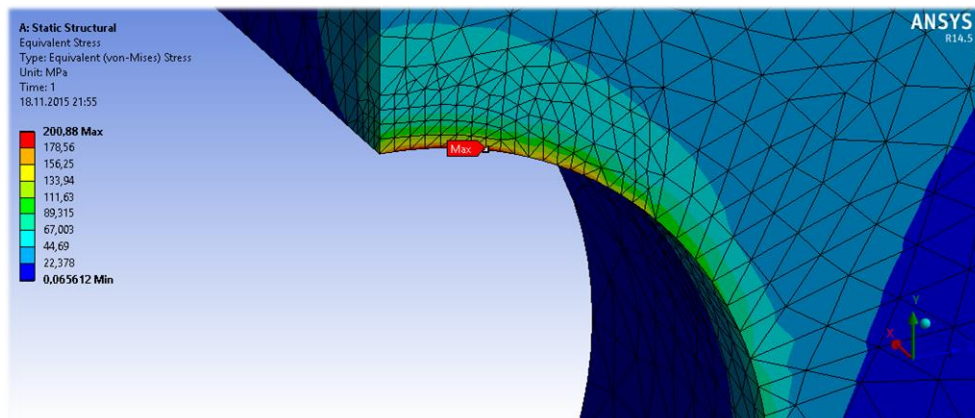

Figure 4.7: Singularity region on clevis.

109
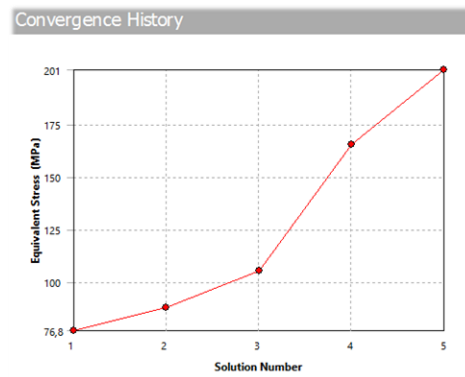
Figure 4.8: Convergence history of clevis and pin.

Distribution of von Mises stress in frictional contact situation is given in Figure 4.9
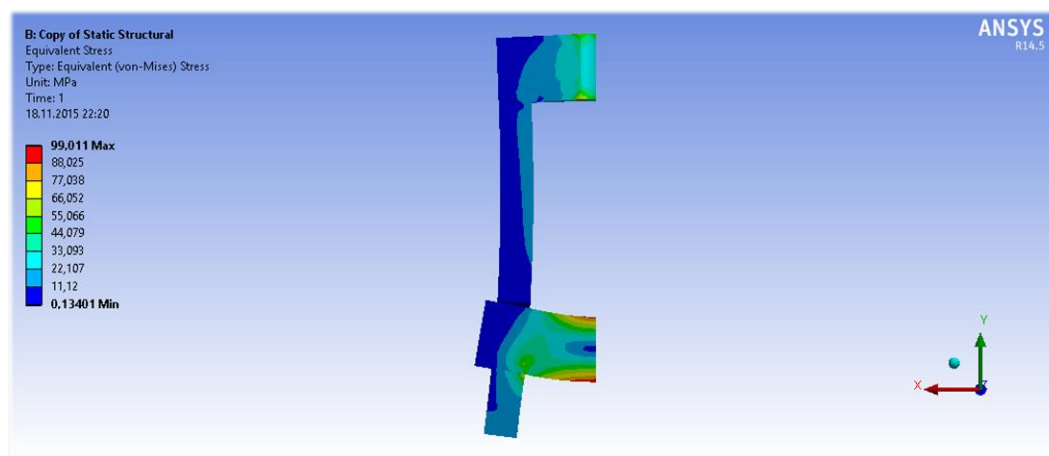
Figure 4.9: Distribution of von Mises stress in frictional contact situation.

It is seen that model easily converged in frictional contact situation (Figure 4.10). In that case contact status and pressure needs to be investigated. It looks like most of the contact area in near or sliding status. Contact pressure is mostly around 15MPa, which sounds reasonable.
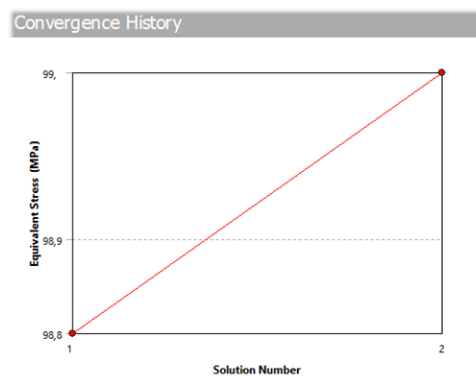
Figure 4.10: Convergence history of clevis and pin in frictional contact.

110

4.1.2.2 Torque arm

Torque arm is comprised of four different parts, welded with each other. A U-shaped profile is closed with a plate, then a slot and a billet is welded into it. Because of welded joints, all the contacts in the structure are defined as bonded. Contact status may again constitute a source of singularity in this model. Weld beads are not modelled and a perfect bonding is assumed to be provided between welded parts.

Torque arm is modelled as a single and symmetric body. It is fixed on inner surfaces of billet and design loading of 70kN is applied on flat surfaces of slot. Mesh is again refined in higher stress regions, according to convergence steps. A displacement around 1mm is obtained in y-axis, which can be seen in Figure 4.11, that could be presumed rigid for a body of this size. It is seen that von Mises stress are concentrated around billet edges.
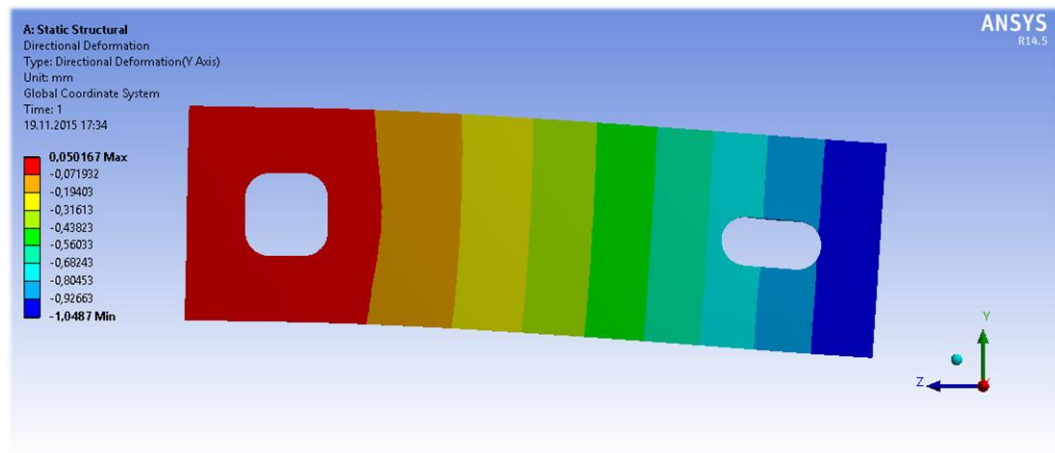

Figure 4.11: Deformation of torque arm in y-axis.

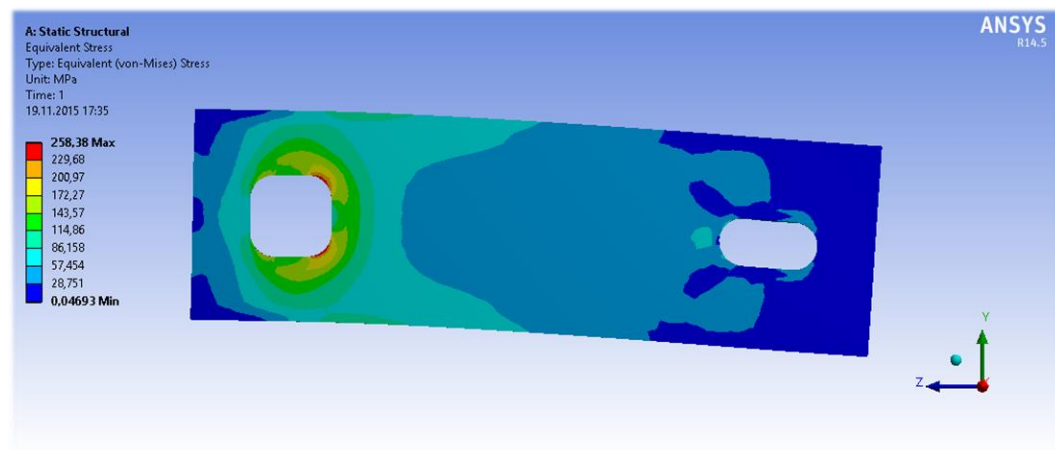Distribution of von Mises stress on torque arm is provided in Figure 4.12.

Figure 4.12: Distribution of von Mises stress on torque arm.

111

Torque arm model has converged in a mere three steps, which are shown in Figure 4.13. Difference is less than 1% in latest two models. Two iterations proved enough to show convergence.
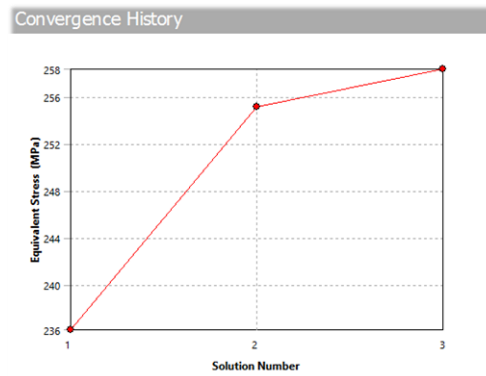

Figure 4.13: Convergence history of torque arm.

4.1.2.3 Shaft

Shaft is the component which would transmit the torque from torque arm to the driveshaft. It has a rectangular section in the ends while it is a cylinder of 100mm diameter in the middle. Shaft is fixed in one rectangle and testing torque of 35000mm applied on the rectangle in the other end.

Deformation in circumferential direction and distribution of von Mises stress on the shaft is shown in Figure 4.14 and Figure 4.15 respectively. Deformations and von Mises stresses are rather larger than expected, concentrated around where cylinder and rectangles meet.
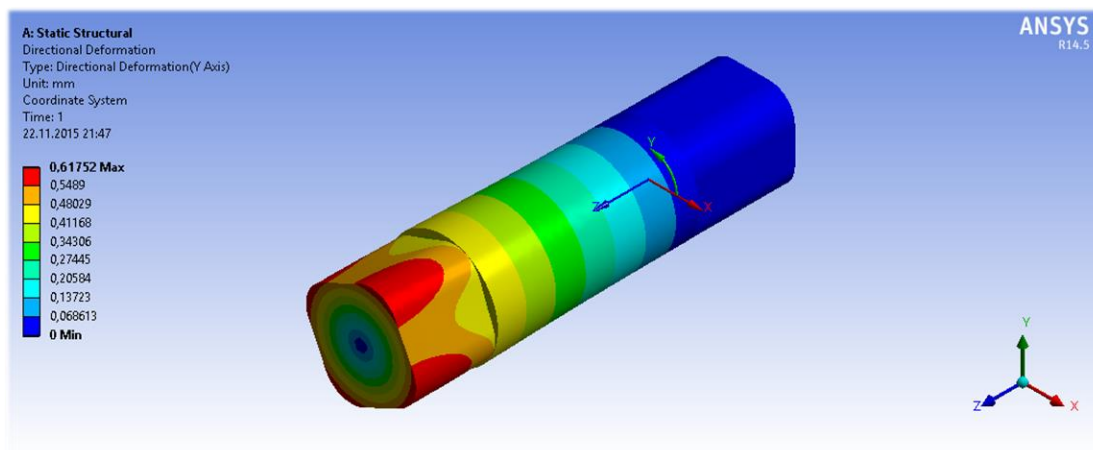

Figure 4.14: Deformation of shaft in circumferential direction.
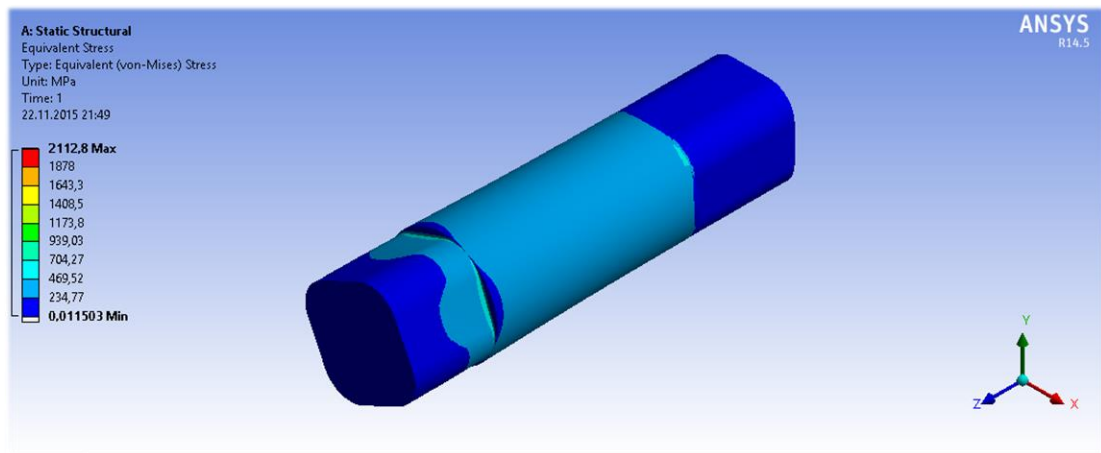
Figure 4.15: Distribution of von Mises stress on shaft.

Further inspection of convergence steps reveal that for decreasing mesh size stresses tend to increase around these regions which indicates the existence of a singularity, shown in Figure 4.16 and Figure 4.17.
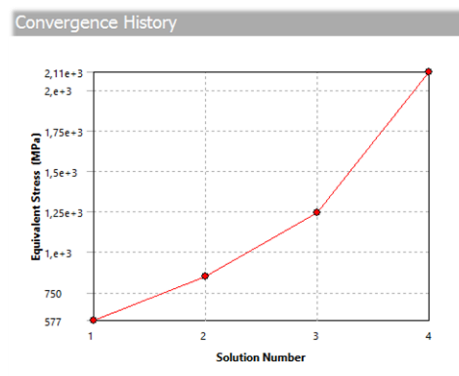

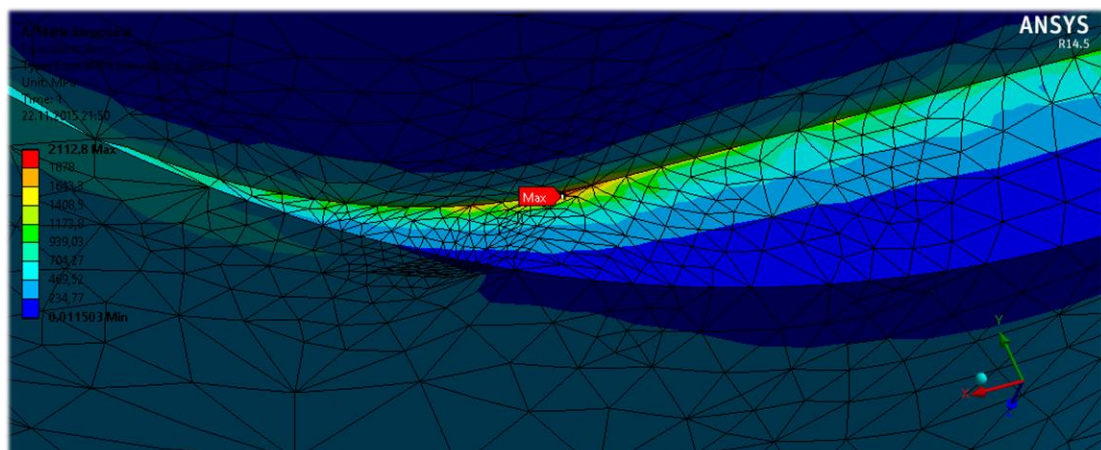**Figure 4.16:** Convergence history of shaft.

Figure 4.17: Singularity region on shaft.

It is evaluated that singularity is a result of geometric transition. Definition of radii on these regions could not be able to eliminate singularity, marginally improving the situation. Source of the singularity is geometric; however, the same geometry is not suitable for a more appropriate transition. Thus a nonlinear material model would be employed in order to relieve stress singularity around problematic geometry.

Deformation of the model in circumferential direction is shown in Figure 4.18 and distribution of von Mises stress are provided in Figure 4.19. It is observed that deformations increased marginally due to some plastic strain due to material nonlinearity; however, maximum von Mises stress on the structure decreased to 291MPa, in a substantial fashion. Deformations and stresses on the cylinder is pretty much the same for both linear and nonlinear situations.
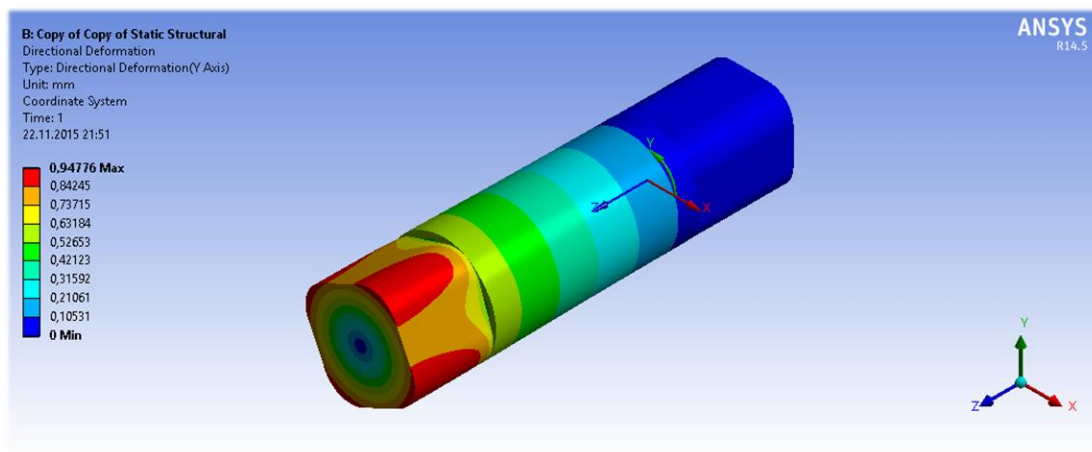
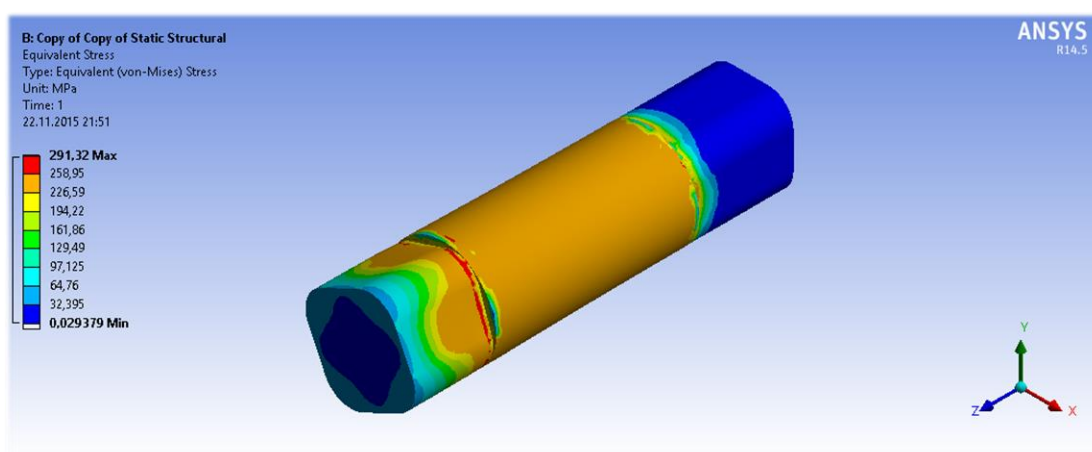**Figure 4.18:** Deformation of nonlinear shaft in circumferential direction.

Figure 4.19: Distribution of von Mises stress on nonlinear shaft.

Convergence steps in Figure 4.20 reveal that the model is convergent. Figure 4.21 shows a plastic strain of 2.5% which is lower than fracture strain value of the material, still a considerably high value. It is clear that if the maximum torque of 35000Nm is imposed on test rig shaft, some plastic deformations on a visual level could occur.
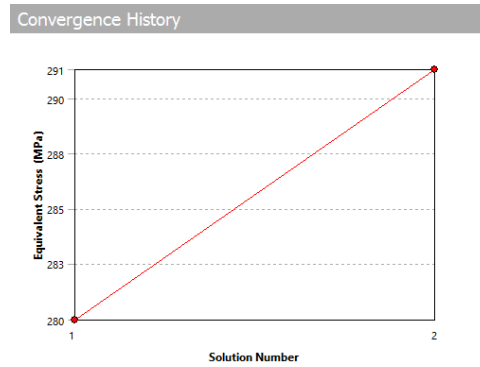

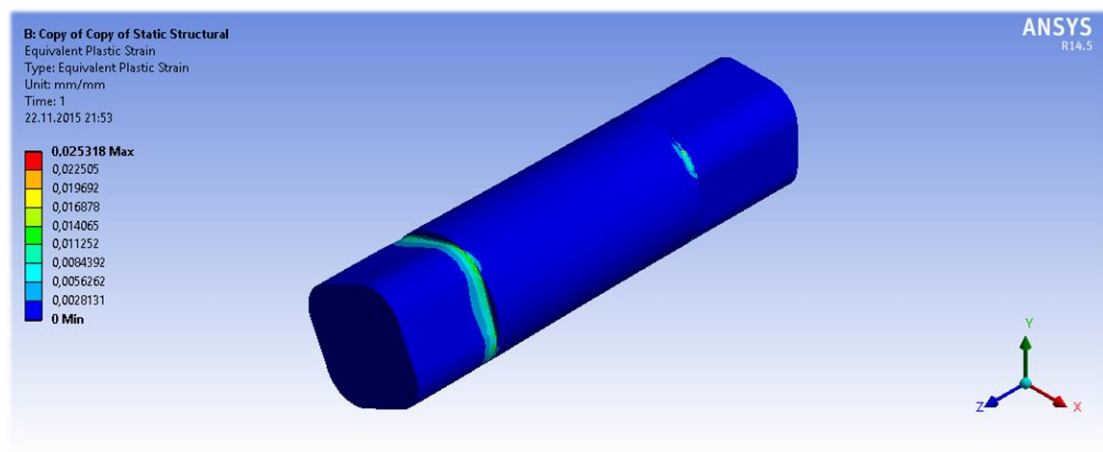**Figure 4.20:** Convergence history of nonlinear shaft.

Figure 4.21: Plastic strains on nonlinear shaft.

4.1.2.4 Bearing billet

Bearing billet is the component supporting bearing unit and the bearing itself. It is manufactured of two different bodies, modelled as a single body in structural analysis though. As an apparent source of singularity, some edges are given some small radii.

Billet is fixed on its sledges and a force of 70kN in y direction and a bending moment of 700Nm around x axis is imposed on the surface which the bearing would be mount. A frictionless support is defined on the bottom surface of the part.

Deformations in x and y directions are marginally small, shown in Figure 4.22 and Figure 4.23 respectively. It could be assumed rigid for a part of that scale.
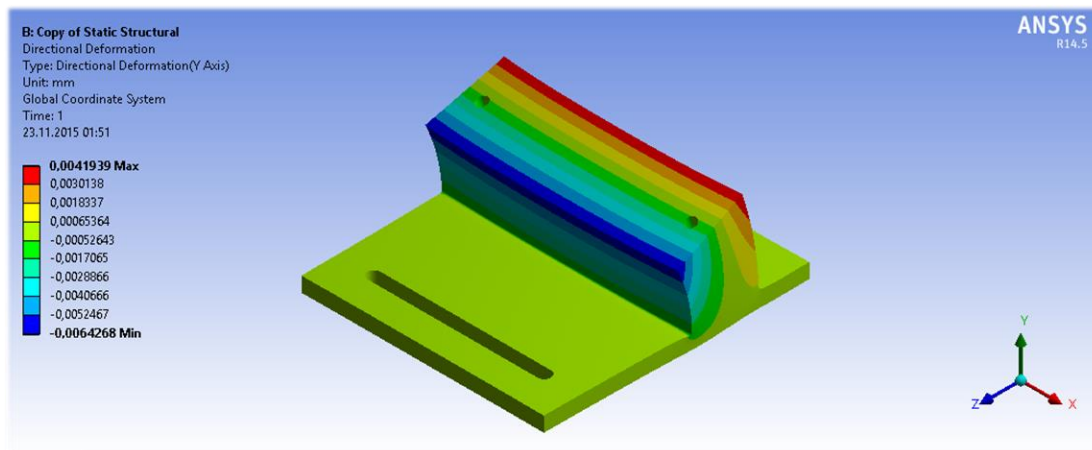
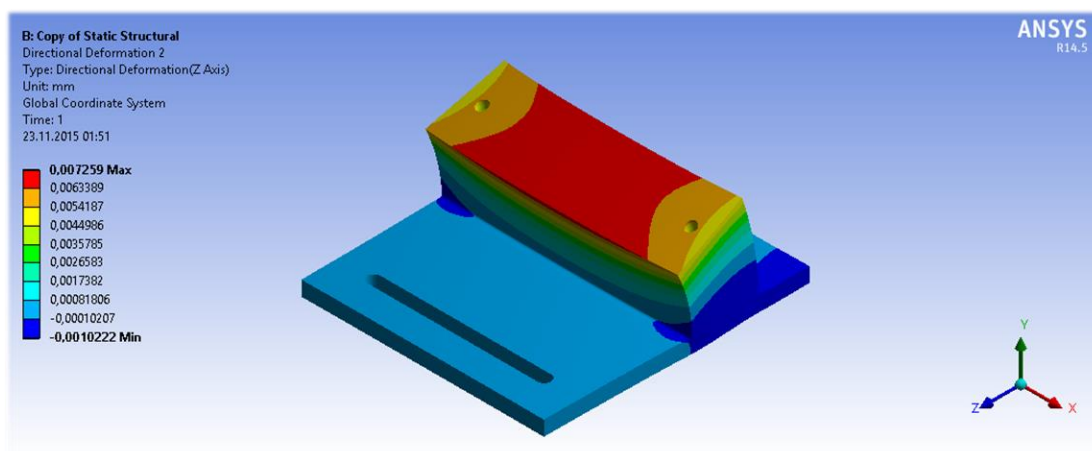**Figure 4.22:** Deformation of bearing billet in y-axis.

Figure 4.23: Deformation of bearing billet in z-axis.

Maximum von Mises stress present on the model, given in Figure 4.24, is 18MPa, which is way below the yield stress of the material. Convergence steps in Figure 4.25 shows that the model is convergent.
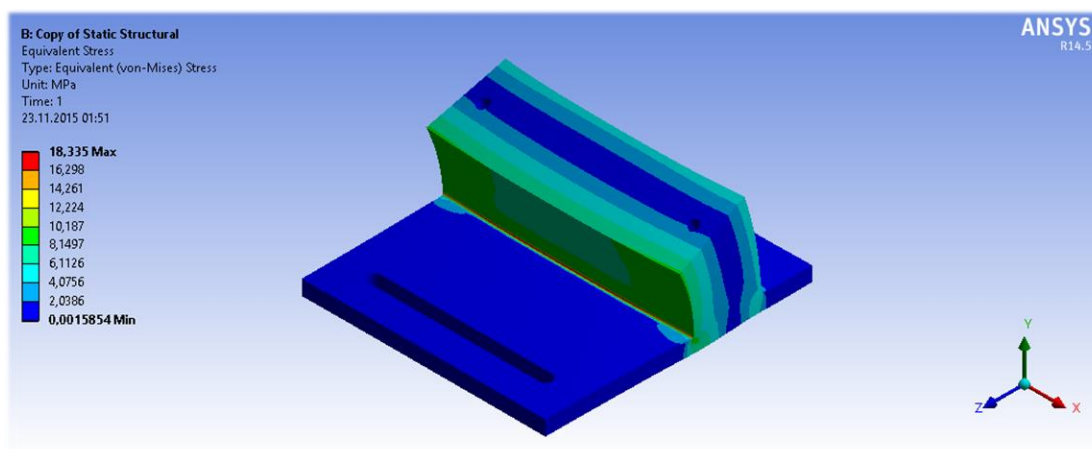

Figure 4.24: Distribution of von Mises stress on bearing billet.
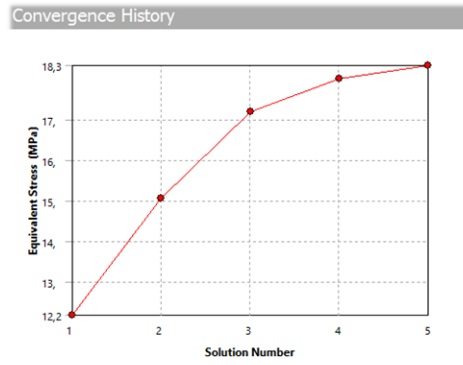
Figure 4.25: Convergence history of bearing billet.

4.1.2.5 Bearing unit

Bearing unit is mounted on the bearing billet and it is the structure that carries the bearing itself. It is fixed by two bolts on the bearing billet, and the bushing is mount in the central hole.

Deformation of the bearing unit model, in x and y directions, are presented in Figure 4.26 and Figure 4.27 respectively.

Figure 4.26: Deformation of bearing in y-axis.

Figure 4.27: Deformation of bearing in z-axis.

117

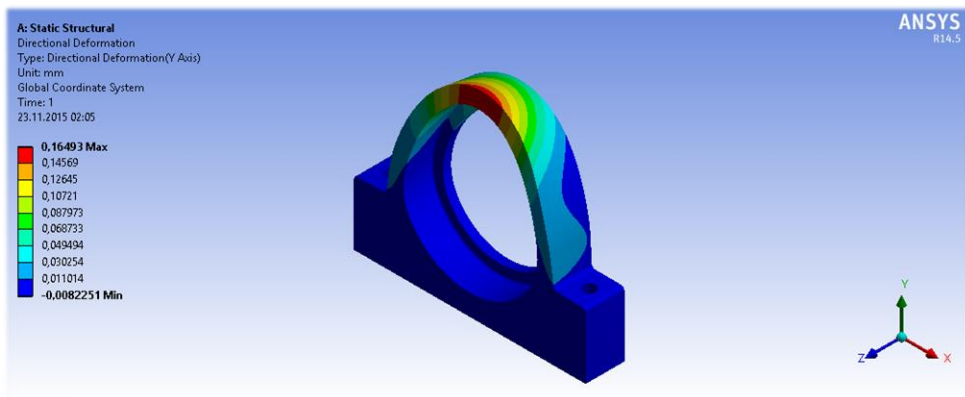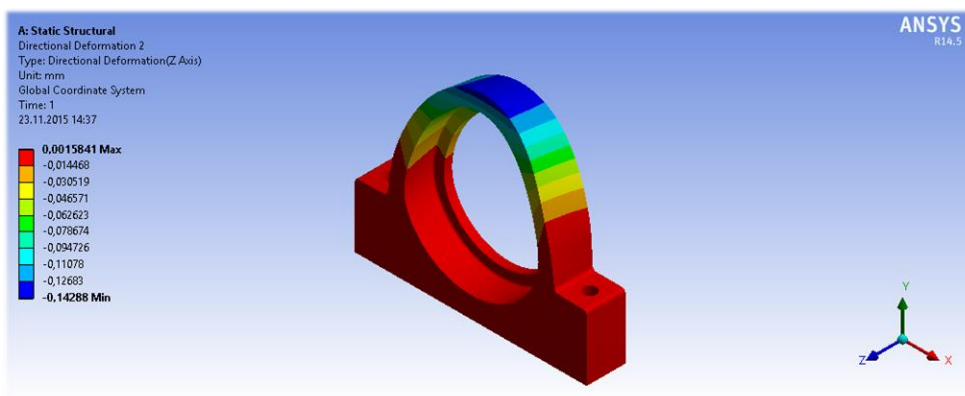It is understandable that vertical displacement is much larger than the lateral, since the bearing force is applied on the same direction. Situation poses no problems since the magnitudes are marginally small values.

Figure 4.28 reveals von Mises stress distribution on the bearing unit. Maximum stress present on the model is 212,5MPa which is a little bit close but still lower than the yield strength of the material.
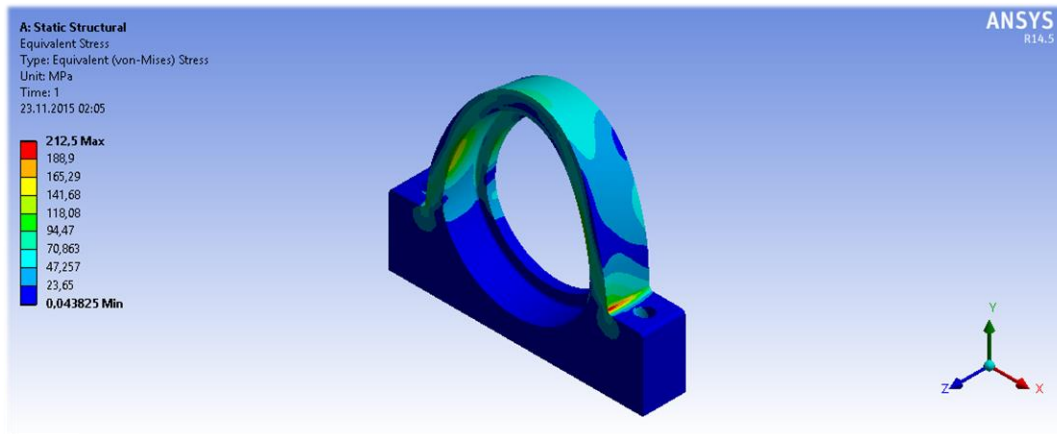
Figure 4.28: Distribution of von Mises stress on bearing.

4.1.2.6 Connecting plate

As the last remaining component of the test rig assembly, strength of the connecting plate is investigated. Plate is fixed by the sleds and testing torque of 35000Nm is imposed on the bolt holes. A frictionless support is present on the rear face of the body, in the place of a bracket.

Deformation of the model in circumferential direction is presented in Figure 4.29 while distribution of the von Mises stress over the body is shown in Figure 4.30.
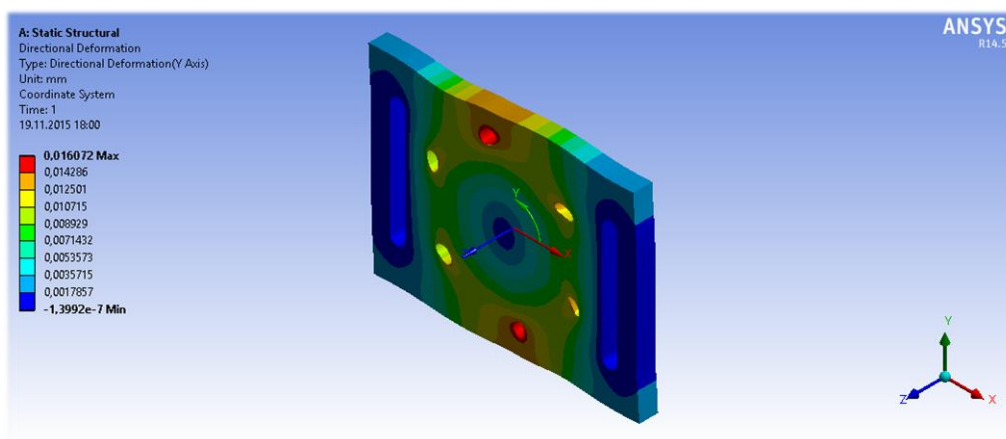
Figure 4.29: Deformation of connecting plate in circumferential direction.
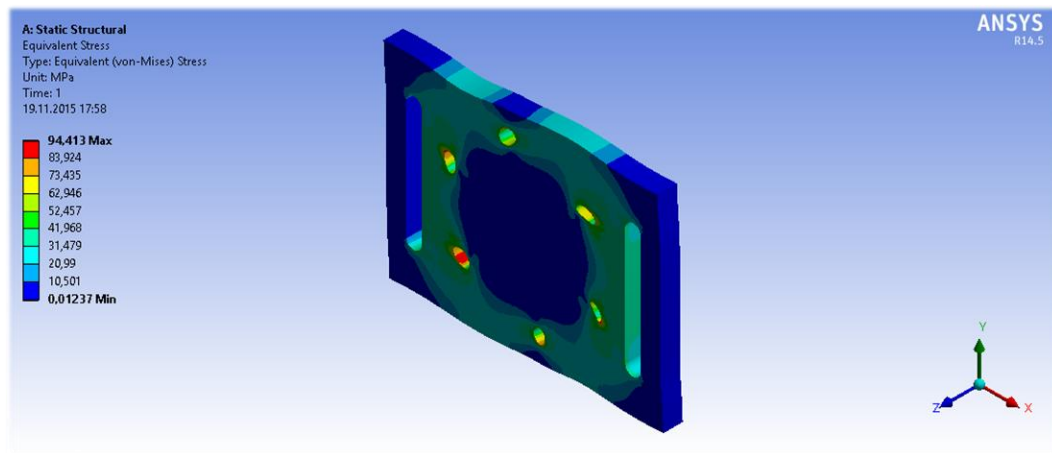
Figure 4.30: Distribution of von Mises stress on connecting plate.

It is predictable that element count and stress values are concentrated around sockets. Deformations in circumferential direction are low and a maximum stress of 94,8MPa is reached after two iterations in Figure 4.31, which shows the model is convergent.
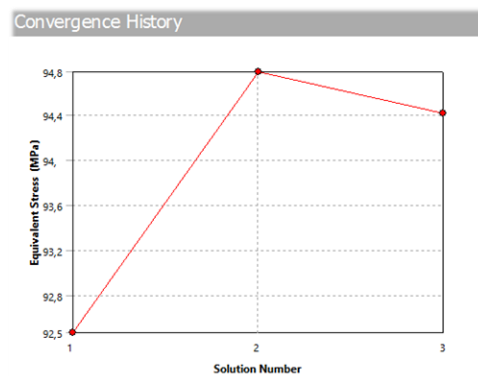
Figure 4.31: Convergence history of connecting plate.

4.2 Static and Fatigue Testing of the Prototype Driveshaft

Prototype driveshaft is ready for testing; however, test rig is still waiting for assembly until the date due to ongoing tests on MTS322.21 universal testing machine. Manufactured components can be seen in Figure 4.32.

Figure 4.32: Test rig components awaiting assembly.

5. CONCLUSIONS AND RECOMMENDATIONS

In this paper, design and analysis of a single piece composite driveshaft that would replace a 2-piece steel driveshaft for a heavy weight vehicle is achieved. 28 kg of weight is saved in total, which constitutes to 35% of the structure. Design requirements are fulfilled, except for the natural frequency which might be attributed to the lower moduli of the production material. Bear in mind that it is achieved with a material that has inferior properties than expected. There is still room for further weight savings through improvement of material properties by better production process. Better planning of the filament winding process would yield a production material with better properties resulting in further weight savings and a higher natural frequency for a production shaft.

REFERENCES

[1] **Ford Otosan**, Driveshaft Training, 2015

[2] **Leslie, J. C., Troung, L., Blank, B., & Frick, G.** (1996). *Composite driveshafts: technology and experience* (No. 962209). SAE Technical Paper.

[3] **Talib, A. A., Ali, A., Badie, M. A., Lah, N. A. C., & Golestaneh, A. F.** (2010). Developing a hybrid, carbon/glass fiber-reinforced, epoxy composite automotive drive shaft. *Materials & Design*, *31*(1), 514-521.

[4] **Lin, K. Y.** (2014). *AA432x – Composite Materials Overview for Engineers*, University of Washington, Massive Open Online Course Notes.

[5] **Skinner, M. L.** (2003). *The Economics of Composites focusing on focusing on Filament Winding & Pultrusion Filament Winding & Pultrusion*, Skinner Creative Inc.

[6] **Pollard, A.** (1999). Polymer matrix composite in drive line applications. *GKN technology, Wolverhampton*.

[7] **Mazziotti, P. J.** (1965). *Dynamic characteristics of truck driveline systems* (No. 650189). SAE Technical Paper.

[8] **Rossoni, A.** (1990) *Vibration Analysis of #4 MSP Drive Train.* ASR Analysis

[9] **Szadkowski, A., & Naganathan, N. G.** (1994). *TORAN™: A Comprehensive Simulation Tool for Driveline Torsionals* (No. 942322). SAE Technical Paper.

[10] **Keys, C., Kinkler, W., Santiago, A.** (2006) *Composite Driveshaft: Efficiency, Safety, and Economics*. Texas A&M University, Kingsville.

[11] **American Chemistry Council** (2006) *Composite driveshafts can increase torque and can help prevent injuries*.

[12] **Van Laarhoven**, D. (1989) Cooling Tower Fan, Gear Drive Operating Problems Solved; *Power Engineering*; Jan 1989, 38-40

[13] **Badie, M. A., Mahdi, A., Abutalib, A. R., Abdullah, E. J., & Yonus, R.** (2006). Automotive composite driveshafts: investigation of the design variables effects. *International Journal of Engineering and Technology*, *3*(2), 227-237.

[14] **Rastogi, N.** (2004). *Design of composite driveshafts for automotive applications* (No. 2004-01-0485). SAE Technical Paper.

[15] **Fourney, W. L., & Poesch, J. G.** (1973). Dynamic modulus and damping in graphite composites. *Polymer Engineering & Science*, *13*(5), 395-397.

[16] **Gireesh, B., Sollapur Shrishail, B., & Satwik, V. N.** (2013). Finite element & experimental investigation of composite torsion shaft. *Int. J. Engg. Research and Applications*, *3*(2), 1510-1517.

[17] **Badie, M. A., Mahdi, E., & Hamouda, A. M. S.** (2011). An investigation into hybrid carbon/glass fiber reinforced epoxy composite automotive drive shaft. *Materials & Design*, *32*(3), 1485-1500.

[18] **Shokrieh, M. M., Hasani, A., & Lessard, L. B.** (2004). Shear buckling of a composite drive shaft under torsion. *Composite structures*, *64*(1), 63-69.

[19] **Badie, M. A., Mahdi, A., Abutalib, A. R., Abdullah, E. J., & Yonus, R.** (2006). Automotive composite driveshafts: investigation of the design variables effects. *International Journal of Engineering and Technology*, *3*(2), 227-237.

[20] **Kaw, A. K.** (2005). *Mechanics of composite materials*. CRC press.

[21] **Erkliğ, A.** (2014) *ME429 – Composite Materials*, University of Gaziantep, Lecture Notes.

[22] **Ummuhaani, A. M., & Sadagopan, P.** (2011). *Design, Fabrication and Stress Analysis of a Composite Propeller Shaft* (No. 2011-28-0013). SAE Technical Paper.

[23] **Cook, R., Malkus, D., Plesha, M., & Witt, R.** (2002). Concepts and applications of finite element analysis.

[24] Release, A. N. S. Y. S. (2009). 12.1 Documentation. *Element Reference, Element Library*.

[25] **Peters, S. T., Humphrey, W. D., & Foral, R. F.** (1991). *Filament winding composite structure fabrication*. SAMPE International Business Office.

[26] **Peters, S. T., McLarty, J. L.** (2001). *Filament Winding*. ASM Handbook, Volume 21: Composites, p536-549, DOI: 10.1361/asmhba0003416

[27] **Sharma, S.** (2002). Economics of composites and reinforcements. Composite materials.

[28] **Kliger, H. S., Yates, D. N., & Davis, G. C.** (1980). *Economic and Manufacturing Considerations for Composite Driveshafts* (No. 800005). SAE Technical Paper.

[29] **Bannister, M.** (2001). Challenges for composites into the next millennium—a reinforcement perspective. *Composites Part A: Applied Science and Manufacturing*, *32*(7), 901-910.

[30] **ISO 1268-1&5** (2001). Fibre-reinforced plastics – Methods of producing test plates, *Internatinal Organization for Standardization*, Geneve.

[31] **Gibson, R. F.** (2011). *Principles of composite material mechanics*. CRC press.

[32] **ASTM D3039** (2014). Standard Test Method for Tensile Properties of Polymer Matrix Composite Materials, *ASTM International*, West Conshohocken, PA.

[33] **ASTM D6641** (2014). Standard Test Method for Compressive Properties of Polymer Matrix Composite Materials Using a Combined Loading Compression (CLC) Test Fixture, *ASTM International*, West Conshohocken, PA.

[34] **ASTM D3518** (2013). Standard Test Method for In-Plane Shear Response of Polymer Matrix Composite Materials by Tensile Test of a ±45° Laminate, *ASTM International*, West Conshohocken, PA.

[35] **ASTM D792** (2013). Standard Test Methods for Density and Specific Gravity (Relative Density) of Plastics by Displacement, *ASTM International*, West Conshohocken, PA.

[36] **Brace, M. W., & Tzioumis, E.** (2010). *U.S. Patent No. 7,682,256*. Washington, DC: U.S. Patent and Trademark Office.

[37] **Lawrie, D. J.** (2012). *U.S. Patent Application No. 13/493,719*.

[38] **Borges, J. S., Trevisanut, V. R., & Scarr, D. R.** (2008). *U.S. Patent No. 7,419,435*. Washington, DC: U.S. Patent and Trademark Office.

[39] **Yates, D. N., & Presta, J. C.** (1980). *U.S. Patent No. 4,236,386*. Washington, DC: U.S. Patent and Trademark Office.

[40] **Yates, D. N., & Presta, J. C.** (1980). *U.S. Patent No. 4,187,135*. Washington, DC: U.S. Patent and Trademark Office.

[41] **Yates, D. N., & Presta, J. C.** (1980). *U.S. Patent No. 4,238,540*. Washington, DC: U.S. Patent and Trademark Office.

[42] **Shinoara, J., Murotani, H., Yamatsuta, K.** (1992) *EP0511843A1. European Patent Office*

[43] **Duggan, J. A.** (1997). *U.S. Patent No. 5,601,494*. Washington, DC: U.S. Patent and Trademark Office.

[44] **Myers, G. L.** (1997). *U.S. Patent No. 5,632,685*. Washington, DC: U.S. Patent and Trademark Office.

[45] **Smiley, A. J., Higgins, M. H., & Scholley, F. G.** (1995). *U.S. Patent No. 5,397,272*. Washington, DC: U.S. Patent and Trademark Office.

[46] **Bergsma, O. K., & Huisman, J.** (1988). Deep drawing of fabric reinforced thermoplastics. *Computer aided design in composite material technology*, 323-334.

[47] **Van Der Weeën, F.** (1991). Algorithms for draping fabrics on doubly-curved surfaces. *International journal for numerical methods in engineering*, *31*(7), 1415-1426.

[48] **Potter, K. D.** (1979). The influence of accurate stretch data for reinforcements on the production of complex structural mouldings: Part 1. Deformation of aligned sheets and fabrics. *Composites*, *10*(3), 161-167.

[49] **Wang, J., Paton, R., & Page, J. R.** (1999). The draping of woven fabric preforms and prepregs for production of polymer composite components. *Composites Part A: Applied Science and Manufacturing*, *30*(6), 757-765.

[50] **Van West, B. P., & Luby, S. C.** (1997). Fabric draping simulation in composites manufacturing. Part II: Analytical methods. *Journal of advanced materials*, *28*(3), 36-41.

[51] **Mohammed, U., Lekakou, C., & Bader, M. G.** (2000). Experimental studies and analysis of the draping of woven fabrics. *Composites Part A: Applied Science and Manufacturing*, *31*(12), 1409-1420.

[52] **Prodromou, A. G., & Chen, J.** (1997). On the relationship between shear angle and wrinkling of textile composite preforms. *Composites Part A: Applied Science and Manufacturing*, *28*(5), 491-503.

[53] **Potter, K.** (2002). Bias extension measurements on cross-plied unidirectional prepreg. *Composites Part A: Applied Science and Manufacturing*, *33*(1), 63-73.

Url-1 *<http://repairguide.autozone.com>*

Url-2 *<http://www.acpt.com/Products/Composite-Driveshafts.aspx>*

Url-3 *<http://navyaviation.tpub.com/14018/css/14018_596.htm>*

Url-4 *<http://mostreal.sk/html/elem_55/chapter4/ES4-181.htm>*

Url-5 *<https://www.coursehero.com/file/10016676/Composite-Lecture-overview>*

Url-6 <*http://www.cstcomposites.com>*

Url-7 *<http://www.teufelberger.com/en/innovation/t-igelr.html>*

Url-8 *<http://www.saarstahl.de >*

CURRICULUM VITAE

Name Surname:	Samet TATAROĞLU
Place and Date of Birth:	Bursa/TR – 22.08.1989
E-Mail:	samettataroglu@gmail.com
EDUCATION:	
B.Sc.:	YTU, Mechanical Engineering, 2011

PROFESSIONAL EXPERIENCE AND REWARDS:

- 2011, **Yıldız Technical University Honor Student**
- YTU IEEE Community Sectoral Development Symposium '09
  1st Prize in Article Competition about Defence / Aerospace Industry and Technologies
  with the article titled "Advent and the Future of UAS Concept"

PUBLICATIONS, PRESENTATIONS AND PATENTS ON THE THESIS:

▪ Türkmen H. S., Doğan V. Z., Mecitoğlu Z., **Tataroğlu S.**, Ok E., Akay E., Süsler S., Kaya S., Şen A. A., 2015: Analytical Development of a Composite Drive Shaft for Heavy Duty Commercial Vehicles. *International Conference on Advances in Composite Materials and Structures*, April 13-15, 2015 Istanbul, Turkey.